The Pennsylvania State University

The Graduate School

ADVANCING INTEGRATED NUCLEIC ACID TESTING FOR HIV SELF-TESTING AND PERSONALIZED VIRAL LOAD MONITORING

A Dissertation in

Electrical Engineering

by

Tianyi Liu

Submitted in Partial Fulfillment
of the Requirements
for the Degree of
Doctor of Philosophy

December 2024

The dissertation of Tianyi Liu was reviewed and approved by the following:

Weihua Guan

Associate Professor of Electrical Engineering

Dissertation Advisor

Chair of Committee

Zhiwen Liu

Professor of Electrical Engineering

Mehdi Kiani

Associate Professor of Electrical Engineering

Cunjiang Yu

Associate Professor of Engineering Science and Mechanics

Madhavan Swaminathan

Professor of Electrical Engineering

Department Head of Electrical Engineering

ABSTRACT

The Human Immunodeficiency Virus (HIV) remains a significant global public health challenge, particularly in resource-limited settings where access to timely and accurate viral load monitoring is constrained. This dissertation presents the development of a portable, user-friendly device designed for quantitative HIV detection from finger-prick blood samples, aiming to address the critical need for accessible HIV viral load testing in these regions.

The developed device integrates advanced nucleic acid testing (NAT) techniques, such as reverse transcription loop-mediated isothermal amplification (RT-LAMP) and reverse transcription polymerase chain reaction (RT-PCR), into a compact, portable format. This innovation facilitates a seamless 'sample-to-answer' solution, enabling self-testing with rapid and accurate results without the need for extensive laboratory infrastructure or professional expertise.

This dissertation focuses on the development of a portable, user-friendly device for quantitative HIV detection from finger-prick blood samples, tailored for use in resource-limited settings. The research encompasses the following key advancements:

1. NAT-on-USB Device: The creation of a fully integrated NAT device for HIV self-testing. This device features a microfluidic reagent cartridge and an ultra-compact analyzer interfaced via USB. It simplifies the testing process, requiring only minimal user interaction, and achieves a detection limit of 214 viral RNA copies/mL within 60 minutes.
2. Quantitative Detection Enhancements: Development of quantitative detection capabilities, including a disposable plasma separation card and a syringe-based RNA extraction module. These enhancements ensure efficient plasma separation and viral recovery, achieving 80% and 86% efficiency, respectively. Additionally, a smartphone interface for real-time

semiquantitative RT-LAMP testing was implemented, maintaining stable performance over 16 weeks.

3. Multiplex PCR for HIV-1 and HIV-2: Advancing the device to perform multiplex RT-PCR for simultaneous detection of HIV-1 and HIV-2 viral loads. This portable PCR analyzer, designed for resource-limited settings, demonstrates high sensitivity and specificity, confirming its reliability and effectiveness.
4. Simultaneous Detection of HIV and HCV: Refinement of the multiplex PCR device to allow rapid self-testing for both HIV and Hepatitis C Virus (HCV) viral loads. The battery-operated system completes PCR amplification in 45 minutes and shows high accuracy and reliability, comparable to benchtop PCR systems.

These innovations represent significant progress in making HIV viral load testing more accessible and practical, particularly in high-prevalence regions with limited healthcare resources. The developed device offers a rapid, accurate, and user-friendly solution for self-testing, which is crucial for improving HIV management and treatment outcomes globally.

TABLE OF CONTENTS

LIST OF FIGURES

LIST OF TABLES

ACKNOWLEDGEMENTS

First and foremost, I express my deepest gratitude to my supervisor, Professor Weihua Guan, for his invaluable advice, unwavering support, and patience throughout my Ph.D. journey. His vast knowledge and rich experience have been a constant source of inspiration in my academic pursuits and daily life. It has been a privilege to work with him, and I am profoundly thankful for all his contributions.

I extend my sincere thanks to my dissertation defense committee members: Prof. Zhiwen Liu, Prof. Mehdi Kiani, and Prof. Cunjiang Yu, for their time, guidance, and insightful feedback. I also appreciate all my lab members, whose kindness and support have made my study and life in the USA a truly wonderful experience.

This research was partially funded by the National Institutes of Health (NIH) under Grant R61AI147419 and the National Science Foundation (NSF) under grants No. 1902503, 1912410, and 1710831. The views and opinions expressed in this dissertation do not represent those of the federal funding agencies and should not be used for advertising or product endorsement.

Lastly, I am immensely grateful to my parents for their unwavering love and support. Their faith in me has been a constant source of strength and motivation. I also wish to thank all my relatives and friends who have stood by me over these past eight years. Your encouragement and companionship have made this journey unforgettable and rewarding. Your presence in my life is invaluable, and I am eternally grateful for your support and love.

Tianyi Liu

CHAPTER 1 Introduction and Overview

1.1. Background

The Human Immunodeficiency Virus (HIV) remains a significant global public health concern, with extensive social, economic, and healthcare ramifications [1]. Despite concerted international efforts to curb its spread, numerous challenges continue to hinder progress, particularly in resource-limited environments [2]. The World Health Organization (WHO) and other global health authorities underscore the vital importance of widespread and accessible HIV testing, anchoring it as a pivotal element of effective HIV/AIDS management and prevention strategies [3]. This is aligned with the WHO's ambitious 95-95-95 targets, which aim for 95% of all people living with HIV to know their status, 95% of those diagnosed to receive sustained antiretroviral therapy (ART), and 95% of those receiving ART to achieve viral suppression by 2030 [4]. The introduction of ART has dramatically transformed HIV from a terminal illness into a manageable chronic condition [5], [6]. Nonetheless, the efficacy of ART is contingent upon regular viral load monitoring to assess and enhance treatment outcomes effectively [7].

Nucleic acid testing (NAT) is a crucial method for monitoring HIV viral load, providing accurate and sensitive detection of HIV RNA [8]. Various NAT techniques are utilized to quantify viral load, including reverse transcription polymerase chain reaction (RT-PCR) and reverse transcription loop-mediated isothermal amplification (RT-LAMP) [9], [10]. RT-PCR involves converting viral RNA into complementary DNA (cDNA) using reverse transcription, followed by amplification of specific DNA sequences . This method is highly sensitive and specific, making it the gold standard for HIV viral load testing [11]. Conversely, RT-LAMP is a newer technique that offers several

advantages over RT-PCR, particularly in resource-limited settings [12]. As an isothermal amplification method, RT-LAMP can be performed at a constant temperature, eliminating the need for expensive thermal cycling equipment [13]. This method is faster and simpler, providing results within a shorter time frame while maintaining high sensitivity and specificity [14]. Both RT-PCR and RT-LAMP play critical roles in the effective monitoring of HIV, enabling timely adjustments to ART and improving patient outcomes.

Traditional methods for monitoring HIV viral load rely on nucleic acid molecular testing conducted in healthcare facilities and processed in specialized laboratories by trained professionals [10]. These methods require extensive laboratory infrastructure and skilled handling, which are often unavailable in resource-limited areas where HIV is most prevalent [15]. This results in long turnaround times and raises privacy concerns for individuals wary of social discrimination [16]. The significant gap between the availability of HIV viral load monitoring and the needs of high-prevalence regions underscores a critical demand for more accessible, portable, and user-friendly VL detection devices [17]–[22]. Such innovations could streamline complex detection procedures, ensuring broader implementation and facilitating timely care adjustments [23]–[27]. The unmet need remains for effective HIV viral load testing that allows self-testing in resource-limited areas, utilizing nucleic acid detection methods, and ultimately achieving sample-to-answer functionality.

This thesis focuses on developing a portable, user-friendly device for quantitative HIV detection from finger-prick blood. It addresses the need for accessible HIV viral load testing in resource-limited settings by integrating advanced nucleic acid testing techniques, such as RT-LAMP, into a compact format. The device aims to provide a seamless 'sample-to-answer' solution, enabling self-testing with rapid, accurate results without requiring extensive lab infrastructure or professional

expertise. This innovation seeks to improve HIV management and treatment, especially in high-prevalence, resource-limited regions.

First, we developed a fully integrated nucleic acid testing (NAT) device for streamlined HIV self-testing using finger-prick whole blood. The device includes a microfluidic reagent cartridge and an ultra-compact NAT-on-USB analyzer. Users can easily drop a blood sample into a collection tube with lysis buffer, load the lysate onto the microfluidic cartridge, and read the results via a graphical user interface (GUI). The cartridge handles sample preparation, purification, and real-time reverse-transcription loop-mediated isothermal amplification (RT-LAMP) automatically. This device demonstrated a limit of detection of 214 viral RNA copies/mL of whole blood within 60 minutes, making it suitable for high-risk populations seeking private self-testing at the early stages of exposure.

Second, we enhanced our HIV viral load testing device by incorporating quantitative detection capabilities, moving beyond simple qualitative testing. We designed a disposable plasma separation card to efficiently separate plasma from finger-prick blood samples and developed a syringe-based RNA extraction module for on-site plasma processing. These innovations achieved an 80% efficiency in plasma separation and an 86% viral recovery efficiency. Additionally, we integrated a smartphone interface for real-time semiquantitative RT-LAMP testing, ensuring stable performance over 16 weeks with lyophilized reagents. The device accurately categorized viral load into low, medium, and high levels with 95% accuracy, providing a convenient and long-term solution for home-based ART treatment monitoring.

Third, we advanced the device to perform multiplex PCR for HIV-1 and HIV-2 viral load determination from finger-prick whole blood. This portable PCR analyzer, designed for resource-limited settings, incorporates multiplex RT-PCR technology with high specificity and sensitivity.

The device simplifies the process by separating plasma, extracting RNA using a portable centrifuge-based device, and performing real-time PCR with fluorescent labeling. The diagnostic performance showed high sensitivity (100% for both HIV-1 and HIV-2) and specificity (100% for HIV-1 and 90.91% for HIV-2), confirming its reliability and effectiveness in various testing environments.

Fourth, we further refined the multiplex PCR device to enable simultaneous self-testing detection of HIV and HCV viral loads. This battery-operated system significantly reduces the time required for point-of-care testing, completing PCR amplification in just 45 minutes. It includes innovations like a custom plasma separation card, portable RNA extraction, and state-of-the-art multiplex RT-PCR technology. Our system provides concurrent measurements of viral loads for HIV and HCV. The novel portable PCR system shows high correlation coefficients (0.96 to 0.99) when compared to the Bio-Rad benchtop PCR, highlighting its accuracy and reliability. These performance figures underscore the device's effectiveness in detecting both HIV and HCV across different infection stages, making it a critical tool for home-based self-testing.

1.2. Overview of work presented

The first part of the dissertation (Chapters 2 and 3) details the development and enhancement of a portable HIV viral load testing device based on RT-LAMP. Chapter 2 introduces a fully integrated nucleic acid testing (NAT) device for streamlined HIV self-testing using finger-prick whole blood for qualitative analysis. This device includes a microfluidic reagent cartridge and an ultra-compact NAT-on-USB analyzer, demonstrating suitability for high-risk populations seeking private self-testing. Chapter 3 builds on this by incorporating quantitative detection capabilities, discussing the design of a disposable plasma separation card and a syringe-based RNA extraction module.

Additionally, it introduces a smartphone interface for real-time semiquantitative RT-LAMP testing, ensuring stable performance over 16 weeks and accurately categorizing viral load levels. The second part of the dissertation (Chapters 4 and 5) focuses on enhancing the device's diagnostic capabilities based on RT-PCR. Chapter 4 details the development of a portable PCR analyzer for resource-limited settings, incorporating multiplex RT-PCR technology for simultaneous detection of HIV-1 and HIV-2 viral loads from finger-prick whole blood. This chapter highlights the device's high sensitivity and specificity, confirming its reliability and effectiveness. Chapter 5 further refines this technology, enabling simultaneous self-testing detection of HIV and HCV viral loads with a battery-operated system that completes PCR amplification rapidly. This chapter showcases the device's diagnostic performance, demonstrating its potential for widespread use in resource-limited settings. Finally, Chapter 6 offers conclusions based on the work presented in the preceding chapters and perspectives for future development. It synthesizes key findings and outlines potential future enhancements to improve the accessibility, efficiency, and accuracy of HIV viral load testing devices, particularly in resource-limited settings.

CHAPTER 2 Quantitative Fingerpick Blood-Based Nucleic Acid Testing on A USB Interfaced Device Towards HIV Self-Testing

In this chapter, we present a fully integrated nucleic acid testing (NAT) device towards streamlined HIV self-testing using 100 µL finger-prick whole blood. The device consists of a ready-to-use microfluidic reagent cartridge and an ultra-compact NAT-on-USB analyzer. The test requires simple steps from the user to drop the finger-prick blood sample into a collection tube with lysis buffer and load the lysate onto the microfluidic cartridge, and the testing result can be easily read out by a custom-built graphical user interface (GUI). The microfluidic cartridge and the analyzer automatically handle the complexity of sample preparation, purification, and real-time reverse-transcription loop-mediated isothermal amplification (RT-LAMP). With a turnaround time of ~60 min, we achieved a limit of detection (LoD) of 214 viral RNA copies/mL of whole blood at a 95% confidence level. Due to its ease of use and high sensitivity, we anticipate the HIV NAT-on-USB device would be particularly useful for the high-risk populations seeking private self-testing at the early stages of exposure.

2.1. Introduction

According to the World Health Organization (WHO), HIV continues to be a significant global public health issue, having claimed 36.3 million lives so far [28]. Early and accurate HIV diagnosis is a critical step to initiate timely antiretroviral therapy (ART), which could suppress HIV, stop the progression of HIV disease, and reduce the viral load (VL) to undetectable levels [29]. The Joint United Nations Program on HIV/AIDS (UNAIDS) has thus put forth the ambitious goal to end AIDS as a global public health threat by 2030. This goal will highly depend on the increases in

HIV testing, treatment, and viral suppression to prevent the onward transmission of HIV[30]. To this end, HIV self-testing is proposed as a new approach where an individual who wants to know HIV status collects a specimen, performs a test, and interprets the result privately [31], [32]. In recent years, uptake of HIV self-testing has gained increasing acceptance both in the US and internationally [31], [33]–[36].

Existing HIV self-testing methods rely exclusively on widely adopted RDTs to detect the presence of HIV-1/2 antibodies [37]. While HIV RDT is very well suited for the primary screening process due to its low cost and fast turnaround time [38]–[41], it could miss a significant portion of asymptomatic HIV carriers during the 2-4 weeks of the window period [32], [42]. A possible alternative is to use nucleic acid testing (NAT), one of the most sensitive methods available for identifying the presence of HIV RNA and/or DNA [32]. NAT devices for HIV testing are readily available in centralized labs. However, a NAT device suitable for HIV self-testing is still lacking. In a recent report [43], WHO surveyed a list of HIV detection platforms such as Aptima HIV-1 Quant Assay (Hologic), GeneXpert HIV-1 Viral Load Test (Cepheid), Alere q system (Alere), cobas LiatTM System (Roche), and EOSCAPE-HIVTM HIV Rapid RNA Assay system (Wave 80 Biosciences). Most of these systems rely on relatively complex and expensive analyzers and replace conventional real-time PCR machines with portable thermal cyclers [44]. They often require plasma as a testing specimen which is prepared from venipuncture whole blood in laboratory conditions. Thus these NAT devices are not well suited for self-testing, in which a self-obtainable sample type such as finger-prick whole blood [45]–[47] or oral fluid would be preferred. To make the technologically intense HIV NATs more readily available in the resource-limited setting such as self-testing, there are increasing efforts in developing alternative isothermal amplification techniques that do not require thermal cycling and expensive instrumentation [44], [48]–[57]. These assays include loop-mediated isothermal amplification (LAMP), nucleic acid sequence-based

amplification (NASBA), recombinase polymerase amplification (RPA), as well as helicase-dependent amplification (HDA). Among isothermal methods, LAMP has been observed to be more resistant than PCR to inhibitors in complex samples such as blood [58]. HIV LAMP assay [59]–[64] has enabled the recent development of point-of-care HIV NAT devices, such as Smart Cup [65] and microRAAD [66]. Despite significant progress, no HIV NAT technologies can be used by a layperson to perform self-testing due to the complexity in sample handling [67].

An ideal HIV self-test should combine the benefits of RDTs (minimal training, minimal sample handling, and rapid) and NAT (highly sensitive, specific, and quantitative capability). To this end, it would require a fully integrated sample preparation by automating the assay process with a cost-effective microfluidic chip and analyzer. Here, we present an integrated 'finger-prick blood sample in, answer out' HIV NAT device to address this challenge. The device consists of a microfluidic reagent cartridge and an ultra-compact NAT-on-USB analyzer. We showed that the device can work with a reduced whole blood volume of 100 µL (readily available with finger-pick method) as compared to traditional methods using ~10 ml of venous blood [68]. The test requires simple steps from the user to drop the finger-prick blood sample into a collection tube with lysis buffer and load the lysate onto the microfluidic cartridge, and the testing result can be easily read out on a custom-built graphical user interface (GUI). The microfluidic cartridge can automatically handle the complexity of sample preparation, purification, and real-time reverse-transcription Loop-mediated Isothermal Amplification (RT-LAMP). The automation is facilitated by a novel programmable electromagnetic (EM) pulse method. The highly portable analyzer is USB interfaced and integrates cooperating subsystems (electronic, optical and mechanical) into an ultra-compact form factor. Since USB ports are universally available and provide connections for both the power and the data, we anticipate the HIV NAT-on-USB would significantly enhance the device usability by the lay individuals. Through these innovations, we anticipate that HIV self-testing could be performed as

simply as a home blood glucose test. The rapid, low-cost, easy-to-use HIV NAT-on-USB would be particularly useful for the high-risk populations seeking private, highly sensitive self-testing at home.

2.2. Methods

2.1.1 Materials and Chemicals

All the electronic and optical components used to build the NAT device (listed in **Table 2-1**) were purchased from Digikey, unless otherwise stated. All RT-LAMP and RT-PCR primers were synthesized by IDT. Isothermal buffer, $MgSO_4$, deoxyribonucleotide triphosphates (dNTPs), Bst 2.0 DNA polymerase, WarmStart reverse transcriptase are from NEB (New England Biolabs). Betaine, Calcein, $MnCl_2$, and EDTA-buffer solution (pH 8.0) were purchased from Sigma-Aldrich. The TaqMan Fast Virus 1-Step Master Mix and the ChargeSwitch™ Total RNA Cell Kit (CS14010) for extracting RNA were purchased from ThermoFisher. The assay was validated in a benchtop real-time PCR instrument (Bio-Rad CFX96). Purified HIV-1 RNAs (Subtype B, USA) were obtained commercially from SeraCare Life Science (cat. 0400-0078). We obtained samples of whole blood collected in potassium EDTA tubes from Innovative Research, Inc (Novi, MI).

Table 2-1. Bill of materials

System	Description	Part#	Function	Unit Cost ($)	Unit Qty.	Ext. Cost ($)
Electronics	Arduino Nano	7630049200173	Microcontroller	22	1	22.00
Electronics	36-pin stripe male header	392	Headpins	4.95	0.1	0.50
Electronics	DC Barrel Power Jack/Connector	PRT-00119	Power Connector	1.25	1	1.25
Electronics	Stacking Headers for Arduino	85	Wire Sockets	1.95	0.83	1.62
Electronics	Male/Male Jumper Wires	758	Wires	3.95	0.1	0.40
Electronics	Power Resistor, 3Ω	MP930-3.00F	Power stabilizing	5.2	1	5.20
Electronics	Capacitor 10uF	P10425CT	Power stabilizing	0.147	1	0.147
Electronics	IC 16-channel I/O Expander	SX1509BIULCT	EM control	2.06	1	2.06

Electromagnetic	SMD Resistor, 1kΩ	311-1.00KHRCT	Temperature/EM control	0.0072	24	0.17
Electromagnetic	N Channel Power MOSFET	DMN1019USN-7DICT	Switch for PCB coils	0.354	24	8.50
Magnet	Neodymium Disc Magnet Nickel	58605K33	Holding magnetic beads	2.69	1	2.69
Thermal	Cold Plate	CP-0.91-0.91	Heating Stage	5.75	0.25	1.44
Thermal	2Ω Power Resistor	MP725-2.00-FCT	Heater	7.01	1	7.01
Thermal	SMD Resistor, 1kΩ	311-1.00KHRCT	Temperature/EM control	0.0072	1	0.01
Thermal	Thermistor	235-1057	Temperature sensing	7.94	1	7.94
Thermal	SMD Resistor, 10kΩ	RNCP0603FTD10K0CT	Temperature control	0.1	1	0.10
Thermal	N Channel Power MOSFET	DMN1019USN-7DICT	Switch for heater	0.354	1	0.35
Optics	SMD Resistor, 10kΩ	RNCP0805FTD10K0CT	Optical module	0.0277	3	0.08
Optics	IC Color Sensor	TCS34725FNCT	Optical detection	2.6	1	2.60
Optics	SMD LED, Blue	1497-1138-1	Fluorescence excitation	0.528	1	0.53
Enclosure	ABS Filament (Black)	-	3D platform material	69	0.05	3.45
Enclosure	Screws (M2 cap screw)	91290A015	Assembly	0.14	10	1.40
			Total Cost			**$69.43**

2.1.2 NAT-on-USB analyzer and cartridge instrumentation

The overall design of the instrument is completed by PTC Creo software, and the device housing is fabricated by 3D printing (METHOD X, MakerBot). The PCB is designed in Autodesk Eagle software and fabricated by OSH Park. The electronic components and MCU on the PCB are manually soldered in the laboratory. A resistive-heating element (PWR263S-20-2R00J, Digi-Key) was attached to the backside of the customized aluminum heating plate using thermal paste (AATA-5G, Artic Alumina). A thermistor (95C0606, Digi-Key) was embedded in the center of the heating plate for real-time temperature monitoring. Negative thermal feedback control was performed using N-channel power MOSFET (63J7707, Digi-Key) to maintain the desired temperature during NAT. The one-time use cartridge was designed by AutoCAD, and each layer was patterned using a CO_2 laser cutting machine (Universal Laser Systems). All patterned layers were aligned and laminated with adhesive solvent. The control GUI software is written in Python, and the GUI establishes connection and communication with the device through USB serial communication.

2.1.3 HIV-1 RT-LAMP reaction

The RT-LAMP reaction mix (total volume: 25 µL) contains isothermal buffer (20 mM Tris-HCl, 10 mM $(NH_4)_2SO_4$, 50 mM KCl, 2 mM $MgSO_4$, 0.1% Tween 20, pH 8.8), PCR grade H_2O, Betaine (0.8 M), $MgSO_4$ (7 mM), deoxyribonucleotide triphosphates (dNTPs, 1.4 mM), Bst 2.0 DNA polymerase (16U), DNA template, WarmStart reverse transcriptase (2U) and primer sets (0.2 µM F3 and B3c, 1.6 µM FIP and BIP, 0.8 µM LPF and LPB).

2.1.4 HIV-1 RT-PCR reaction

We used a one-step, two-enzyme RT-PCR protocol for HIV-1 assays. The reaction has a total volume of 20 µL, consisting of 5 µL TaqMan Fast Virus 1-Step Master Mix (cat. 4444432, Thermofisher), forward primer (0.6 µM), reverse primer (0.6 µM), probe (0.25 µM), and 1 µL RNA templates as well as 11 µL PCR grade water. We used a previously validated HIV-1 RT-PCR primer set [11]. The RT-PCR was performed by the following thermal cycling sequences: 50 ℃ for the first five minutes without repeating to reverse transcription reactions which convert HIV-1 RNA into cDNA, then 95℃ for 20 seconds without repeating to initiate amplification, followed by 40 cycles of amplification stage consisting of 3 seconds of 95℃ and 30 seconds of 60℃ thermal-cycling. Primers Forward (5’-CATGTTTTCAGCATTATCAGAAGGA-3') and Reverse (5’-TGCTTGATGTCCCCCCACT-3') (600 nM) and Probe (5′FAM-CCACCCCACAAGATTTAAACACCATGCTAA-Q 3') (250 nM), where FAM indicates a reporter 6-carboxyfluorescein group and Q indicates a 6-carboxytetramethylrhodamine group quencher conjugated through a linker arm nucleotide.

2.1.5 Mock whole blood HIV sample

Purified HIV-1 RNAs (Subtype B, USA) were obtained commercially from SeraCare Life Science (cat. 0400-0078). As-received RNAs were serially diluted to form linearity panels with concentrations ranging from 1 to 10^5 copies/µL. Aliquots of the linearity panels were stored at -80°C until use. To form the mock whole blood HIV sample, 1 µL of these purified HIV-1 RNAs was spiked into 99 µL of healthy whole blood to generate 100 µL of mock samples at concentrations from 10 to 10^6 copies/mL immediately before testing. Note that our protocol did not use Proteinase K to inactivate RNases in the whole blood for simplified sample preparation. The volume of the mock sample used in our study is 100 µL unless otherwise indicated.

2.1.6 Statistical analysis

The fluorescence signals from assays run on the USB device were expressed as the mean of ≥3 independent reactions ± standard deviation (SD). Customized MATLAB code was used to calculate one-way analysis of variance (ANOVA), obtain the optimized threshold for positive/negatives, and calculate linear regression of standard curve.

2.3. Results and discussion

2.3.1. Overall instrumentation

As shown in **Figure 2-1a**, the HIV NAT-on-USB device consists of a highly portable palm-sized analyzer (footprint of 10×5×5 cm^3, weighing 170 g) and a ready-to-use, disposable reagent cartridge. The inset of **Figure 2-1a** shows the cartridge design with an overall dimension of 9 cm

(l)×1.5 cm (w)×0.58 cm (h). It consists of three-patterned polymethyl methacrylate (PMMA) layers, laminated with an adhesive solvent. The assembled cartridge has a binding chamber (800 µL), a washing chamber (450 µL), and a reaction chamber (25 µL). Each of these functional chambers was separated by an oil valve chamber [55]. Reagents were preloaded to the cartridge before use.

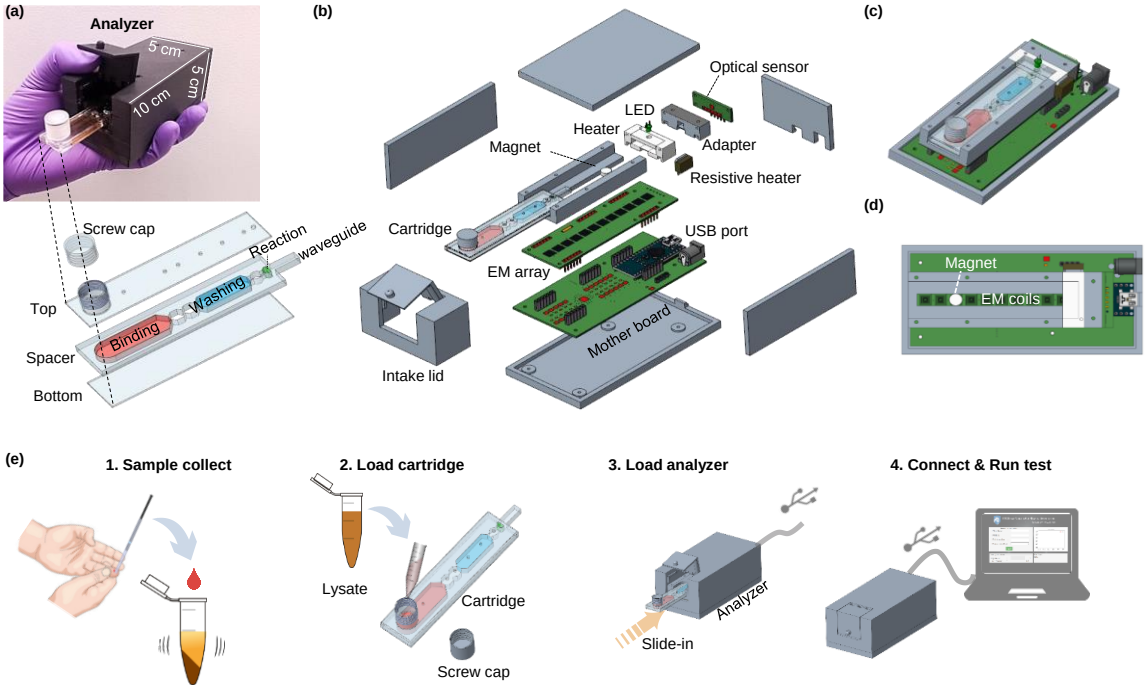

Figure 2-1. Overall HIV NAT-on-USB device and microfluidic cartridge design. **(a)** Photo image of the device held by hand. The enlarged inset shows the exposed view of the cartridge. **(b)** Exposed view of the analyzer. The analyzer was designed to be USB-interfaced for data connection. Optical, thermal, and electromagnetic array subsystems are seamlessly integrated to perform streamlined nucleic acid testing. **(c)** The assembled view of the analyzer with the cartridge in the operation position. **(d)** Top view of the analyzer, showing the electromagnetic array and the permanent magnet. **(e)** Overall operation workflow of HIV NAT-on-USB device. The user self-collects 100 µL of finger-prick blood into the lysis tube (premixed with lysis buffer and the magnetic beads) and shakes it for thorough mixing (step 1). The lysate mixture is loaded to the binding chamber of the microfluidic cartridge. After loading, the cartridge inlet is sealed with a screw cap (step 2). The sealed cartridge is then inserted into the USB analyzer (step 3). The analyzer is connected to a PC through the USB port. The test will be automatically recognized and administrated by a graphic user interface (GUI). The final positive/negative results will be displayed at the end of the automated process (step 4).

Figure 2-1b&c shows the exposed view and the assembled view of the analyzer, respectively. The USB-interfaced analyzer integrates the optical modules (excitation/detection), thermal modules (actuation/sensing), and mechanical modules (PCB coil electromagnet driver). These modules are controlled by a microcontroller unit (MCU) to fully automate the sample-to-answer process on the disposable cartridge. The working principle of the optical and thermal modules is similar to those used in our previous AnyMDx instrument [55], with modifications in spatial configurations. After assembly, we validated that the optical sensor has a linear response to the Calcein concentration from 0 to 25 μM (**Figure 2-2**), confirming its suitability for real-time monitoring of the amplification process. In addition, we validated that the resistive heating module can reach the desired 60°C within 1.5 mins and the root mean squared (RMS) value of the temperature is 0.53°C after stabilization (**Figure 2-3**), which can meet the temperature requirement of the LAMP assay [59]. For actuating the nucleic acid-bearing magnetic beads on the cartridge, we designed a double-sided planar coil array on a printed circuit board (PCB). This PCB coil can be programmed to generate a localized electromagnetic (EM) field for actuating a permanent magnet (**Figure 2-1d**).

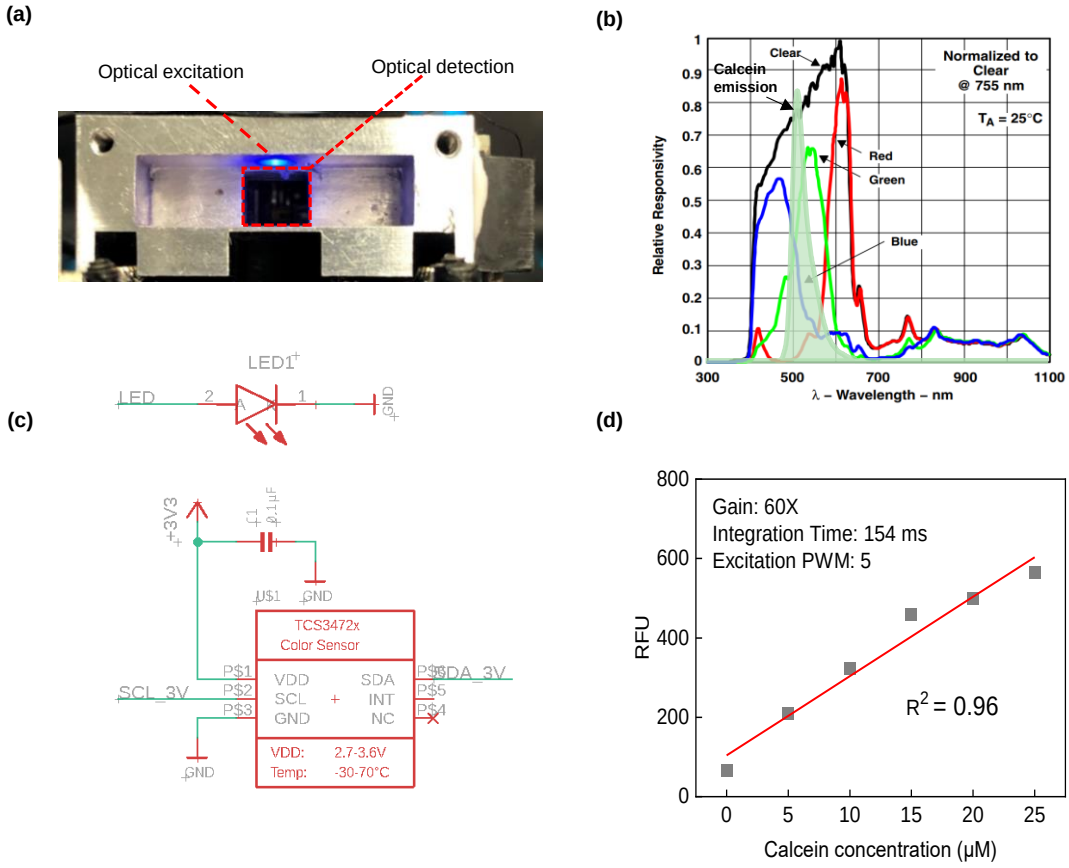

Figure 2-2. (a) Photo image of the optical module. On the excitation side, an LED light source (λ = 488 nm) illuminates the LAMP reaction chamber. On the detection side, the emitted light from the LAMP reaction chamber is guided to the optical sensor through PMMA. The incident direction of the excitation LED light is perpendicular to the optical sensor to minimize the diffracted excitation light entering the optical sensor, thereby improving the signal-to-noise ratio. **(b)** Optical responsibility of the optical sensor as well as the calcein emission profile. The optical sensor can collect the signals from the red, green, and blue channels. The analyzer uses the red channel of the optical sensor to monitor the emission signal. **(c)** The circuit schematic diagram of the excitation and emission sensing module. **(d)** Characterization of the optical sensor with calcein. The optical sensor showed a linear response to the concentration of Calcein from 0 to 25 µM. The test is performed with gain 60x, the integration time 154 ms, and PWM of the excitation LED control is 5.

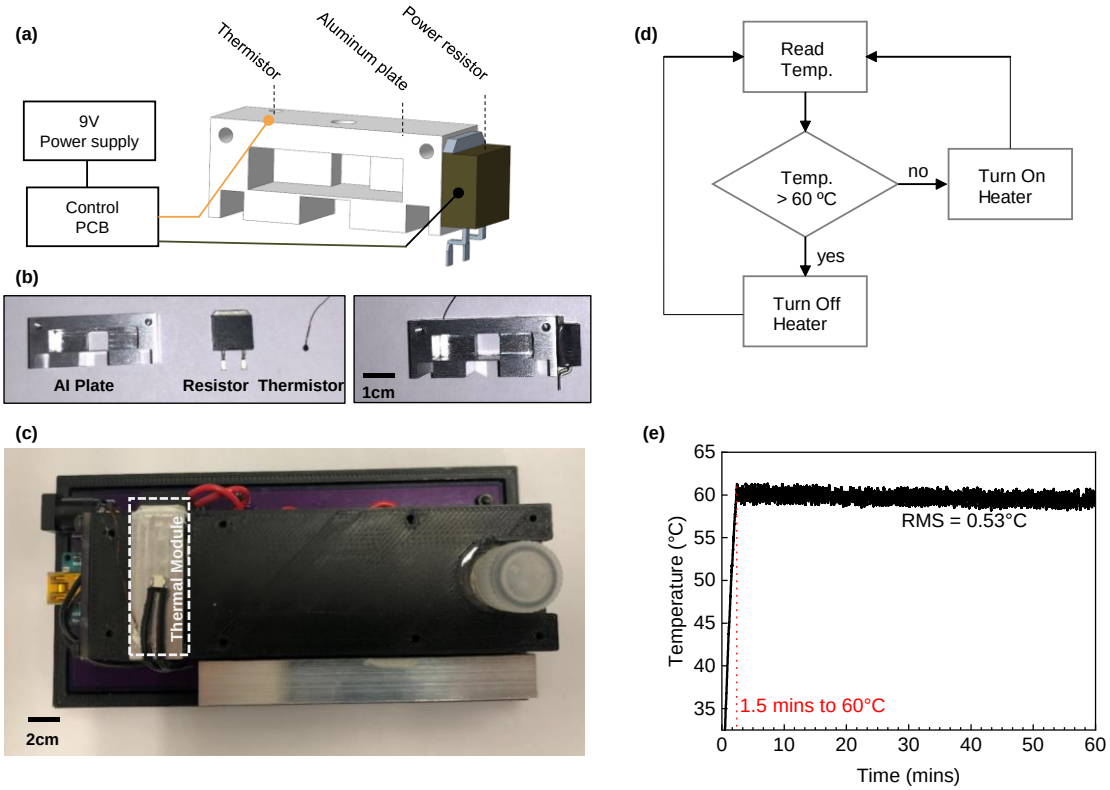

Figure 2-3. (a) The thermal module is composed of a power resistor as a heating source, a thermistor as a temperature feedback sensor, and a CNC aluminum plate. **(b)** Photo image of each component in the heating module (left) and the assembled heating module (right). **(c)** Photo image of the thermal module assembled on the analyzer (top view). **(d)** Flow chart of the thermal control algorithm. **(e)** The thermal module can reach the required 60°C within 1.5 minutes, and the root mean square (RMS) value of the temperature after stabilization is 0.53°C, which can meet the temperature requirements of LAMP detection.

Figure 2-1e shows the overall workflow of the HIV NAT-on-USB. The user would self-collect ~100 µL of finger-prick blood using an exact volume transfer pipet and drop it into a collecting tube pre-filled with 800 µL lysis buffer, 200 µL binding buffer, and 15 µL charge switchable magnetic beads. After the blood is collected into the lysis tube, the user can shake the tube to promote the mixing and binding. After 1 min, the lysate is loaded onto the cartridge through the extruded inlet, which can be completely sealed with a screw cap by hand tightening. The sealed cartridge is then inserted along a sliding rail into the analyzer through a hinged intake lid. After closing the lid, the analyzer is connected to a personal computer (PC) through a USB port. A

customized PC graphical user interface (GUI) was developed for interfacing the analyzer and interpreting the data in a user-friendly way. The GUI can automatically detect a new analyzer connection, request user information, initiate the nucleic acid test, and report the 'yes/no' qualitative result (see **Figure 2-4** for software flowchart). It is noteworthy that the USB-interfaced analyzers can be used in a plug-and-play (PnP) fashion. In addition, multiple USB-interfaced analyzers can be simultaneously and independently connected to a PC through a USB hub for enhanced throughput, if needed. The material cost per test is $3.30 per reagent cartridge and $69.43 per analyzer (**Table 2-1 & Table 2-2**). It is noteworthy that the microfluidic cartridge is an enclosed system after the sample is loaded. It is disposable after each test. Therefore, cross-contamination between tests is not a concern. The overall HIV NAT-on-USB workflow requires minimal user intervention and is simple enough for the laypersons to perform HIV self-testing. **Supplementary Video S2-1** shows the overall workflow of the test.

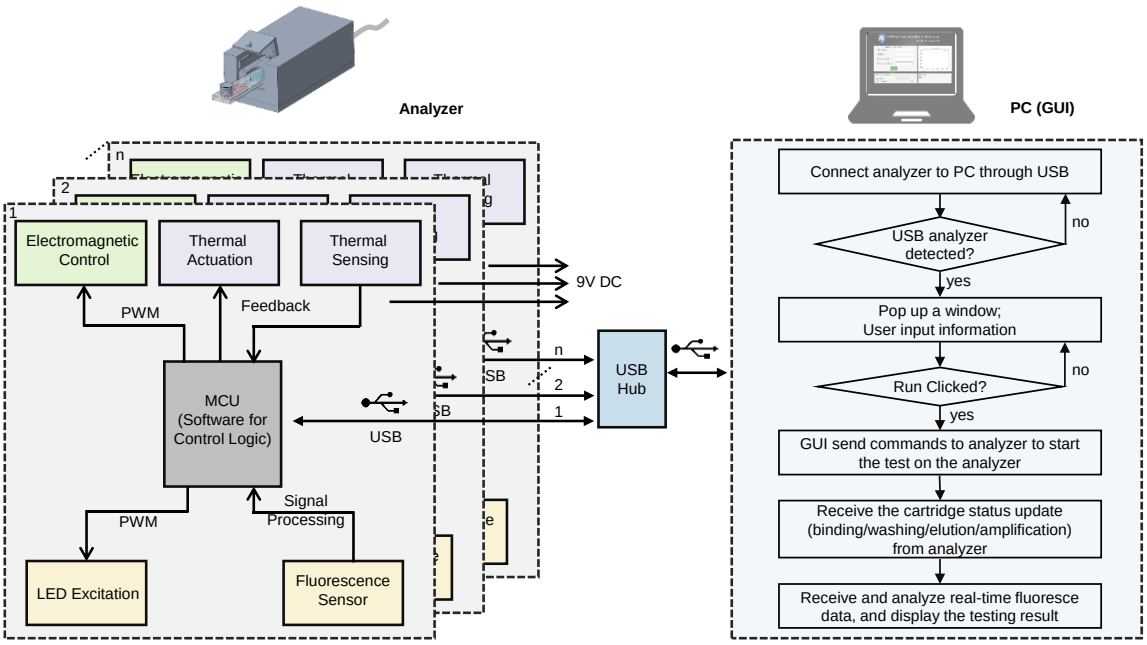

Figure 2-4. Schematic diagram of the device software and hardware. On the analyzer side, the optical, thermal, and electromagnetic modules are seamlessly integrated and controlled by an MCU for automated nucleic acid testing. The analyzer is designed to be USB-interfaced for data connection. Multiple analyzers can be used concurrently through a single USB hub. On the PC side,

a graphic user interface (GUI) is designed to automatically recognize and administrate the analyzer inserted through the USB port. The device status, real-time amplification data, and the final positive/negative results will be displayed on GUI to the end-user.

Table 2-2. Microfluidic cartridge and reagent cost per test

Reagents	Vendor	Function	Stock Vol. (ml)	Unit Cost ($)	Vol. (µl)	Ext. Cost ($)
PCR Grade Water	VWR	LAMP master mix	20	91.88	1	0.0046
F3	IDT	LAMP master mix	4.8	9.4	0.15	0.0003
B3	IDT	LAMP master mix	4.3	8.46	0.15	0.0003
FIP	IDT	LAMP master mix	0.9	62.68	1.2	0.0836
BIP	IDT	LAMP master mix	0.9	64.56	1.2	0.0861
LF	IDT	LAMP master mix	4.6	9.4	0.6	0.0012
LB-HEX	IDT	LAMP master mix	4.3	75.34	0.6	0.0105
LB-BHQ1	IDT	LAMP master mix	1.2	143.58	0.6	0.0718
Betaine	Sigma-Aldrich	LAMP master mix	1.5	24.25	2.4	0.0388
dNTP Mix	Thermo Fisher	LAMP master mix	3.2	107	2.1	0.0702
Bst polymerase	NEB	LAMP master mix	1	264	1	0.5280
WarmStart RT	NEB	LAMP master mix	1	292	0.3	0.0876
NEB Isothermal Buffer	NEB	LAMP master mix	6	24	1.5	0.0060
$MgSO_4$	NEB	LAMP master mix	6	20	1.2	0.0040
Lysis Buffer	Invitrogen	Sample Prep.	100	12.68	1000	0.1268
Purification Buffer	Invitrogen	Sample Prep.	20	2.54	200	0.0254
Wash Buffer	Invitrogen	Sample Prep.	100	12.68	500	0.0634
Proteinase K	Invitrogen	Sample Prep.	1	33.20	10	0.3320
Magnetic Beads	Invitrogen	Sample Prep.	2	356.00	10	1.7800
Acrylic Adhesive	Inventables	Compact disc	118	9.69	1.5	0.0001
1/32" Acrylic Sheet	Inventables	Compact disc	-	14.98	-	0.0250
1/16" Acrylic Sheet	Inventables	Compact disc	-	17.72	-	0.03
					Total Cost	**$ 3.38**

2.3.2. Programmable electromagnetic pulse for sample preparation on cartridge

We have previously demonstrated the use of charge-switchable magnetic beads for streamlining nucleic acid binding, purification, and elution by rotating a microfluidic disc against a stationary magnet [55]. To completely remove the bulky moving parts for actuating the magnetic beads in the NAT-on-USB device, we here further developed a programmable electromagnetic method using double-sided planar coil arrays (**Figure 2-5a**). The planar coil is designed into two layers in a single PCB. There are 12 coils on the top layer and 11 coils on the bottom layer (1×23 array). The permanent magnet can be programmed to the center of any of these 23 coils. This is because a deviation from the 'ON' coil will result in a restoring force to bring the permanent magnet to its equilibrium position (center of the 'ON' coil) (**Figure 2-5b-d**).

It is noteworthy that several previous studies [69]–[71] had tried to use planar coils to generate electromagnets for direct manipulation of the magnetic beads. However, due to the small size and weak relative magnetic susceptibility of magnetic beads (χ_r<<1), the magnetic beads must be significantly polarized by strong permanent magnets. Moreover, a strong electromagnet field with ~ 1 A DC current is required, in which excessive heat can be generated due to the Joule heating [71]. Our approach here uses the programmable pulsed EM field to actuate a permanent magnet that further controls the magnetic beads on the cartridge (**Figure 2-5e&f**). Since the permanent magnet itself has a substantial susceptibility, a small electromagnet field (*i.e.*, a reduced power consumption) is sufficient to drive its motion. In addition, the actuation of the permanent magnet only requires 100 ms of 'ON' time on the desired coil. With this pulsed operation, we found that a minimum of 450 mA is sufficient to actuate the permanent magnet in our device. The temperature generated by the Joule heating was found to be operation frequency-dependent. At the normal 1 Hz operation, the measured max temperature did not exceed 30 °C for 5 min operation (**Figure 2-5g&h**), suggesting that the reagents and assays in the cartridge would not be affected by the electromagnetic actuation, alleviating the overheating problems in previous methods.

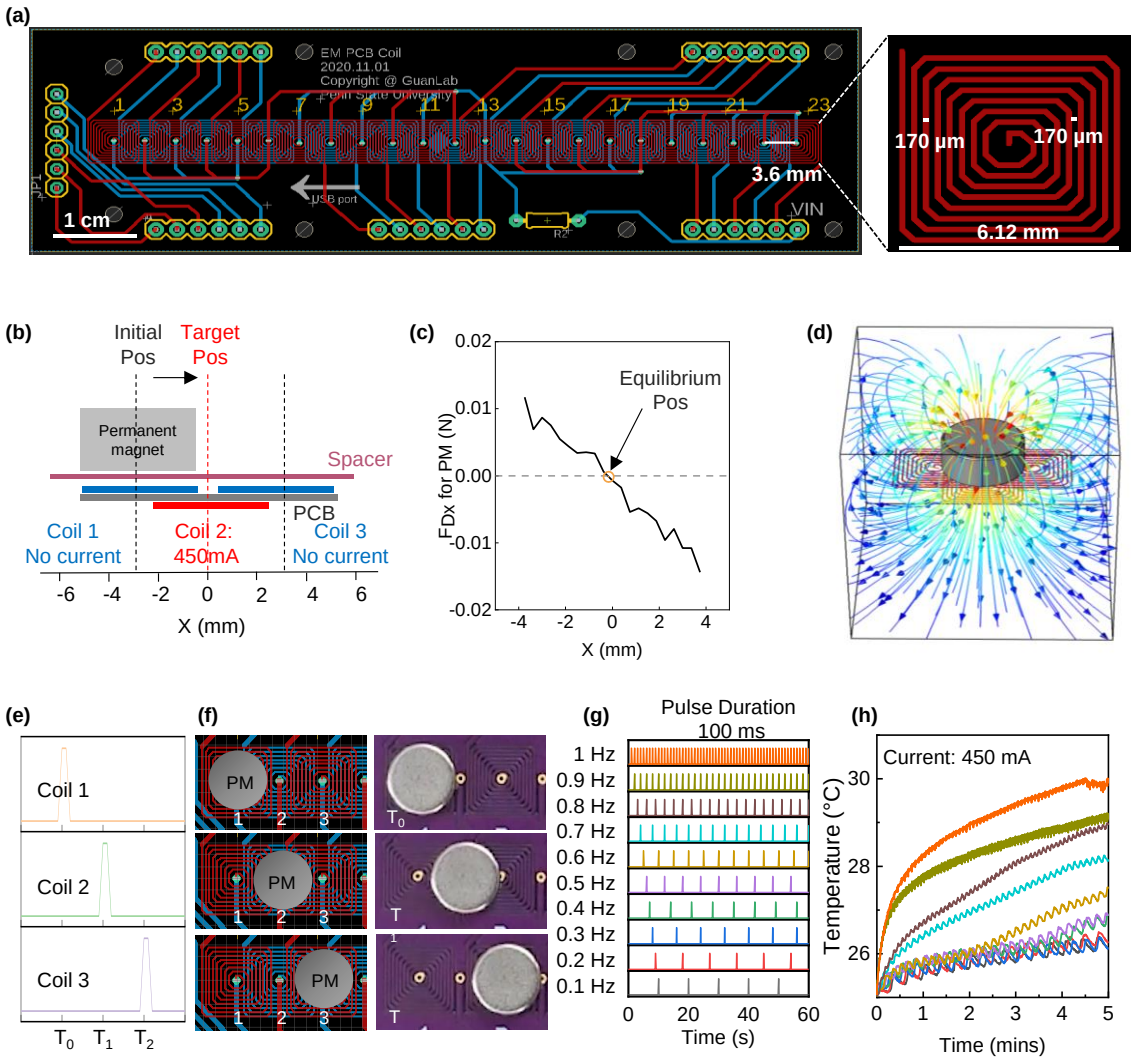

Figure 2-5. (a) The PCB design of the double-sided planar coil array. The planar coil is designed as two layers in a single PCB with a vertical distance of 0.78 mm. Each rectangular coil has a winding width of 170 μm, a spiral pitch of 170 μm, a thickness of 35 μm, and nine turns (enlarged inset). The coils on the top and bottom layers are offset by 3.6 mm horizontally, yielding an effective motion step of 3.6 mm. **(b)** The operation diagram of the permanent magnet being moved from an initial position to a new adjacent position by turning on a specific coil (coil 2 in this case). **(c)** Calculated force on the permanent magnet as a function of the relative displacement of the permanent magnet to the coil center. **(d)** COMSOL simulation of the electromagnetic field generated by the planar coil. **(e)** The sequence of the current pulse to move the permanent magnet from position 1 to position 3. Each pulse is 100 ms in duration. **(f)** The corresponding permanent magnet position at each time spot during the pulsed operation. **(g)** Joule heating evaluation for the programmable electromagnetic pulse. The current pulse waveform with 0.1 Hz to 1 Hz operating frequencies. The duration of each pulse is fixed at 100 ms. (h) The time course

of the temperature measured on the planar coil surface at different operating frequencies (color corresponding to these in (g)). The current pulse amplitude is 450 mA. With 0.1 to 1 Hz operation frequencies, the measured temperature does not exceed 30 °C for 5 min of operation.

Figure 2-6 illustrates the automated sample preparation and amplification on cartridges enabled by the EM actuation of charge-switchable magnetic beads [55]. In the first step, the negatively charged RNAs in the lysate bind to the positively charged magnetic beads at pH 5 in the binding chamber. During the binding process, the permanent magnetic under the cartridge was actuated back and forth at a frequency of 1/3 Hz to ensure thorough mixing. In the second step, the RNA binding beads were transferred to the washing chamber (buffered at pH 7) by the EM array. The beads were horizontally agitated by the programmed EM sequence at 1/3 Hz. In the third step, the washed beads were transferred to the reaction chamber with the master mix buffered at pH 8.8. The RNAs were directly eluted to the master mix due to the positive charge on the magnetic bead surface. After elution, these magnetic beads were moved away from the reaction chamber (step 4) before starting the RT-LAMP reaction (step 5). The entire sample preparation could be completed in less than 15 minutes with minimum user interaction. **Supplementary Video S2-2** presents a typical workflow of the EM array-enabled automated sample preparation and amplification on the cartridge.

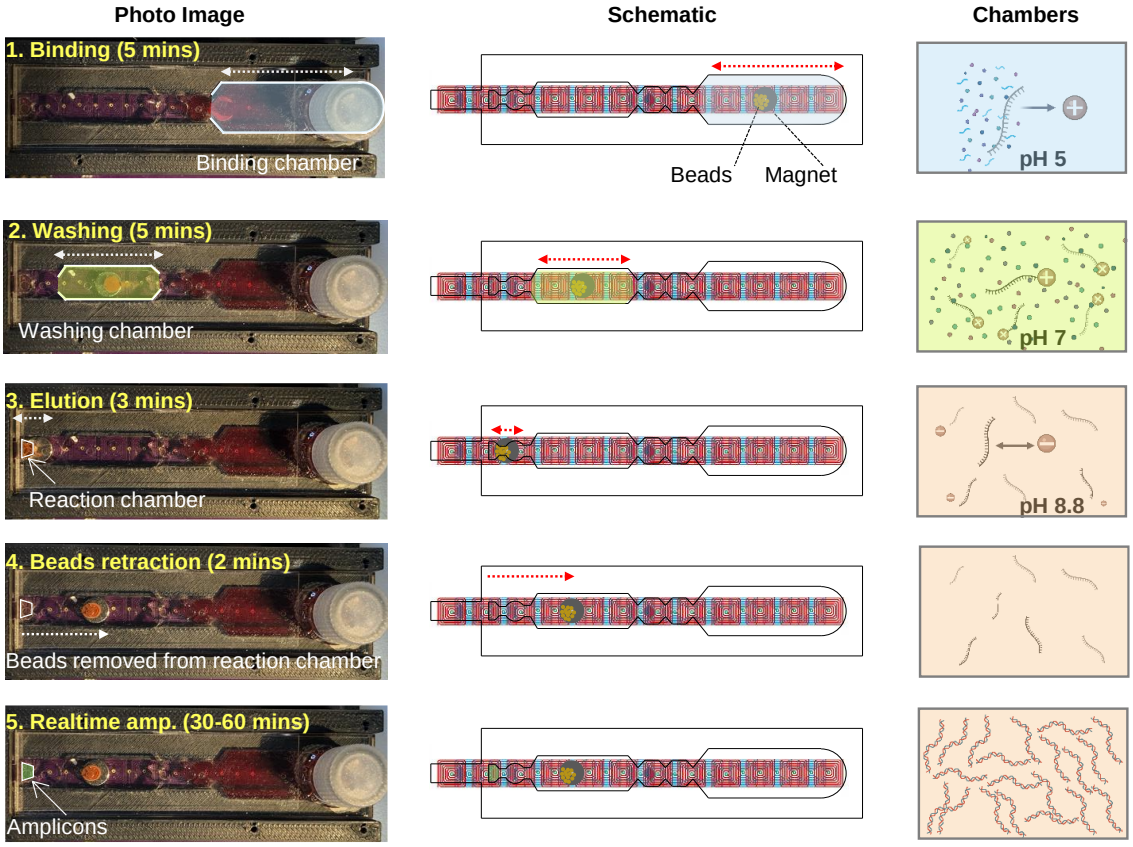

Figure 2-6. Automated sample preparation and amplification on cartridges enabled by the EM pulsed actuation of charge-switchable magnetic beads. The entire sample preparation could be completed in less than 15 minutes with minimum user interaction. The left, middle and right panels show the photo image of the actual device, the schematic of the relative position of the cartridge chambers to the EM driven magnet, and the schematic interactions of molecules with magnetic beads, respectively. In step 1, the negatively charged RNAs in the lysate binds to the positively charged magnetic beads at pH 5 in the binding chamber. In step 2, RNA binding beads were transferred to the washing chamber (buffered at pH 7). In step 3, the washed beads were transferred to the reaction chamber with the master mix buffered at pH 8.8. After elution, these magnetic beads were moved away from the reaction chamber (step 4) before starting the RT-LAMP reaction (step 5).

2.3.3. Copy Number sensitivity of HIV-1 RT-LAMP

We used a previously validated HIV-1 LAMP primer set against the highly conserved region of the integrase gene within subtype B [50] with a modified fluorescent reporter of Calcein [72]. We first validated the intrinsic copy number sensitivity of the HIV-1 RT-LAMP assay by performing the

RT-LAMP reaction against the quantitative panel of HIV-1 RNAs at concentrations ranging from 10^5 copies/µL down to 1 copy/µL. **Figure 2-7a&b** summarized the RT-LAMP primers, the reaction setup, and the real-time RT-LAMP results. As shown in **Figure 2-7c-f,** the copy number sensitivity of the HIV-1 RT-LAMP was determined to be four copies. Changes in temperature or storage time can affect the performance of LMAP. The prepared LAMP should be kept in a refrigerated environment, and it is best to use it immediately.

(a)

Primer	Sequence (5' → 3')
F3	AGTTCCCTTAGATAAAGACTT
B3	CCTACATACAAATCATCCATGT
FIP	GTGGAAGCACATTGTACTGATATCTTTTTGGAAGTATACTGCATTTACCAT
BIP	GGAAAGGATCACCAGCAATATTCCTCTGGATTTTGTTTTCTAAAAGGC
Loop F	GGTGTCTCATTGTTTATACTA
Loop B	GCATGACAAAAATCTTAGA

(b)

Component	Volume (µl)/test	Final Concentration
Isothermal Buffer	2.5	1 X
F3	0.25	0.2 µM
B3	0.25	0.2 µM
FIP	2	1.6 µM
BIP	2	1.6 µM
LF	1	0.8 µM
LB	1	0.8 µM
Betaine	4	0.8 M
MgSO4	1.75	7 mM
Calcein	0.63	25 µM
MnCl2	1.88	75 µM
dNTP Mix	3.5	1.4 mM
Bst polymerase	2	0.64 U/ul
Warmstart RT	0.5	0.3 U/ul
RNA sample	1	1 ul/rxn
PCR Grade Water	0.75	-

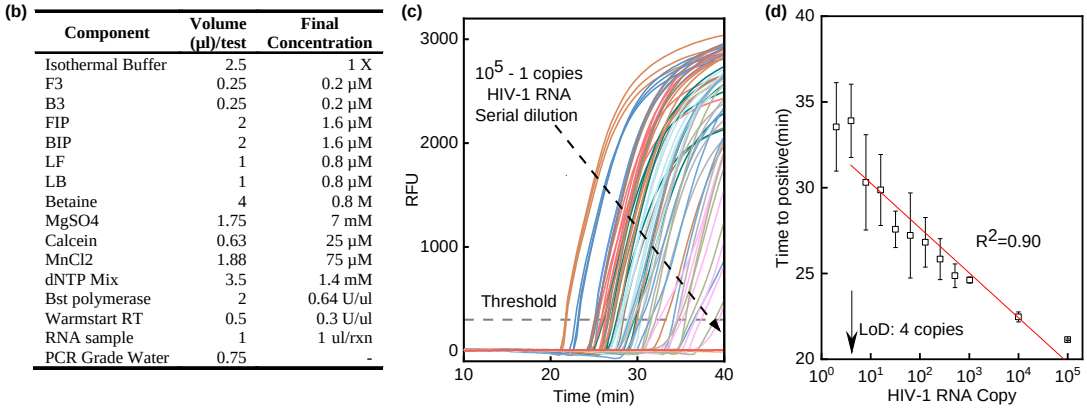

(e)

HIV-1 RNA (copy)	1	2	4	8	16	32	64	128	256	512	1024	10^4	10^5
No. positive/ no. of replicates	0/6	4/6	6/6	6/6	6/6	6/6	6/6	6/6	6/6	6/6	6/6	6/6	6/6
Hit rate (%)	0%	66.7%	100%	100%	100%	100%	100%	100%	100%	100%	100%	100%	100%

Figure 2-7. Validation of the HIV-1 RT-LAMP assay with the quantitative panel. **(a)** Primer set for HIV-1 subtype B RT-LAMP amplification. **(b)** RT-LAMP reaction setup. **(c)** Real-time RT-LAMP amplification data with serially diluted HIV RNA standards (each concentration was repeated six times). **(d)** Time to positive value at different HIV-1 RNA concentrations. The time to positive is defined as the time needed for the RFU to reach the threshold level of 300 (dashed line in c). **(e)** Summary of the hit rate. All six reactions with four or more copies of RNAs can be amplified successfully. The copy number sensitivity of the HIV-1 RT-LAMP was determined to be four copies.

2.3.4. Whole blood HIV-1 RT-LAMP assay

To further test the impact of the whole blood matrix and the reagent on the HIV-1 RT-LAMP assay, we formed mock HIV-1 positive samples by spiking the HIV-1 RNA into healthy whole blood. The 100 µL of mock samples at concentrations from 10 to 10^6 copies/mL were mixed with 500 µL lysis buffer, 200 µL binding buffer, and 15 µL charge switchable magnetic beads for lysis and binding. The beads were then washed with 450 µL of washing buffer. The RNAs were directly eluted into a 25 µL master mix for RT-LAMP reaction. **Figure 2-8a** presents the real-time RT-LAMP results (each concentration was repeated six times). **Figure 2-8b** shows the fluorescent image of the reaction tubes under the ultraviolet (UV) light. **Figure 2-8c** shows the gel electrophoresis results in 2% agarose gel, in which clear ladder-like patterns with multiple bands of different molecular sizes were observed due to the stem-loop DNA structures with several inverted repeats within LAMP amplicons [9], [72]. The fluorescent image and the gel images agreed well with each other.

To estimate the LoD of whole blood HIV-1 RT-LAMP assay, we examined the hit rates at different RNA concentrations [73]. The hit rate is defined as the number of amplified samples over all samples. As shown in **Figure 2-8d,** the LoD of the whole blood RT-LAMP assay is determined to be 214 copies/mL at the 95% confidence level. This LoD is higher than that obtained with the HIV-1 quantitative panels (4 copies, **Figure 2-7e**). We believe the following factors are responsible for the deteriorated LoD in the whole blood samples. First, although we used the spiked sample as soon as we prepared it, the HIV-1 RNA can still experience a certain degree of degradation in the whole blood. Second, inhibitors could exist with the whole blood sample. Third, there is a possibility of material loss during the sample preparation process. We further examined the time to positive as a function of the RNA concentrations in whole blood. As shown in **Figure 2-8e,** linear fit produced the R^2 with 0.89, similar to those obtained with the HIV-1 quantitative panels (**Figure 2-7d**).

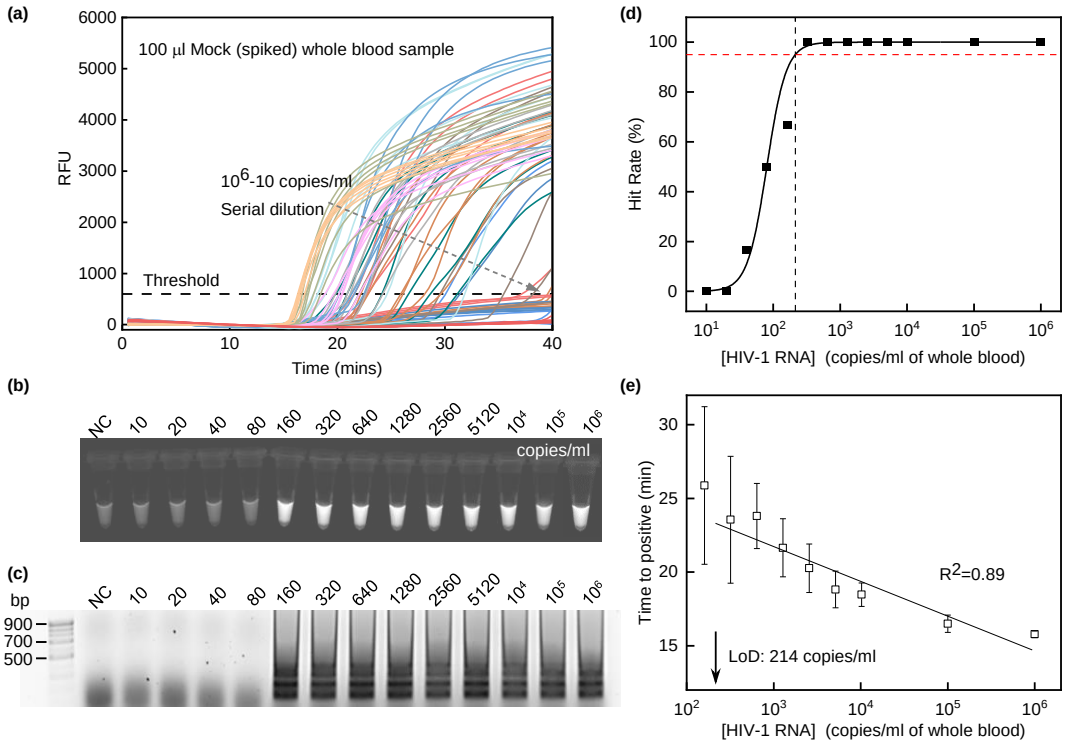

Figure 2-8. RT-LAMP assay validation with spiked whole blood mock sample. **(a)** RT-LAMP amplification curves with serially diluted HIV RNA standards. **(b)** Photo image of RT-LAMP products observed in the reaction tubes under a UV light. **(c)** Gel image of RT-LAMP products analyzed by agarose gel electrophoresis. **(d)** The extracted hit rate at various RNA concentrations to establish the assay LoD, which is determined to be 214 copies/mL at the 95% confidence level. **(e)** Time to positive value at different HIV-1 RNA concentrations in whole blood.

2.3.5. Intra- and inter-device performance test

After validating the automated sample preparation and the HIV-1 RT-LAMP assay, we went out to test the intra- and inter-device performances. It is noteworthy that the multiple USB-interfaced analyzers can be used simultaneously and independently in a plug-and-play (PnP) fashion (**Figure 2-9a** and **Supplementary Video S2-1)**.

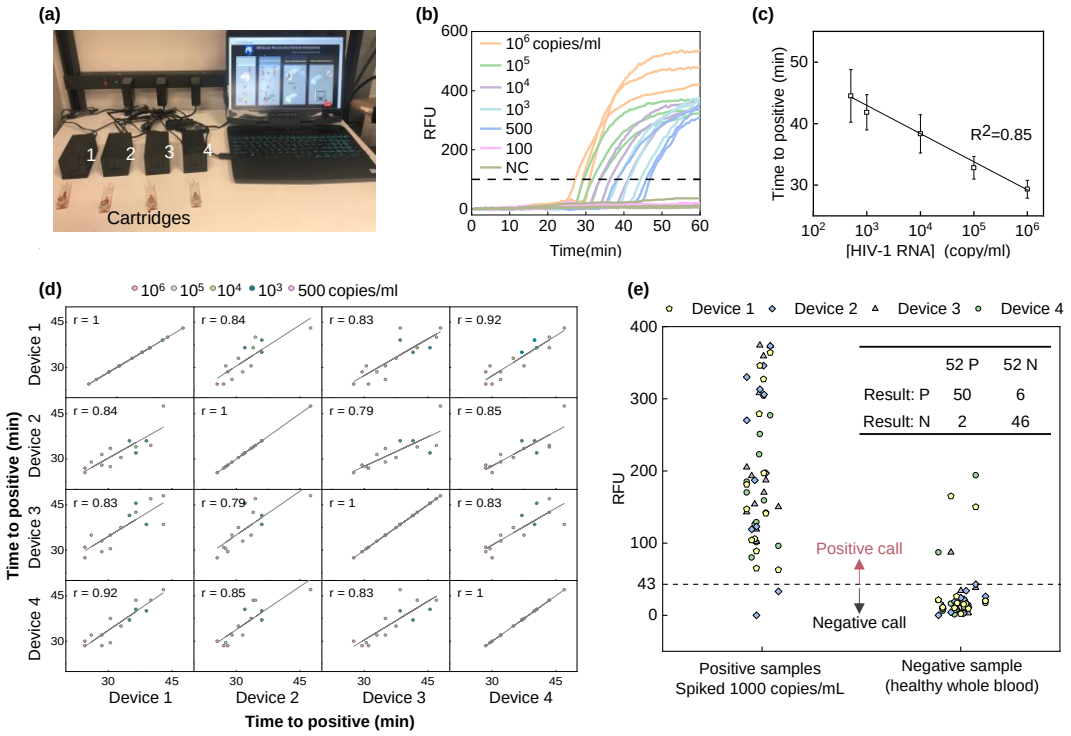

Figure 2-9. Intra- and inter-device performance. **(a)** Photo image showing multiple analyzers being used simultaneously through a single USB hub. **(b)** The real-time RT-LAMP data in the intra-device test with a serially diluted mock blood sample. Each concentration was tested in triplicates. **(c)** Extracted time to positive value for the intra-device test. **(d)** The scattering plot of the time to positive value between two devices. **(e)** The end-point fluorescence values for a total of 104 whole blood samples (52 negatives and 52 positives) were tested with four different analyzers. The dashed line of the value 43 is the receiver operating characteristics (ROC)-optimized fluorescence threshold. The inset table shows the summarization of the results.

For the intra-device verification, we tested a series of mock samples with different HIV-1 RNA concentrations. **Figure 2-9b** shows the real-time data obtained from testing a triplicate panel of these samples with a single USB interfaced analyzer. As shown, HIV-1 RNA concentrations at 500 copies per mL of whole blood were all amplified successfully (in par with these obtained in the tube, **Figure 2-8d**). **Figure 2-9c** shows the time to positive as a function of the input RNA concentrations. A linear fit produced the R^2 with 0.85, indicating the feasibility of using the USB-

interfaced analyzer for a semi-quantitative test on the whole blood (*i.e.*, differentiating between high, medium, and low viral load).

For the inter-device verification, we tested four independent devices with multiple triplicated mock samples. **Figure 2-10** summarizes the real-time data obtained from these tests. We benchmarked the time to positive between any two devices and examined their Pearson correlation coefficient. As shown in **Figure 2-9d**, the device to device showed Pearson correlation coefficients ranging from 0.79 to 0.92, suggesting a good quantitative agreement between these devices.

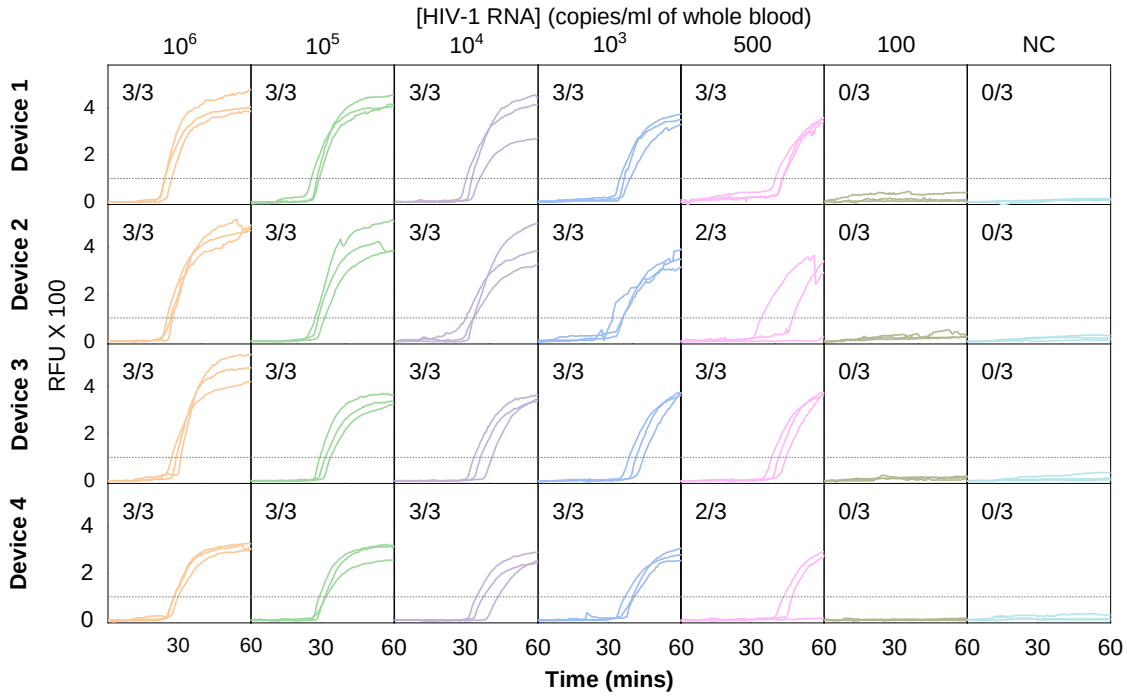

Figure 2-10. The real-time RT-LAMP curves for the inter-device test (4 devices) at different HIV-1 RNA concentrations in whole blood. The hit rate for RNA concentrations above 1000 copies/mL is 100% for all devices tested. The hit rate dropped to 83% (10/12) with samples of 500 copies/mL. No amplification curves were observed for samples at 100 copies/mL and negative control samples.

To determine the diagnostic ability of the HIV NAT-on-USB, we tested a total of 104 whole blood samples (52 negatives and 52 positives) with four different analyzers. The 52 positive samples were

constructed by spiking the HIV-1 RNA into 100 μL human whole blood to form a concentration of 1000 copies/mL, a clinically relevant viral load threshold used for routine monitoring of HIV in resource-limited settings [74], [75]. We examined the fluorescence values for all samples at 60 min (**Figure 2-9e)**. As shown, the RFU values of positives were significantly higher than that of the healthy controls. To find the optimal fluorescence threshold to differentiate the positives and negatives, we analyzed the receiver operating characteristic (ROC) curve [76], [77] by varying the threshold from 1 to 500 RFU. In general, increasing the threshold will improve the specificity but deteriorate the sensitivity. The optimal RFU threshold from ROC analysis is 43 (dashed line in **Figure 2-9e**). The inset of **Figure 2-9e** summarized the diagnostic performance with this optimized threshold. 50 out of 52 positives were detected as true positives, and 46 out of 52 negatives were detected as true negatives. The sensitivity, and specificity of the test was 96.2% (95% CI=90.9%-100%) and 88.5% (95% CI= 79.8%-97.1%). The tests performed with all four different devices showed excellent accuracy (93%) in differentiating the clinically relevant viral load threshold at 1000 copies/mL.

2.4. Summary

In summary, we developed an integrated 'finger-prick blood sample in, answer out' full auto sample preparation and detection HIV NAT device towards HIV self-testing using 100 μL of a self-obtained finger-prick blood sample. The device consists of an ultra-compact NAT-on-USB analyzer and a ready-to-use microfluidic cartridge. The test requires simple steps from the user to drop the finger-prick blood sample into a collection tube with lysis buffer and load the lysate onto the microfluidic cartridge, and the testing result can be easily interpreted by the user through a GUI. We fully automated the process of on-chip RNA extraction, purification, and isothermal amplification from a whole blood sample and achieved an LoD of 214 copies per mL of whole

blood at the 95% confidence level. Although the HIV NAT-on-USB device is designed for self-testing, the test can be easily scaled up to conduct multiple tests simultaneously through a USB hub. This makes the device also suitable for use in primary care settings as well. To further develop this technology for self-testing, there are several outstanding issues we need to address, including validation with clinical HIV-positive samples, evaluating performance across different subtypes of HIV-1, incorporating an internal control, and the lyophilization of the LAMP reagents to allow ambient storage at room temperature. With these efforts, we anticipate the rapid, low-cost, easy-to-use HIV NAT-on-USB device could enable laypersons to perform highly sensitive self-testing at home.

CHAPTER 3 Compact Point-of-Care Device for Self-Administered HIV Viral Load Tests from Whole Blood

In this chapter, we explored a point-of-care HIV viral load device to address this need. This device can perform streamlined plasma separation, viral RNA extraction, and real-time RT-LAMP semiquantitative testing in an ultra-compact device. We developed an absorption-based membrane plasma separation method suitable for finger-prick blood samples, achieving an efficiency of 80%. We also designed a syringe-based RNA extraction method for on-site plasma processing with a viral recovery efficiency of 86%. We created a portable device with a smartphone interface for real-time semiquantitative RT-LAMP, useful for monitoring viral load. The device uses lyophilized reagents, processed with our lyophilization method, which remain stable for 16 weeks. The device can accurately categorize viral load into low, medium, and high categories with 95% accuracy. We believe this point-of-care HIV self-test device, offering convenience and long-term storage, could aid patients in home-based ART treatment monitoring.

3.1. Introduction

HIV remains a severe global health issue, claiming over 40.1 million lives to date, according to the World Health Organization (WHO) [1]. Nonetheless, implementing Antiretroviral Therapy (ART) has markedly mitigated morbidity and mortality in HIV-1 infected patients [5], [6]. ART's main objective is the reduction of the HIV viral load (VL) to levels that are undetectable, thereby rendering the virus unable to perpetuate transmission [78], [79]. In the year 2020, the Joint United Nations Program on HIV/AIDS (UNAIDS) articulated a robust 95-95-95 target: by the year 2025, 95% of all individuals affected by HIV are expected to be aware of their status; 95% of those identified should be recipients of ongoing antiretroviral therapy; and 95% of all those engaged in

therapy ought to achieve viral suppression [4]. The realization of these objectives demands significant augmentations in HIV diagnostics, the assimilation of treatment, and the containment of the virus, as the curtailment of future HIV transmission intrinsically relies on these components. However, while ART can suppress viral replication, it is not a cure. Lifelong therapy is necessary due to viral persistence, residual inflammation, and metabolic disturbances, all linked to the existence of viral reservoirs [80]. These factors can lead to disease progression towards acquired immune deficiency syndrome (AIDS), even in those receiving ART. Regular viral load monitoring thus becomes indispensable for ensuring treatment success, the current practice of which is regular visits to healthcare facilities [7].

The rapid and accurate quantification of HIV viral load is critical for the effective management of HIV infection [8]. However, creating and advancing point-of-care (POC) devices for assessing HIV viral load introduces substantial and intricate challenges [81]. While highly sensitive and specific, traditional laboratory-based testing methodologies, such as reverse transcription-polymerase chain reaction (RT-PCR), are time-consuming, resource-intensive, and necessitate advanced laboratory infrastructure and trained personnel [10]. These factors often result in prolonged turnaround times for results, particularly for low-resource settings where the HIV burden is often the highest. Moreover, access to regular viral load monitoring is challenging in rural or remote regions due to the geographical distance to equipped laboratories [15]. This lack of accessibility can delay treatment adjustments and potentially accelerate disease progression [82]. Additionally, the need for venous blood sampling can be an obstacle due to the discomfort and expertise required for the procedure. Hence, a POC device for (semi)quantitative HIV viral load testing that is affordable, user-friendly, rapid, and requires minimal infrastructure could revolutionize HIV management by enabling timely and accessible monitoring, particularly in low-resource settings.

Several commercially available instruments, like the GeneXpert HIV-1 Viral Load Test (Cepheid), the Alere q system, Roche's Cobas Liat™ System, and the EOSCAPE-HIV™ HIV Rapid RNA Assay system from Wave 80 Biosciences, have been developed for HIV viral load detection. Typically, these devices utilize plasma as the specimen for testing, extracted from venipuncture whole blood within a controlled laboratory environment. As a result of this requirement, these instruments are not particularly suited for self-administered testing procedures, where more readily accessible sample types such as finger-prick whole blood would be more desirable [45], [83], [84]. In the domain of quantitative POC HIV self-testing, there have been efforts, though limited, to create and optimize systems [85]. The majority of these methodologies are dependent on complex, high-cost analyzers and opt for the use of portable thermal cyclers instead of traditional real-time PCR machinery [44].

Isothermal amplification technologies, such as reverse transcription loop-mediated isothermal amplification (RT-LAMP), have seen increased adoption in POC settings [9]. Unlike conventional PCR tests, RT-LAMP doesn't require a thermocycler. RT-LAMP maintains a comparable level of specificity and sensitivity to PCR tests [86], but provides a faster time to result and better tolerance to impurities [12]. These attributes contribute to making RT-LAMP quicker, easier to use, and more cost-effective than RT-PCR assays [13], solidifying its suitability for POC diagnostics [87]. RT-LAMP has demonstrated resilience to inhibitors in complex samples such as blood, a distinct advantage over PCR [14]. There's a growing focus on developing Nucleic Acid Testing (NAT) devices employing isothermal amplification. This innovation eliminates the need for thermal cycling and costly apparatus, marking substantial progress in the field [17], [44], [88]–[94]. Nevertheless, despite advances in developing these devices, significant limitations persist. At present, there exists no POC device capable of facilitating HIV viral load self-testing due to the following challenges: the inability to process whole blood samples [22], the absence of quantitative

or semiquantitative capabilities within a single run [17]–[21], and the requirement for reagents to be stored at room temperature for extended periods. These pressing issues highlight the critical need for the development of an advanced HIV viral load monitoring device, one that operates from sample to answer and is suited for point-of-need usage.

In this study, we demonstrated an ultra-compact POC device with lyophilized reagents for semiquantitative self-testing of HIV viral load. Starting from 100 µL of whole blood, the device streamlines plasma separation, viral RNA extraction, and real-time RT-LAMP with built-in internal references for semi-quantification tests. We developed an efficient membrane absorption-based plasma separation technique to overcome the challenges of the limited volume of plasma under test. We achieved 80 ± 2.3% (Hematocrit is 40%) plasma separation efficiency using this approach. We also developed a facile instrument-free syringe-based viral RNA extraction method and achieved 86 ± 1.7% (VL = 25 copies/µL) viral recovery. To facilitate the user experience, we developed a smartphone-based interface for real-time viral load monitoring. Furthermore, we also developed the lyophilized reagents in-house and demonstrated their stability at room temperature for at least 16 weeks. We assessed the performance of our device using contrived whole blood samples in conjunction with clinically obtained plasma samples. The results demonstrated an accuracy of 95% and displayed a 99% agreement with the standard benchtop RT-PCR method. These results suggested the developed device would be ideal for frequent HIV viral load self-testing at home, enhancing the monitoring of the ART treatment. We envision this device could serve as a starting point for providing rapid and easy-to-use HIV viral load self-testing solutions for the betterment of patient care.

3.2. Methods

3.2.1. Materials and chemicals.

Components for this study were sourced from various suppliers. Vivid™ Plasma Separation GR was from Pall Corp. RNA extraction materials came from McMaster (**Table 3-1**), while most electronic and optical parts for the HIV analyzer were from DigiKey (**Table 3-2**). RT-LAMP and RT-PCR primers were by IDT. Essential mixes and chemicals were from Meridian Life Science, Sigma-Aldrich, and ThermoFisher. The Bio-Rad CFX96 was used for assay validation. HIV-1 RNAs were from SeraCare, while blood samples were from Innovative Research. Clinical HIV samples were sourced from Penn State Hershey Medical Center. All materials were used as received and stored following manufacturer guidelines.

Table 3-1. Bill of materials of the analyzer

System	Description	Part#	Function	Unit Cost ($)	Unit Qty.	Ext. Cost ($)
Electronics	Arduino Nano	7630049200173	Microcontroller	6.00	1	6.00
Electronics	Adafruit Bluefruit LE SPI	2633	Bluetooth Low Energy	14.00	1	14.00
Electronics	Capacitor 10uF	P10425CT	Power stabilizing	0.147	1	0.15
Electronics	DC Barrel Power Jack/Connector	PRT-00119	Power Connector	1.25	1	1.25
Electronics	36-pin stripe male header	392	Headpins	4.95	0.1	0.50
Thermal	Aluminum CNC block	CP-0.91-0.91	Heating Stage	5.75	0.25	1.44
Thermal	2Ω Power Resistor	MP725-2.00-FCT	Heater	7.01	1	7.01
Thermal	SMD Resistor, 1kΩ	311-1.00KHRCT	Temperature/EM control	0.0072	1	0.01
Thermal	Thermistor	235-1057	Temperature sensing	3.5	1	3.50
Thermal	SMD Resistor, 10kΩ	RNCP0603FTD10K0CT	Temperature control	0.1	1	0.10
Thermal	N Channel Power MOSFET	DMN1019USN-7DICT	Switch for heater	0.354	1	0.35
Optics	Res Cermet Trimmer 500K ohm	3296W-1-501RLF	Adjust LED intensity	0.6	3	1.80
Optics	SMD Resistor, 1kΩ	RNCP0805FTD1K0CT	Optical module	0.0277	3	0.08
Optics	SMD Resistor, 10kΩ	RNCP0805FTD10K0CT	Optical module	0.0277	8	0.22
Optics	IC Color Sensor	AS7341	Optical detection	3.00	3	9.00

Optics	SMD LED, Blue	1497-1138-1	Fluorescence excitation	0.528	3	1.58
Optics	Capacitor 10uF	P10425CT	Power stabilizing	0.147	3	0.44
Optics	Capacitor 0.1uF	P01425CT	Power stabilizing	0.147	1	0.15
Optics	Voltage Regulator	AP7312-3.3/1.8	Power supplier	0.8	1	0.80
Optics	I2C Multiplexer	TCA9548A	I2C expender for sensor	1.10	1	1.10
Enclosure	ABS Filament (Black)	-	3D platform material	69.00	0.05	3.45
Enclosure	Screws (M2 cap screw)	91290A015	Assembly	0.14	10	1.40
			Total Cost			**$54.33**

Table 3-2. Cost per test

Reagents	**Vendor**	**Function**	**Stock Vol (mL)**	**Unit Cost ($)**	**Volume (μL)/rxn**	**Ext Cost/rxn**
RT-LAMP Mixes	Meridian Life Science	LAMP master mix	5	198	6.25	0.2475
F3	IDT	LAMP master mix	4.8	9.4	0.15	0.0003
B3	IDT	LAMP master mix	4.3	8.46	0.15	0.0003
FIP	IDT	LAMP master mix	0.9	62.68	1.2	0.0836
BIP	IDT	LAMP master mix	0.9	64.56	1.2	0.0861
LF	IDT	LAMP master mix	4.6	9.4	0.6	0.0012
LB	IDT	LAMP master mix	4.3	75.34	0.6	0.0105
Calcein	Sigma-Aldrich	LAMP master mix	1.5	24.25	2.4	0.0388
MnCl2	Sigma-Aldrich	LAMP master mix	3.2	107	2.1	0.0702
MgSO4	NEB	LAMP master mix	6	20	1.2	0.004
Lysis Buffer	Invitrogen	Sample Prep.	25	6	200	0.02
Wash Buffer	Invitrogen	Sample Prep.	37.5	54	500	0.12
Elution Buffer	Invitrogen	Sample Prep.	11	35	30	0.1
Ethanol	Sigma-Aldrich	Sample Prep.	100	10	200	0.02
Material	**Vendor**	**Function**	**Stock Vol (sq. m.)**	**Unit Cost ($)**	**Volume (sq. mm)/rxn**	**Ext Cost/rxn**
1/32" Acrylic Sheet	ePlastics	PSM card	0.5	16.13	20	0.65
Vivid PSM-GR	Pall Corporation	PSM card	0.06	30.00	200	0.30
Tygon PVC Tubing	McMaster	RNA extraction	25 ft	11.50	1 ft	0.46
Quick-Turn Coupling	McMaster	RNA extraction		0.50	3	1.50
Silica column	Qiagen	RNA extraction		2.00	1	2.00
Syringe	VWR	RNA extraction		0.30	2	0.60
PCR tube		Fisher scientific		0.01	1	0.01

Total **$6.32**

3.2.2. HIV-1 lyophilized RT-LAMP assay reaction

The RT-LAMP assay reaction, optimized for the detection of HIV-1, is detailed in **Table 3-3**. This assay involves a reaction mix with a total volume of 25 µL, composed of several critical components. This mix contains an isothermal buffer, which includes Tris-HCl, $(NH_4)_2SO_4$, KCl, $MgSO_4$, Tween 20, and dNTPs, along with Bst, PCR grade H_2O and $MgSO_4$ (7 mM) were also included in the reaction mixture. Additionally, the RNA template was integrated in conjunction with a specifically designated collection of primers, consisting of 0.2 µM of F3 and B3, 1.6 µM of FIP and BIP, as well as 0.8 µM of LPF and LPB. The reaction was performed at a controlled temperature of 60 ℃ for a duration of 45 minutes. In this assay, we utilized our pre-validated primers, listed in **Table 3-4**. These primers were added to the commercial master mix. The resulting samples were then frozen at -80 ℃ for 12 hours to stabilize them. After this freezing step, the samples underwent lyophilization at -50 ℃ and 0.02 mbar using a freeze-dryer from LabCon Co. This process rendered the samples stable and ready for subsequent analyses.

Table 3-3. RT-LAMP reaction setup

Component	Volume (µl)/test	Final Concentration
Lyo-Ready RT-LAMP master mix	6.25	4 X
F3	0.05	0.2 µM
B3	0.05	0.2 µM
FIP	0.4	1.6 µM
BIP	0.4	1.6 µM
LF	0.2	0.8 µM
LB	10.2	0.8 µM
$MgSO_4$	1	4 mM

Calcein	0.63	25 µM
$MnCl_2$	1.88	75 µM
RNA sample	1	1 ul/rxn
PCR Grade Water	12.95	-

Table 3-4. RT-LAMP primer set targeting HIV-1

Primer	Sequence (5' → 3')
F3	AGTTCCCTTAGATAAAGACTT
B3	CCTACATACAAATCATCCATGT
FIP	GTGGAAGCACATTGTACTGATATCTTTTTGGAAGTATACTGCATTTACCAT
BIP	GGAAAGGATCACCAGCAATATTCCTCTGGATTTTGTTTTCTAAAAGGC
Loop F	GGTGTCTCATTGTTTATACTA
Loop B	GCATGACAAAAATCTTAGA

3.2.3. HIV-1 RT-PCR reaction

In the study, a two-enzyme, single-step RT-PCR technique was implemented for conducting HIV-1 examinations. The procedure involved a total reaction volume of 20 µL, comprising 5 µL of TaqMan Fast Virus 1-Step Master Mix, along with forward and reverse primers (each at 0.6 µM concentration), a probe (0.25 µM), 1 µL of RNA templates, and 11 µL of water that meets PCR-grade standards. A previously authenticated set of HIV-1 RT-PCR primers was utilized in this investigation [95]. The RT-PCR process was carried out with specific thermal cycling patterns, initiating at 50 ℃ for an initial five-minute duration for the singular non-repeating reverse transcription phase, converting HIV-1 RNA into complementary DNA (cDNA). This was succeeded by a 95 ℃ phase for 20 seconds without repetition to commence the amplification process, followed by a series of 40 amplification cycles. Each cycle involved a three-second heating at 95 ℃ and a thirty-second thermal cycling at 60 ℃. The primers used in the investigation were Forward (5'-CATGTTTTCAGCATTATCAGAAGGA-3') and Reverse (5'-TGCTTGATGTCCCCCCACT-3') at 600 nM, along with a Probe (5'FAM-

CCACCCCACAAGATTTAAACACCATGCTAA-Q 3') at 250 nM. In this context, FAM refers to the reporter 6-carboxyfluorescein group, while Q symbolizes the 6-carboxytetramethylrhodamine group that functions as a quencher and is conjugated through a linker arm nucleotide.

3.2.4. Whole blood HIV sample

We created a whole-blood HIV sample by integrating a known concentration of HIV-1 clinical plasma sample with healthy whole blood. The process involved several stages. Initially, we centrifuged clinical whole blood samples at 1000 rpm for 10 minutes, separating plasma and red blood cells and storing them separately. We then combined 6 ml of clinical plasma with 4 ml of red blood cells, mixing and vertexing to obtain a 10 ml blood sample with an estimated hematocrit ratio of 40%. An EKF Diagnostics Hemo Control analyzer was used to confirm this ratio. Notably, our method omitted the use of Proteinase K to deactivate RNases in the whole blood, streamlining sample preparation. Unless specified otherwise, the volume of whole blood sample used in our study was 100 µL.

3.2.5. Disposable plasma separation card

The design of this disposable plasma separation card was executed using AutoCAD software. Each layer of the card was meticulously patterned using a CO_2 laser cutting machine (Universal Laser Systems). Following this, all the patterned layers were aligned with exceptional precision and laminated with double-sided adhesive tape. This procedure ensured a consistent and robust assembly of the plasma separation card apparatus. By combining innovative design with precise

construction techniques, we were able to manufacture an effective and reliable module, paving the way for convenient, one-time-use plasma separation.

3.2.6. Syringe-based RNA extraction module

The design of a syringe-based RNA extraction module can be separated into three parts. Firstly, a silica membrane filter was designed to bind to RNA effectively at a high salt concentration. The QIAamp Viral RNA Kits Total RNA (52904) were modified by cutting and retrofitting the silica column. Quick-Turn Tube Couplings were connected to the modified column, and a sealing adhesive was used to secure and seal the connections, effectively transforming it into a silica membrane filter. Secondly, flexible Tygon PVC tubes (procured from McMaster) were employed to store the washing and elution buffers. Each segment of the reagent was separated by a custom-made manual valve. Each tube was equipped with a lure lock at its end to facilitate a quick and secure connection to a syringe. This feature accelerated the overall extraction process and minimized the risk of leaks or contamination. Finally, two syringes were used to generate a negative pressure, enabling the reagent in the flexible tubes to pass through the silica membrane filter. One syringe was dedicated to collecting the washing buffer, while the other was assigned to collect the eluted RNA. These syringes were procured from VWR.

3.2.7. Analyzer design and fabrication

The entire architecture of the analyzer was conceived and developed using PTC Creo software, while the containment unit for the device underwent fabrication via three-dimensional printing, utilizing METHOD X on a MakerBot system. The Printed Circuit Board (PCB) was intricately designed with Autodesk Eagle software, with manufacturing carried out by OSH Park. Laboratory

personnel manually soldered the electronic constituents and Microcontroller Unit (MCU) onto the PCB. For heating regulation, a resistive-heating element (PWR263S-20-2R00J, Digi-Key) was adjoined to the reverse side of a specially tailored aluminum heating block through the application of thermal compound (AATA-5G, Artic Alumina). In the core of the heating plate, a thermistor (95C0606, Digi-Key) was carefully positioned for the continuous surveillance of temperature. To sustain the requisite temperature during Nucleic Acid Testing (NAT), negative thermal feedback control was executed by deploying an N-channel power Metal-Oxide-Semiconductor Field-Effect Transistor (MOSFET) (63J7707, Digi-Key). Our optical components comprised an adjustable Res Cermet Trimmer (3296W, Digi-Key) for LED intensity control, an IC Color Sensor (AS7341, Digi-Key) for optical detection, and a blue SMD LED (1497-1138-1, Digi-Key) for fluorescence excitation. Power stabilization for the optical components was provided by the capacitors, and a voltage regulator supplied the necessary power. An I_2C Multiplexer was used as the I_2C expander for the sensor. The control graphical user interface (GUI) software was developed using the MIT App Inventor. This GUI facilitates easy control and communication with the device via Bluetooth, offering a user-friendly control interface for the instrument.

3.2.8. Statistical analysis.

All statistical analysis and regression modeling were performed using MATLAB R2020 (Natick, MA). All plots displaying data represent the mean and 3 standard deviations from triplicate testing unless stated otherwise. MATLAB was used for all data processing. All figures and plots were generated using MATLAB and PowerPoint.

3.3. Results and discussion

3.3.1. Overall workflow

Figure 3-1a shows all the required materials for the whole workflow. **Figure 3-1b** shows the comprehensive workflow of the HIV viral load self-testing device. The workflow includes these steps: Step 1 - The user activates the app on their Android phone, which provides instructions for all subsequent steps. Step 2 - The user independently collects approximately 100 μL of blood through a finger prick, employing a disposable pipette. This blood sample is then introduced into a plasma separation card. The plasma separates from the blood cells as the blood sample passes through the card's membrane and is collected onto an absorbent paper. According to the datasheet of Vivid™ Plasma Separation GR, it is recommended to wait for 1 minute to ensure complete filtration. The now isolated plasma is readily collected for downstream analysis, serving potential applications in diagnostics, medical research, and transfusion medicine. Step 3 - The user employs disposable tweezers to detach the absorbent paper from the plasma separation card along the predefined perforated line. The absorbent paper is transferred into a collection tube preloaded with 800 μL of lysis buffer. After the transfer, the user agitates the tube to facilitate lysing and mixing. Step 4 - Concurrently, the user assembles the RNA extraction silica column onto a 10 mL syringe within the RNA extraction module using a connector and removes the tube's transportation valve. Following a one-minute lysis period, the user utilizes a disposable pipette to transfer the solution from the lysis tube to the RNA extraction silica column. The syringe is drawn so that all the lysate within the RNA extraction silica column travels through the silica membrane and enters the syringe. The user then disconnects the lysis tube and connects tube one (packaged with two wash buffers and deionized water), drawing the syringe to allow the first two blocks to flow through the silica membrane. After completing these steps, the user switches the 10 mL syringe to a 1 mL one, draws the syringe to finalize the elution step, and stores the eluted RNA in the syringe. The connector of the syringe containing the eluted RNA is then removed, and the RNA is injected into the PCR

reaction tube. Step 5 - The user inserts the test tube into the analyzer, initiating the test. Step 6 - Following 40 minutes, the APP generates and reports the final result. **Supplementary Video S3-1** shows the overall workflow of the test. The entire process can be completed independently by the user at home without the need for professional personnel or laboratory equipment, enabling self-testing for HIV viral load.

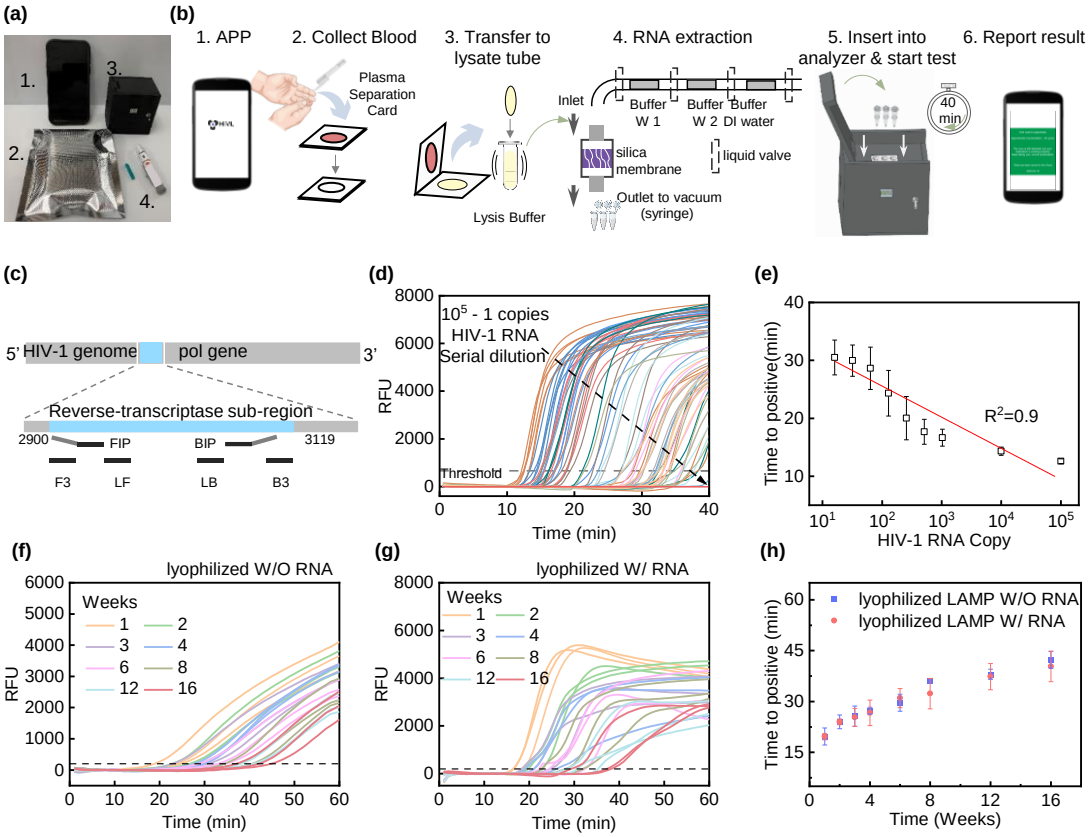

Figure 3-1. Overall Device Workflow and Assay Design. **(a)** An image showing the components of the device, including 1. an Android phone, 2. a syringe-based RNA extraction module, 3. an analyzer, and 4. a lancet. **(b)** The procedure, as comprehensively delineated in the mobile application, involves a user initiating the app, self-collecting a blood sample using a disposable pipette and plasma separation card, transferring the absorbent paper into a pre-filled lysis buffer collection tube, conducting RNA extraction, introducing the eluted RNA and water into the testing tube, and finally, after 40 minutes, receiving the test results via the APP. **(c)** The design of primers. This includes a set of 6 RT-LAMP primers that target the medium region of the pol gene. **(d)** Real-time HIV-1 lyophilized RT-LAMP amplification data preserved when reconstituted from powder with

serially diluted HIV RNA standards (six repeats per concentration). **(e)** Duration to positive value at various HIV-1 RNA concentrations; defined as the time for the RFU to hit a 1000 threshold (dashed line in d). **(f)** Results of HIV-1 lyophilized RT-LAMP real-time amplification over 16 weeks, replicated three times weekly using PCR-grade water and lyophilized RT-LAMP powder, plus 1000 HIV-1 RNA copies. **(g)** Data showing HIV-1 lyophilized RT-LAMP real-time amplification performance within a 16-week period. Each reaction was replicated three times per testing week using only PCR-grade water and lyophilized RT-LAMP powder (containing 1000 copies of HIV-1 RNA) mixed together. **(h)** The results of a test evaluating the shelf-life of lyophilized HIV-1 RT-LAMP.

3.3.2. Development of the lyophilized RT-LAMP assay

In the context of HIV viral load self-testing, it is imperative for the reagents to possess an excellent limit of detection (LOD), high accuracy, specificity, as well as quantitative or semiquantitative detection capacity. Furthermore, these reagents should have the capacity to be stored at room temperature for extended periods, enabling efficient transport and storage. To facilitate the development of the HIV viral load testing assay, we utilized RT-LAMP to amplify the POL (polyprotein) genes of the HIV-1 subtype B (**Figure 3-1c**). We validated the HIV-1 RT-LAMP primer set against the highly conserved region of the integrase gene within subtype B [96], in conjunction with a modified fluorescent reporter of Calcein [17], [87]. For long-term reagent storage, we employed lyophilized reagents [97]. The pre-validated primers were added to the commercial master mix (Lyo-Ready™) to produce lyophilized RT-LAMP (**Table 3-3&4** provides a summary of the HIV-1 lyophilized RT-LAMP primers, the reaction setup).

To test the performance of lyophilized RT-LAMP, especially its quantitative detection capability and limit of detection, we first assessed the intrinsic copy number sensitivity of the HIV-1 lyophilized RT-LAMP assay by conducting the RT-LAMP reaction against a quantitative panel of HIV-1 RNA, at concentrations ranging from 10^5 down to 1 copy/µL. As shown in **Figure 3-1d-e**, the copy number sensitivity of the lyophilized HIV-1 RT-LAMP was determined to be 16 copies

(**Table 3-5**). Moreover, the linear fit produced an R^2 of 0.9, as fresh as when reconstituted from powder, thereby demonstrating the semiquantitative detection capacity of the HIV viral load test.

Table 3-5. Summary of the hit rate

HIV-1 RNA (copy)	**1**	**2**	**4**	**8**	**16**	**32**	**64**	**128**	**256**	**512**	**1024**	**10^4**	**10^5**
No. positive/ no. of replicates	0/6	1/6	3/6	4/6	6/6	6/6	6/6	6/6	6/6	6/6	6/6	6/6	6/6
Hit rate (%)	0	16.7	50	66.7	100	100	100	100	100	100	100	100	100

All six reactions with four or more copies of RNAs can be amplified successfully. The copy number sensitivity of the HIV-1 lyophilized RT-LAMP was determined to be 16 copies.

Having confirmed the functionality of our lyophilized RT-LAMP, we proceeded to examine its long-term storage performance. Two experimental configurations were prepared: one consisting of lyophilized RT-LAMP without RNA (W/O RNA), and the other including lyophilized RT-LAMP with RNA (W/ RNA, 1000 copies/rnx). The latter served as positive controls and internal references for HIV VL examination. All HIV-1 lyophilized RT-LAMP shelf-life trials were conducted at ambient temperature (23 ℃), with specimens securely stored in isolated zipper bags.

During the 16-week evaluation period, the lyophilized RT-LAMP W/O RNA consistently displayed an amplification curve after introducing fresh HIV-1 RNA (1000 copies/rnx), corroborating the effectiveness of the lyophilization process (**Figure 3-1f**). Furthermore, the positive control, equipped with internal RNA lyophilization, also demonstrated functionality (**Figure 3-1g**). Both variations of the samples consistently manifested stable “time to positive” outcomes (**Figure 3-1h**). This consistency indicates the test's accuracy could be maintained for up to 16 weeks of storage, even with the shifts in enzymatic activities.

3.3.3. Plasma separation

Plasma is considered the gold standard for HIV viral load testing. Many endeavors have focused on developing plasma separation technologies from undiluted whole blood for POC applications, particularly those leveraging membrane-based plasma separation [98]–[107]. However, many of these technologies are complex, with low plasma separation efficiency, and challenging to operate by those without expertise or a lab environment. We have developed a straightforward, power-free plasma separation technology that employs a Vivid plasma separation membrane and an absorbent material. For materials and production processes regarding plasma separation card, please refer to the **Methods - Disposable plasma separation card**. **Figure 3-2a** illustrates the plasma separation apparatus we devised, which primarily consists of two sections: the absorber, incorporating the absorbent membrane, and the filter, containing the Vivid plasma separation membrane. These two sections are affixed to the top and bottom covers using double-sided adhesive and are stacked together. In operation, one would drop 100 μL of blood samples, collected from the fingertip, onto the top layer of the separation card. The plasma would then flow through the filter layer and be collected in the storage layer, while red blood cells would be retained within the filter layer. After two minutes, the top surface of the plasma separation membrane appears dry, with the absorbent material transitioning to an orange/pink hue due to plasma absorption, contrasting with its initial white color. The absorbent material can subsequently be extracted and transferred into a test tube containing lysis solution for further processing, using disposable tweezers.

First, we tested the quality of the plasma separated using our plasma separation card and compared it with the traditional laboratory protocol (We used the protocol provided by the manufacturer for QIAamp Viral RNA Kits for Total RNA). One important indicator for measuring the quality of the separated plasma is to measure the hemoglobin content in the plasma. The lower the hemoglobin content in the plasma, the higher the quality of the separation [108]. The testing blood sample

volume was 100 μL, with a hematocrit of 45%. The plasma separation card utilized a separation membrane (PMS) with a diameter of 16mm. Each experimental group was repeated three times. **Figure 3-2b** displays the hemoglobin content measurements, which indicate that the hemoglobin content in plasma separated by our module is significantly lower than in whole blood, mirroring the efficiency of traditional centrifugal separation methods. Concurrently, microscopic imaging validates that the separated plasma is nearly devoid of red blood cells and other residues.

After confirming that the plasma separation card ensures the quality of plasma extraction, we tested the effect of the size of the plasma filtration membrane on the plasma extraction efficiency. We identified the optimal size of the plasma filtration membrane to optimize extraction efficiency. The plasma extraction efficiency of our plasma separation card relies mainly on the size of the plasma filtration membrane [102]. A small membrane may become rapidly clogged by the red blood cells in whole blood, thereby halting filtration. Conversely, an overly large membrane may retain a non-permeable “dead volume” of remaining plasma that the absorbent material cannot capture. In the context of HIV viral load self-testing, we sought to extract 100 μL of whole blood from fingertip samples, utilizing five different diameters of plasma filtration membranes, ranging from 12 to 20 mm. By measuring the plasma paper weight change before and after the absorbing process, we estimated the plasma extraction efficiency. We maintained the diameter of the absorbent material at 16 mm as the initial filtered blood volume was established at 100 μL, and a 16 mm diameter absorbent material can sufficiently absorb 100 μL of plasma. Notably, in a given 100 μL sample of whole blood, the plasma volume commonly represents a maximum proportion of roughly 60 μL. As depicted in **Figure 3-2c**, the 16 mm diameter filter membrane yields an efficiency of about 80%. Importantly, this extraction is less affected by varying hematocrit levels when using the 16 mm diameter filter membrane. Our developed plasma separation card achieves an extraction efficiency

of 80% while ensuring the quality of the extracted plasma. It is user-friendly, cost-effective, and suitable for self-testing applications for HIV viral load tests.

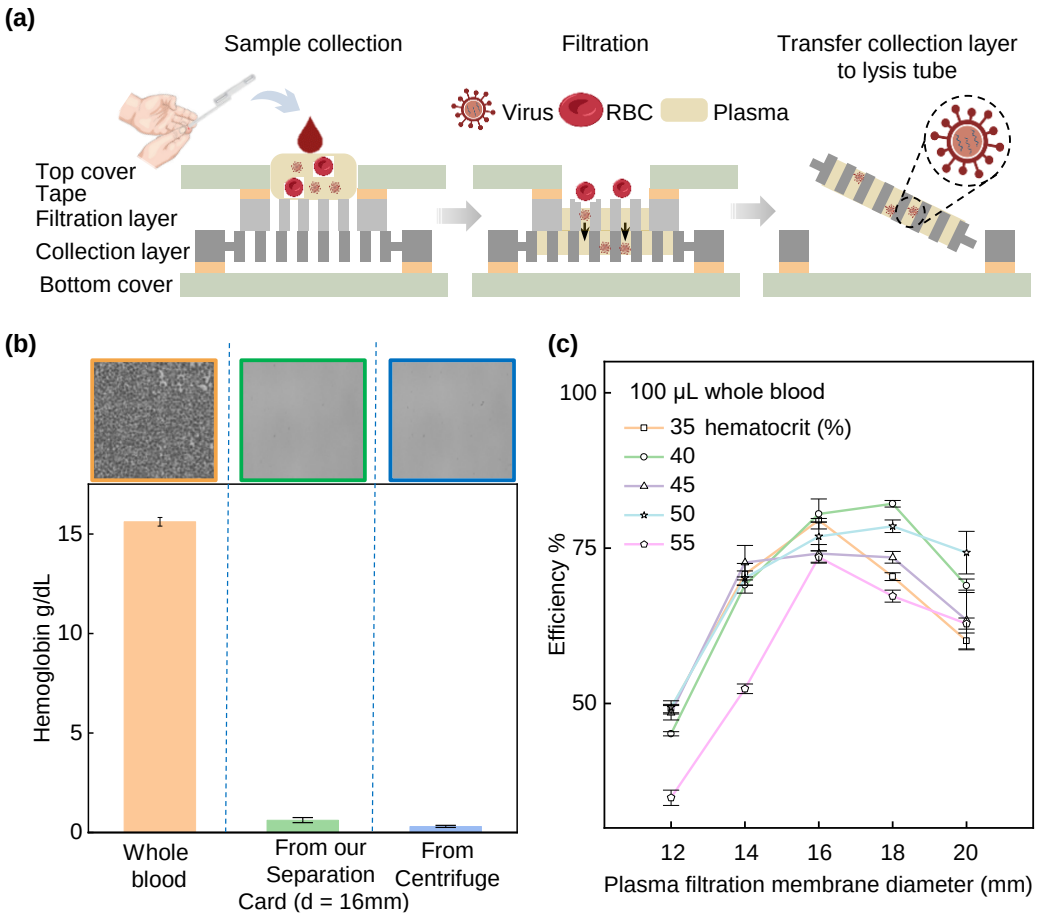

Figure 3-2. Schematic diagram showing its working principle and characterization of the plasma separation card **(a)** Schematic diagram showing its working principle of the plasma separation module. The plasma separation card is divided into six layers. When in use, drop 100 µL of blood samples collected by fingertips into the upper layer of the separation card. The plasma will flow through the filter layer and be stored in the collection layer, while the red blood cells will be trapped in the filter layer. **(b)** The quality (hemoglobin content) difference between plasma separated by a plasma separation card and plasma separated by the laboratory conventional method (centrifugation) was compared. The blood sample volume for testing was 100 µL, with a hematocrit of 45%. The separation membrane (PMS) diameter in the plasma separation card used was 16mm. Each experimental group was repeated three times. **(c)** The variation in the separation efficiency of the plasma separation card, as a function of hematocrit and the diameter of the separation membrane (PMS) in the plasma separation card. The volume of the tested blood sample was 100 µL, and each

experimental group was repeated three times.

3.3.4. Syringe-based RNA extraction module

One of the essential steps in HIV viral load testing is the extraction of RNA from the sample (plasma). The method of solid-phase extraction, employing a silica membrane to engage with RNA alongside chaotropic salts, offers a streamlined alternative for RNA's swift isolation. This approach is facilitated within a singular tube and stands as a comparatively uncomplicated process, applicable for self-testing of HIV viral load [109], [110]. A variety of commercial kits, produced and distributed by several enterprises, are accessible for this purpose. The underlying mechanism involves RNA affixed to silica membranes through chaotropic salts, forming salt bridges. Following multiple wash phases, the RNA is eluted by adjusting the saline concentration [111]. Though this process is both uncomplicated and practical, every stage necessitates centrifugation, an element that may not be practical for in-field applications, particularly within environments constrained by resources [112]. In response to these challenges, our work has paved the path of a centrifugation-independent, syringe-structured viral RNA extraction module for HIV viral load self-testing, thereby enhancing user accessibility.

Figure 3-3a depicts the conceptual design of a syringe-driven RNA extraction module, consisting of three essential elements and its underlying operating mechanism: (i) a silica membrane filter specifically engineered to adhere to RNA molecules under conditions of elevated salt concentration; (ii) flexible tubing employed to contain the wash and elution buffers, delineated by a custom-crafted manual valve that isolates each successive portion of the reagent. (iii) Two syringes are used to create negative pressure, allowing the reagent in the soft tubes to flow through the silica membrane filter. For materials and production processes regarding Syringe-based RNA extraction module, please refer to the **Methods - Syringe-based RNA extraction module**. One

syringe is used to collect the washing buffer, while the other is used to collect the eluted RNA. The absorbent part of the plasma separation card is placed into a lysis tube for sample lysis, releasing RNA into the lysis solution. The lysis tube is connected to the silica membrane and a syringe. By drawing and pushing the syringe, all the solutions flow through the silica membrane, allowing the RNA to bind to the membrane. The valve on the storage buffer reagent tube is released and connected to the silica membrane, replacing the lysis tube. By pulling the syringe, the first two segments of the solution from the storage buffer reagent tube pass through the silica membrane, completing the washing procedure. The syringe is then replaced with a 1-milliliter syringe, and by pulling the syringe again, the last segment of the solution (DI water) from the storage buffer reagent tube flows through the silica membrane and is drawn into the syringe, completing the elution procedure.

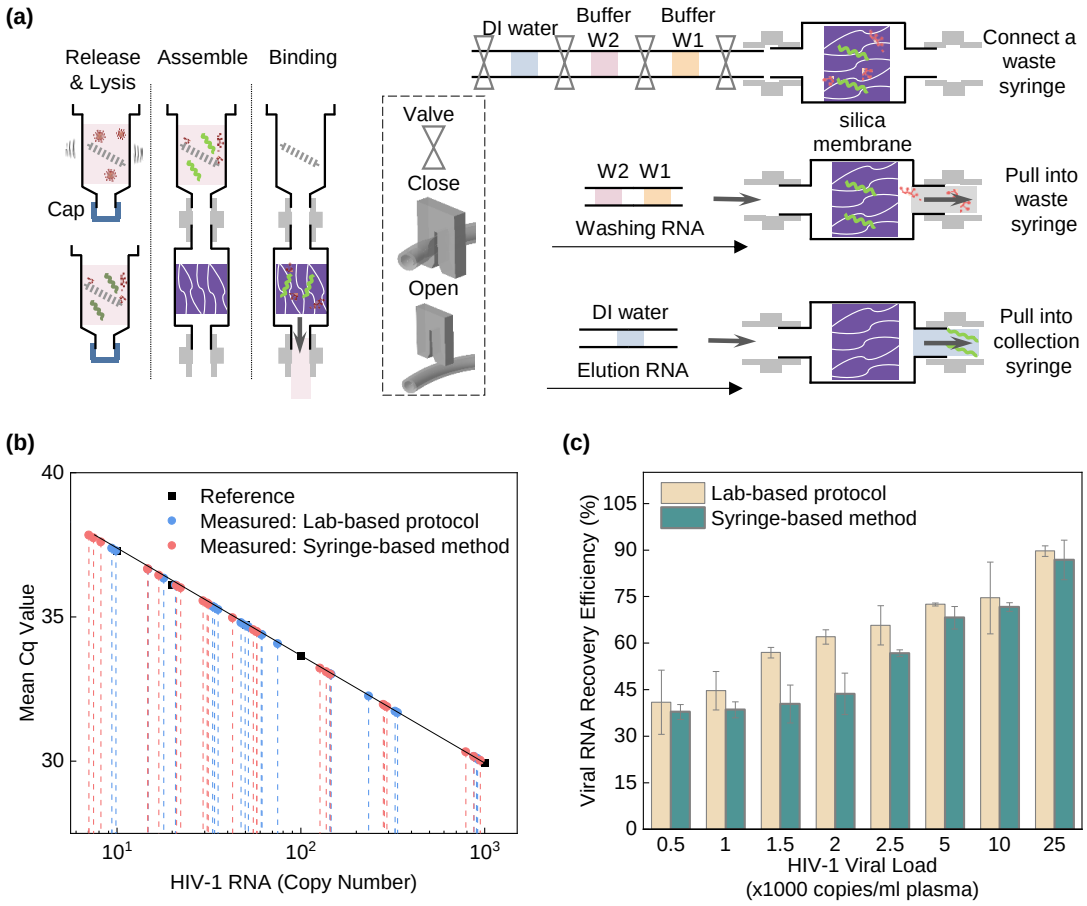

Figure 3-3. Schematic diagram illustrating the working principle and characterization of the syringe-based RNA extraction module. **(a)** Schematic diagram illustrating the working principle of the syringe-based RNA extraction module. The absorbent part is placed in a lysis tube for sample lysis, releasing RNA into the solution. The lysis tube is connected to the silica membrane filter using an injector. Solutions flow through the membrane, binding RNA to it. The storage buffer reagent tube replaces the lysis tube, and the first two segments of its solution flow through the membrane for washing. The last segment (DI water) is flowed through the membrane and drawn into the injector for elution. **(b)** RT-PCR fitted reference line was generated to quantify the copy numbers of extracted RNA. The black squares indicate the reference reaction with known copy numbers. The blue dots represent RNA extracted using the lab-based protocol, while the red dots represent RNA extracted using the syringe-based method. These values are calculated averages obtained from three repeated experiments. **(c)** Comparison of RNA extraction efficiency for plasma samples with varying viral loads between our extraction module and the lab-based protocol. Each group experiment was repeated three times.

In order to test the RNA recovery rate of the Syringe-based RNA extraction module, we prepared mock plasma samples of varying concentrations by mixing different amounts of virus particles into commercial plasma. Each mock plasma sample had a volume of 40 μL, simulating the approximate volume extractable from 100 μL of whole blood using the plasma separation card. The sample concentrations ranged from 500 to 25,000 copies/ml of plasma, covering the typical range of viral loads found in HIV patients. We extracted RNA from the mock plasma samples using our syringe-based RNA extraction module and performed quantitative analysis using RT-qPCR. The real-time HIV-1 RT-qPCR amplification curve can be found in (**Figure 3-4a&b**). We establish a reference line using PCR reactions with known copy numbers. Given the excellent quantification capabilities of PCR (with a linear fit R^2 of 0.99), we can calculate the quantity of RNA in unknown samples by comparing their measured Cq values to the reference line. **Figure 3-3b** shows RT-PCR fitted reference lines were generated to quantify the copy numbers of extracted RNA. The black squares indicate the reference reaction with known copy numbers. The blue dots represent RNA extracted using the lab-based protocol, while the red dots represent RNA extracted using the syringe-based method. These values are calculated averages obtained from three repeated experiments. By using the known viral load and solvent of the mock plasma samples, along with the RNA copy number extracted through PCR Cq values and the reference line, we can calculate the RNA extraction efficiency of the syringe-based RNA extraction module (**Figure 3-4c&d**).

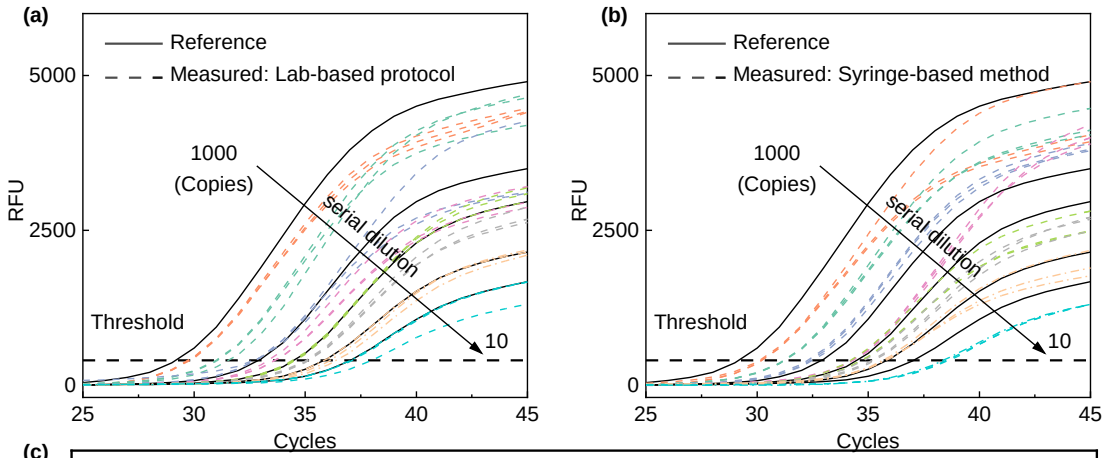

(c)

Recovered RNA Cq value										
RNA (Copies)	Lab-based protocol					Syringe-based method				
	Run 1	Run 2	Run 3	Avg.	Std.	Run 1	Run 2	Run 3	Avg.	Std.
20	38.29	37.38	37.30	37.66	0.45	37.84	37.75	37.60	37.73	0.10
40	36.35	36.66	36.11	36.37	0.22	36.67	36.45	36.66	36.59	0.10
60	35.26	35.37	35.34	35.32	0.05	36.01	36.09	35.56	35.89	0.23
80	34.72	34.66	34.81	34.73	0.06	35.46	34.97	35.48	35.31	0.23
100	34.38	34.40	34.08	34.29	0.15	34.49	34.56	34.50	34.51	0.03
200	33.03	33.02	33.01	33.02	0.01	33.02	33.23	33.11	33.12	0.08
400	32.26	31.73	31.68	31.89	0.26	31.89	31.94	31.97	31.94	0.03
1000	30.09	30.11	30.16	30.12	0.03	30.32	30.04	30.16	30.17	0.12

(d)

Recovered RNA copy number (Copies)										
RNA (Copies)	Lab-based protocol					Syringe-based method				
	Run 1	Run 2	Run 3	Avg.	Std.	Run 1	Run 2	Run 3	Avg.	Std.
20	5.29	9.39	9.89	8.19	2.06	7.05	7.46	8.19	7.57	0.47
40	17.95	14.78	20.84	17.86	2.47	14.66	16.88	14.72	15.42	1.03
60	35.53	33.09	33.89	34.17	1.01	22.21	21.11	29.40	24.24	3.68
80	49.78	51.78	47.24	49.60	1.86	31.35	42.50	30.92	34.92	5.36
100	61.56	60.93	74.72	65.74	6.36	57.63	55.17	57.42	56.74	1.11
200	143.79	145.06	146.12	144.99	0.95	144.85	127.18	137.28	136.44	7.24
400	233.25	325.84	335.62	298.24	46.13	293.98	284.96	280.69	286.54	5.54
1000	914.84	901.52	873.66	896.67	17.16	788.07	944.60	871.73	868.13	63.95

Figure 3-4. Characterization of the syringe-based RNA extraction module. **(a)** Data from real-time HIV-1 RT-qPCR amplification is presented. The solid line represents the reference reaction with known copy numbers, while the dashed line signifies RNA extracted using the lab-based protocol. Each concentration was tested in triplicate. **(b)** Similarly, data from real-time HIV-1 RT-qPCR amplification is shown. The solid line depicts the reference reaction with known copy numbers, and the dashed line illustrates RNA extracted using the syringe-based method. Each concentration was also tested in triplicate. **(c)** The CT value corresponds to the extraction from plasma samples containing HIV-1 RNA with varying copy numbers using two distinct methods. Mean and variance values are also reported. **(d)** Recovered RNA copy numbers were determined from the extraction of plasma samples containing different copy numbers of HIV-1 RNA using two different methods. Mean and variance values are likewise provided.

Figure 3-3c shows RNA extraction efficiency for different concentrations by using our syringe-based RNA extraction module compared with the lab-based protocol (centrifugation). From the figure, we can see that although our syringe-based RNA extraction module efficiency is lower than the laboratory protocol, we can still recover the major RNA which lab-based protocol can recover. For high-concentration samples (VL ~ 25000 copies/ml), our extraction module can reach about 95% of the extraction efficiency. For low-concentration samples (VL ~ 1000 copies/ml), our extraction module can reach about 40% of the extraction efficiency. For the standard protocols of our extraction module and laboratory, the extraction efficiency decreases accordingly when the sample concentration is reduced. One probable reason is that the silicon filter has dead volume and part of the RNA is caught and cannot be extracted. Based on existing data, it can prove that our RNA extraction module can complete the RNA extraction without using power, which is suitable for field testing or self-testing.

3.3.5. First generation Analyzer development and analytical evaluation

Next, we developed a prototype portable analyzer capable of performing RT-LAMP assay amplification and quantifying the resultant fluorescent output. **Figure 3-7a** illustrates the disassembled and assembled views of the analyzer. This compact device features an internal Li-Ion battery and Bluetooth connectivity, integrating electronic, optical, and thermal subsystems into an ultra-portable form factor. Based on the NAT-On-USB device [17], we've updated our analyzer with an optical module featuring three distinct excitation and detection units for real-time fluorescence monitoring. For materials and production processes regarding analyzer, please refer to the **Methods - Analyzer design and fabrication**. We reduced excitation interference by arranging the units perpendicularly. The 555 nm channel was chosen for Calcein detection due to its low interference and optimal responsiveness, and normalization based on the 480 nm channel

minimized potential signal errors. The module displayed a strong linear correlation (R^2 = 0.94) between the relative fluorescence unit and Calcein concentration (**Figure 3-5**). Our thermal module, integrating a power resistor, a thermistor, and an insulated housing, achieves the required 60 ℃ within 3 minutes with a stable temperature of 0.074 ℃ RMS value, meeting the LAMP assay requirements. With the inclusion of thermal insulation made of 3D-printed ABS material and foam sealant, energy consumption during the heating and incubation stages is reduced by about 22%, and the power resistor's duty ratio is effectively decreased (**Figure 3-6**). Our analyzer employs custom circuit boards for temperature and fluorescence management powered by a replaceable lithium-ion battery. Test results are accessible via a Bluetooth-enabled mobile app with a custom GUI.

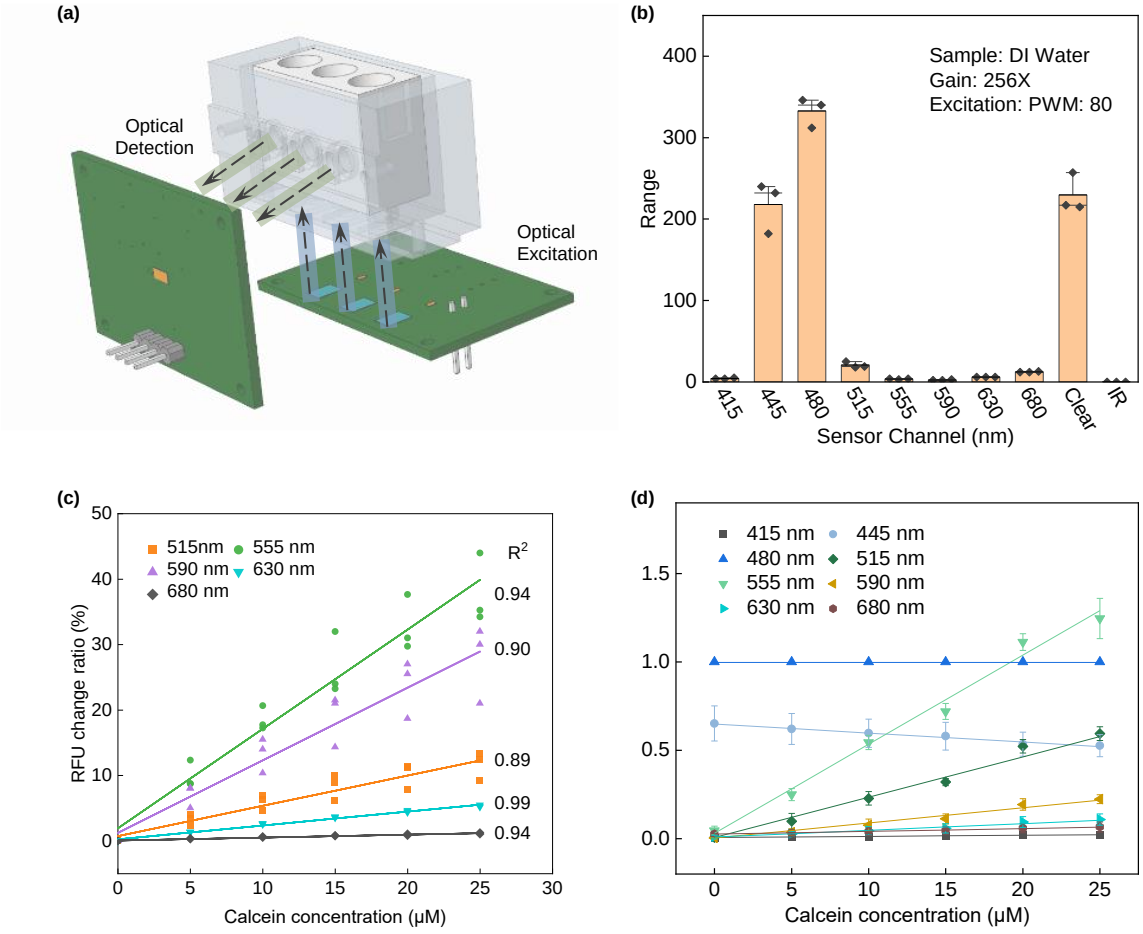

Figure 3-5. **(a)** Schematic of the Optical Module. On the excitation side, an LED light source (λ = 488 nm) illuminates the LAMP reaction chamber. On the detection side, light emitted from the LAMP reaction chamber to the optical senso. The excitation LED light is oriented perpendicularly to the optical sensor to minimize diffracted excitation light entry, thereby enhancing the signal-to-noise ratio. **(b)** Response of each channel in the optical module's sensor to water. The test was conducted at a gain of 256X, an integration time of 154 ms, and an 80% PWM of the excitation LED control. **(c)** Characterization of the optical sensor with Calcein. Each channel of the optical sensor exhibited a linear response to Calcein concentrations ranging from 0 to 25 µM. The test was carried out at a gain of 256X, an integration time of 154 ms, and an 80% PWM of the excitation LED control. **(d)** The optical module's profile when each channel's data from the color sensor is normalized with the channel (480nm) that corresponds to the LED light source (λ = 488 nm).

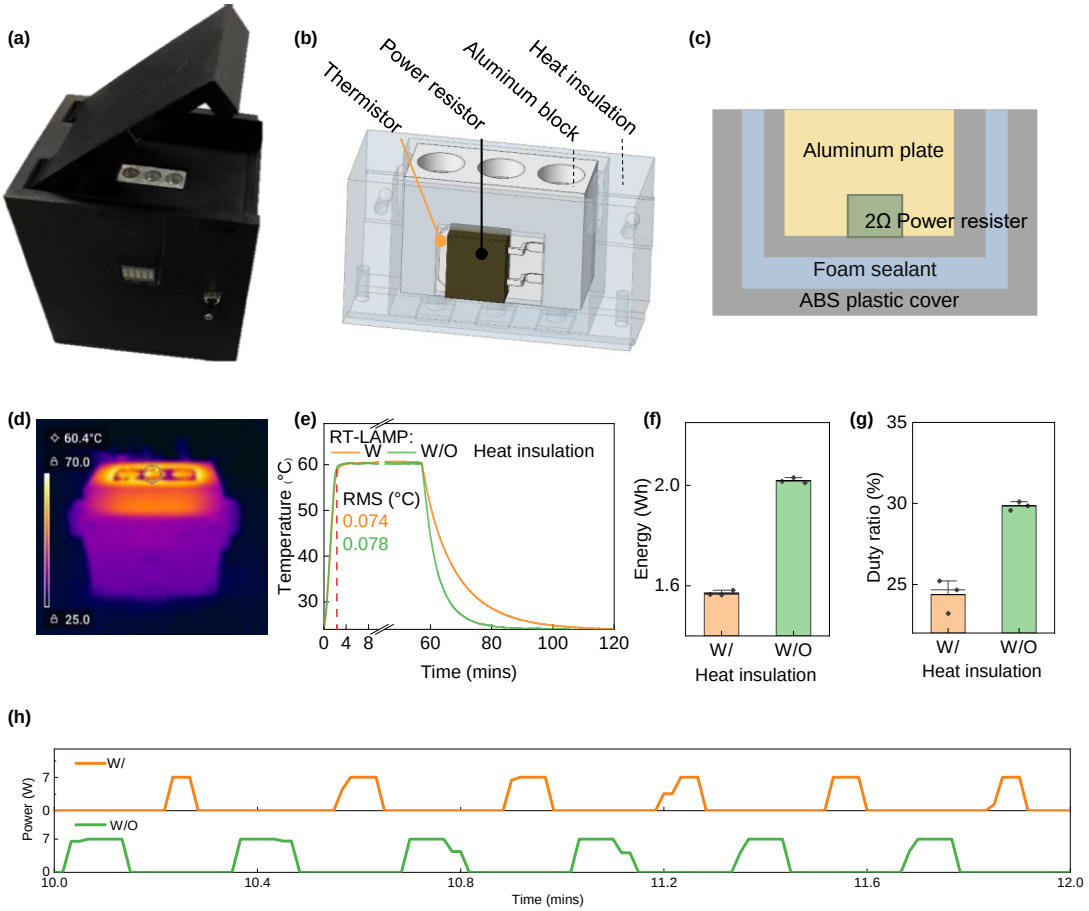

Figure 3-6. **(a)** Photographic depiction of the analyzer, illustrating the process of installing the aluminum block into the heating insulation case and the analyzer. **(b)** The thermal module comprises a power resistor (as a heating source), a thermistor (as a temperature feedback sensor), a CNC aluminum plate, and a housing for heat insulation to conserve energy. **(c)** The inner and outer sides of the thermal insulation module are made of 3D-printed ABS material, with foam sealant filling the middle layer to boost thermal insulation performance. **(d)** Thermal image of the heating module. (The core temperature of the AI

plate is 60 ℃, and the exterior temperature of the insulation layer is around 30 ℃, thus minimizing heat loss.) **(e)** Temperature change curve for RT-LAMP, including the heating up, incubation, and natural cooling stages. The time required for the reaction solution to heat up remains consistent, regardless of the presence of the thermal insulation module. **(f)** Utilizing thermal insulation modules can decrease energy consumption during the heating and incubation phases by approximately 22%. **(g)** With the thermal insulation module, the duty cycle of the heating resistor during the heating and incubation stages is reduced by 16%. (h) The on/off operational profile of heating resistors during incubation for 2 minutes after the temperature remains stable at 60 ℃.

In our quest to assess the quantitative detection performance of our newly designed analyzer, we tested serially diluted HIV-1 RNA samples. With these samples, we undertook the amplification process utilizing our reconstituted lyophilized RT-LAMP. The analyzer's performance was monitored through a panel of these samples tested in triplicate. The real-time data from these tests (**Figure 3-7b**) demonstrated that our analyzer successfully amplified HIV-1 RNA at a concentration of 25 copies per reaction. In addition, the time to positive as a function of the input RNA concentrations (**Figure 3-7c**) shows a clear linear relationship ($R^2 = 0.9$), which suggests the analyzer's practical applicability in semiquantitative clinical sample testing.

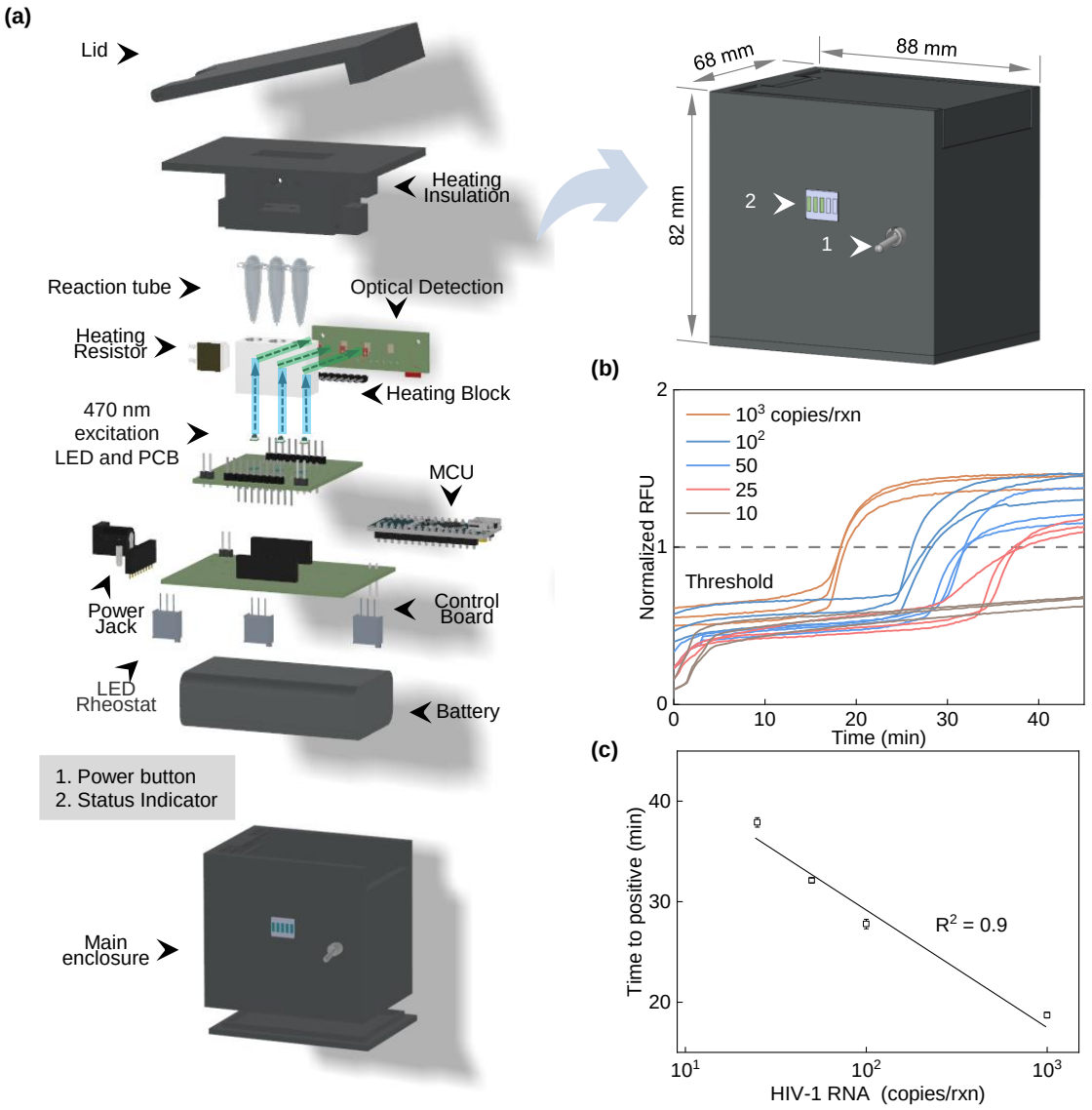

Figure 3-7. The analyzer and its performance for RT-LAMP amplification and detection for HIV semiquantitative self-testing. **(a)** Renderings showcase a fully enclosed analyzer along with a partially exploded view (dimensions: 88×68×82 mm; weight: 200 g). (1) Users activate the analyzer and initiate detection reactions via push buttons, with real-time updates provided by the status indicator. (2) The analyzer is Bluetooth-enabled for data transmission. Optical, thermal, and electromagnetic array subsystems are seamlessly integrated, supporting streamlined nucleic acid testing. The entire analyzer can be powered by an internally rechargeable battery. **(b)** This panel presents real-time RT-LAMP data from a single-analyzer test with serially diluted HIV-1 RNA. Each concentration was tested in triplicate. **(c)** This panel depicts the extracted "Time to positive" value from the single-analyzer test.

3.3.6. Diagnostic performance from sample to answer from first generation analyzer

To illustrate the clinical utility of our HIV self-test device, we examined 20 archived clinical HIV samples sourced from Penn State Hershey Medical Center's HIV/AIDS outpatient clinics. These samples contain 10 HIV-positive patients with three levels of viral load (VL) (Low: 0 - 1,000; Medium: 1,000 - 20,000; High: > 20,000 copies/mL) [113], [114], along with 10 HIV-negative individuals confirmed by Roche COBAS® AmpliPrep. To compare the HIV self-test device with RT-PCR, we tested two identical samples using each method.

To evaluate our device's performance agreement with benchtop PCR, we also extracted RNA using the traditional centrifugation method and performed PCR testing on these samples. Both the RT-PCR process and the HIV self-test device used an identical volume of 25 μL for analysis, with the former employing a column-based extraction method. **Figure 3-9a** displays the real-time RT-PCR results of these clinical samples alongside six concentration references for quantification, with the RT-PCR calibration curve illustrated in **Figure 3-8**. **Figure 3-9b** presents the data obtained through RT-LAMP analysis from our HIV self-test device, encompassing a set of 20 clinical specimens, inclusive of both positive and negative results. For each test, there are two internal references (lyophilized RT-LAMP reagents with known RNA concentrations). These internal references facilitate the differentiation between three levels of viral load.

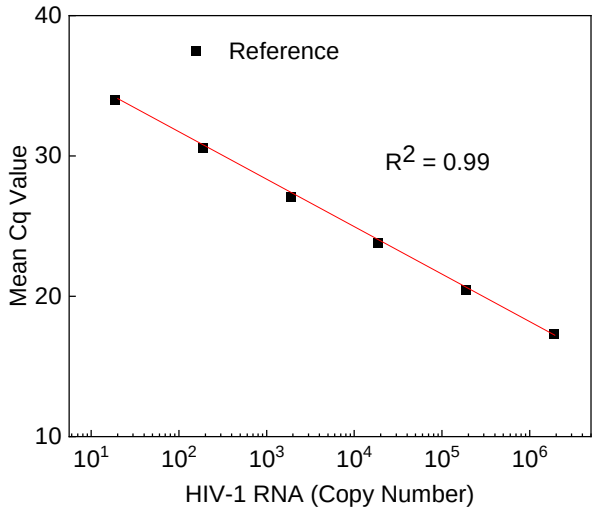

Figure 3-8. The Cq values obtained from the RT-PCR versus the target RNA copies. Cq values showed a logarithmic relationship with the sample concentration and verified our assay.

Figure 3-9c provides a qualitative and semiquantitative analysis using PCR and our device. The green boxes signify clinical samples without HIV infection or from individuals receiving antiretroviral therapy (ART) with a successfully suppressed viral load within a safe range. The orange boxes denote clinical samples with a viral load surpassing the safe range, signaling a necessity for further medical monitoring. The red boxes illustrate samples with a higher viral load, indicative of treatment failure and viral rebound despite ART. By employing Cq values of 33 and 26, we can classify the viral load into three distinct levels. The inset table summarizes the qualitative test results using a 40-minute threshold to determine outcomes in our semiquantitative test. Our analyzer adopts a comparative internal reference method to yield final output results: Low, Medium, and High. The calculated accuracy is 95%, suggesting the ability of our test to categorize viral load into Low, Medium, and High categories.

For the device's quantitative viral load analysis capabilities, we compared the time to positive from our device with the Cq from benchtop PCR. **Figure 3-9d** displays a scatter plot that represents the

correlation between the mean Cq values of RT-PCR results and the Time-To-Positive measured by the analyzer, which showed a strong Pearson correlation of r = 0.99. This indicates excellent agreement between our device and the benchtop PCR instrument. With an accuracy of 95%, we demonstrate that our device is capable of performing semiquantitative HIV viral load tests and that it can inspire confidence for the implementation of the proposed point-of-care platform in areas where HIV viral load tests are necessary.

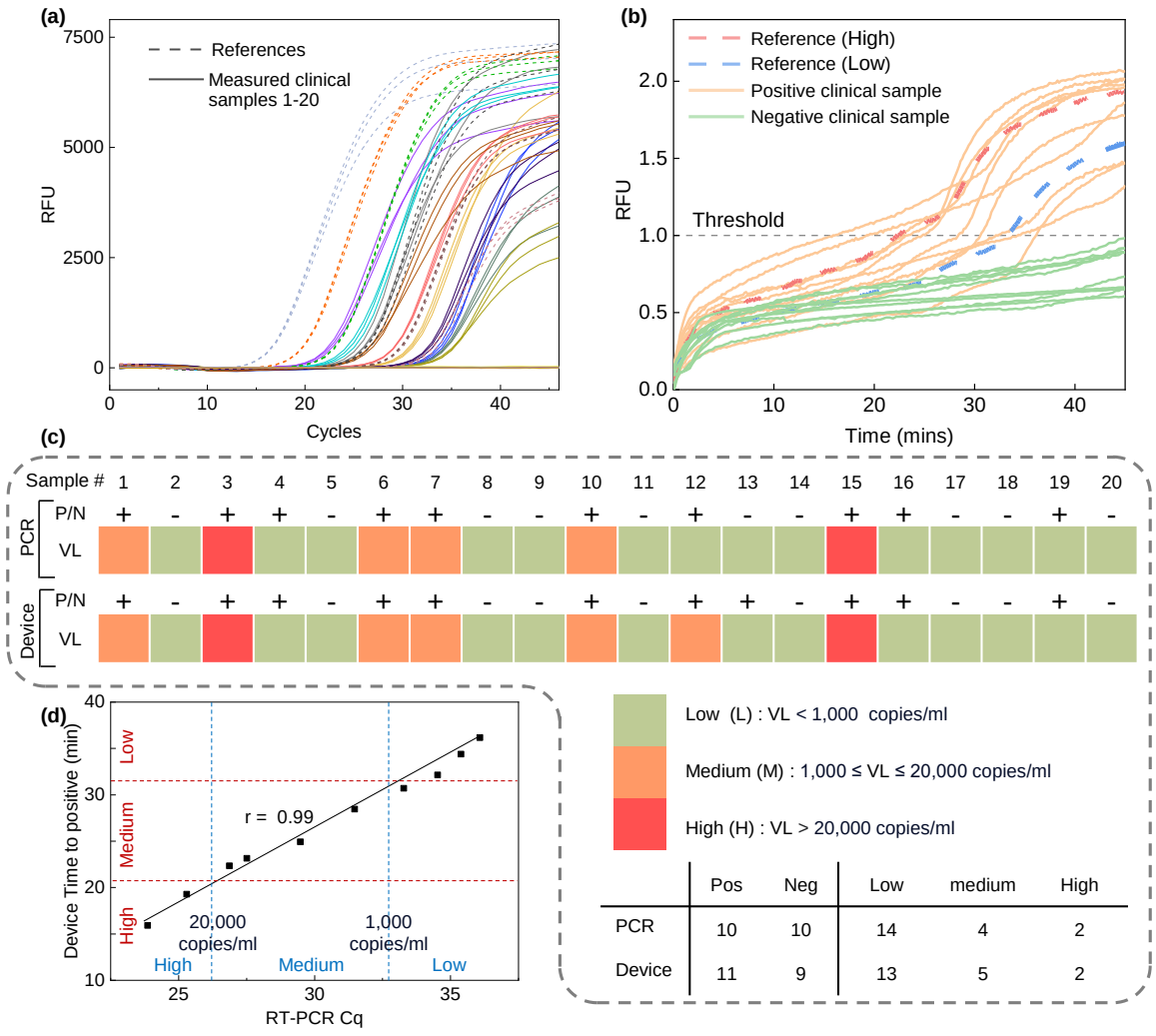

	Pos	Neg	Low	medium	High
PCR	10	10	14	4	2
Device	11	9	13	5	2

Figure 3-9. Testing of clinical samples using our device. **(a)** Real-time RT-PCR results for the clinical sample compared with calibration references. **(b)** Real-time RT-LAMP results were obtained from a single-analyzer test, utilizing both positive and negative clinical

samples. The results were obtained using a 25 µL eluted RNA from 100 µL clinical samples. The total reaction mixture is 25 µL. **(c)** Validation using clinical samples in a blinded test. Clinical samples from 20 patients (10 negatives and 10 positives). We conducted qualitative and semiquantitative analyses using PCR and our device, respectively. **(d)** Scatter plot and the linear fitted line comparing the mean Cq values of RT-PCR results with Time-To-Positive measured by the analyzer (10 positives).

3.3.7. Second generation portable analyzer design and validation of a multiplexed

To enable at home use, we designed and validated a sample-to-answer platform that contains all the necessary stages for nucleic acid testing (

Figure 3-10a-c). From our previous studies we have validated the use of plasma separation membranes[115] to collect samples and portable centrifuges for portable RNA extraction[116]. A Bluetooth paired smartphone app will instruct the user through conducting Sample Collection, RNA Extraction, and Amplification. To begin, a patient will prick their own finger using a lancet and transfer their blood droplet to our plasma separation card with a 100 µL metered pipette (

Figure 3-10a). Next, the plasma will be processed by the user to extract viral RNA using our previously established lab-free protocol (

Figure 3-10b). In several stages, the plasma sample will be liaised, cleaned, rinsed, and dried using our portable device. The user will be guided through each stage by an accompanying smartphone app, which will lead to an isolated sample ready for detection. Last, the extracted sample will be detected using our multiplex RT-LAMP assay. The amplification will be conducted using our portable analyzer and will provide a real-time update to the user on the smartphone app (

Figure 3-10c). Using this workflow, we have successfully designed a portable testing platform for patients to monitor their viral load from the comfort and convenience of their home.

To translate our multiplex LAMP assay outside of lab settings we designed an analyzer capable of multi-fluorophore detection and isothermal amplification. Our previous devices have showed robust isothermal management with relatively low power consumption[117]–[121], but to achieve multiplex detection we incorporated a new optical detection module into this new device. Our device now uses a multi-spectra color sensor that examines 8 discrete bandwidths of light (

Figure 3-10d). Using this sensor, we can analyze broad spectrum output from an assay and train a machine learning model to assist in the conversion from 8 channel signal to fluorophore concentration. The device is constructed using 3D-printed ABS to support the electrical and thermal modules. Inside the device, a 7.4V 2200mAh Li-ion battery provides power to the motherboard, resistive heater, and Arduino MCU. The MCU controls the excitation LEDs, indication LEDs,

resistive heating module, and optical array. Excitation light from the blue LEDs enters the heating block from the bottom where it is incident on the assay tube. Then, emitted light from the assay fluorophores is detected by color sensors positioned 90° off axis of the excitation light. This design enables our device to be battery powered, lightweight, and easy to use while maintaining a highly accurate optical setup.

To analyze a multiplex assay using the multi-spectral color sensor we integrated a machine learning model to convert the 8-channel data received from the sensor into two outputs. We previously established that this method could be used for many fluorophores and demonstrated its capabilities detecting up to four fluorophores simultaneously from one pot. In

Figure 3-10e, an excitation source, here a blue LED, is aimed at the amplification assay. When the LAMP reaction occurs, probes bind to their complementary amplicon and will be excited by the blue LED. The emission from each probe will be detected by the multi-spectra color sensor placed near the assay. The color sensor has 8 channels spaced across the spectrum of visible light (from 415 to 680 nm, bandwidth ~= 20 nm). The data from these 8 channels is converted, using machine learning, into an output layer containing two nodes, one for each fluorophore concentration. This workflow enables us to provide multiplex analysis of RT-LAMP in portable settings with minimal power consumption and real-time analysis.

To evaluate the machine learning model's accuracy, we examined the analyzer's optical detection using synthetic dyes and real-time LAMP assays. To train and evaluate our machine learning model, we prepared six concentrations of FAM and HEX dye (0, 0.2, 0.4, 0.6, 0.8, 1 μM) across

all 36 potential combinations. The portable device was used to collect ten data points per individual combination with four replicates. A training set was formed using 80% of the collected data and used to train a Neural-Network model with eight hidden layers. The remaining 20% of data was used as a test set and when analyzed we found our model performed very well demonstrating very strong linearity for both FAM (R^2=0.994) and HEX (R^2=0.996) across all combinations (

Figure 3-10f-g). These results suggest our analyzer's optical module and machine learning algorithm are well suited for the multiplex analysis of real-time LAMP assays. To verify the analyzer's sensitivity for real-time assays, we conducted several amplification assays on the device. In addition, we duplicated the assays to be operated on the benchtop thermal cycler to compare performance between devices. In

Figure 3-10h-i, we found that the portable analyzer showed great agreement with the benchtop device for both HIV (r=0.985) and RNase P (r=0.962) detection across a range of concentrations. Strong linearity and more than 96% agreement with the benchtop analyzer suggests our device is highly accurate, reproducible, and robust. These features make our device well suited for portable analysis of multiplex assays. Further validation of our device is needed to examine its performance detecting clinical plasma samples.

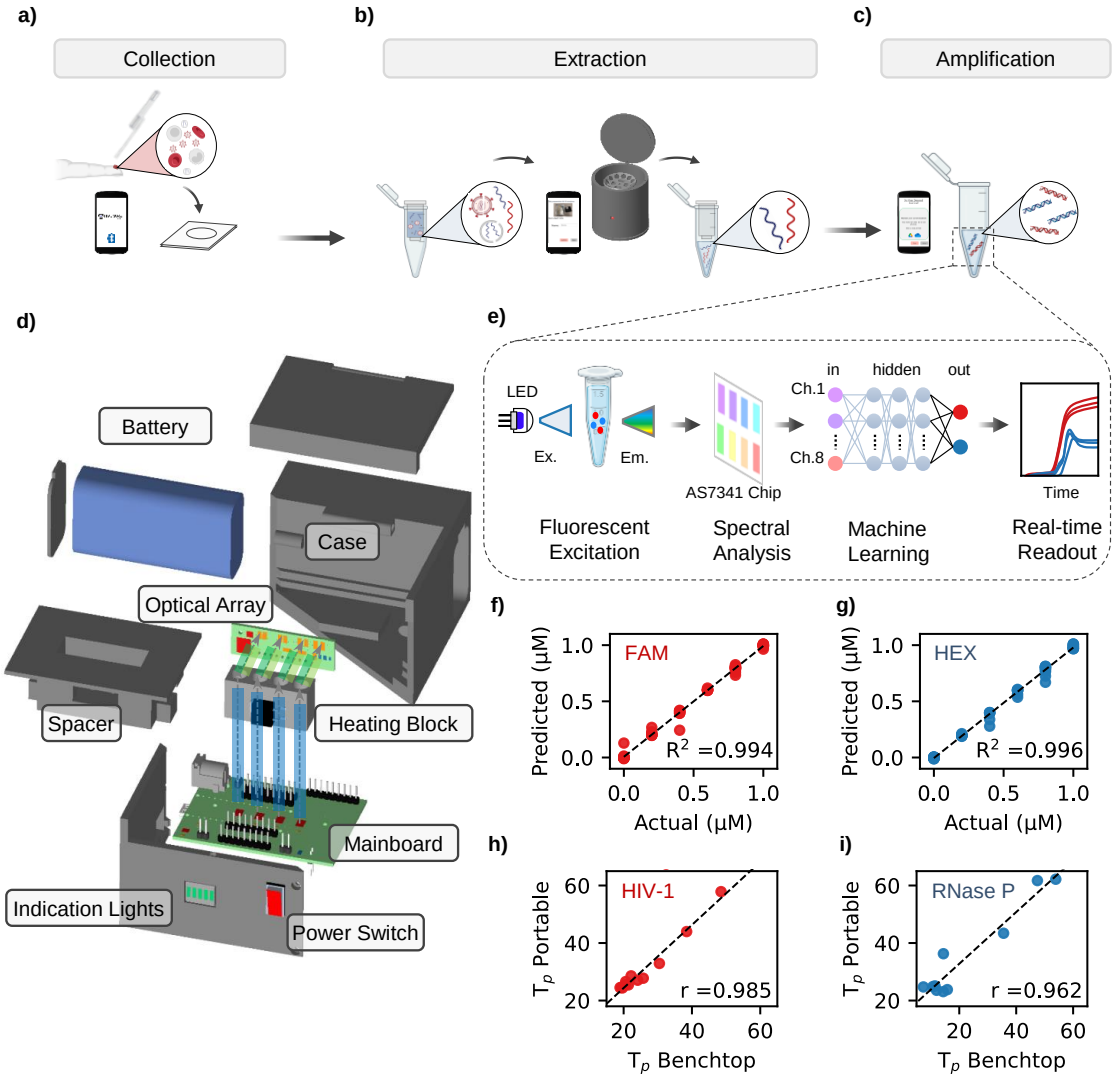

Figure 3-10. Device Validation. **(a)** Our testing workflow begins with a finger prick blood sample collected using a lancet and deposited onto a plasma separation card. **(b)** Next, RNA extraction from the plasma sample results in isolated HIV-1 and RNase P RNA. **(c)** Last, Amplification takes place inside the same tube for both targets and readout is examined using a machine learning pipeline on the portable analyzer (and smartphone). **(d)** Our portable analyzer consists of an interconnected mainboard with MCU, Optical Array (excitation and emission), Heating Block, Battery, User Interface features, and 3d printed case parts. **(e)** Multiplex analysis from one pot begins with fluorescent excitation of both FAM and HEX fluorophores. The emission spectra is examined using a integrated color sensor array (#AS7341). A machine learning model converts the 8-channel output from the color sensor to an output layer of two concentrations for FAM and HEX. These concentrations can be displayed in real-time as amplification curves for the multiplex assay. **(f)** Validation of the machine learning model to distinguish increasing concentration of FAM showed great linearity (R^2 = 0.994) **(g)** Validation of the machine learning model to distinguish

increasing concentration of HEX showed great linearity (R^2 = 0.996) Further validation of the machine learning model to analyze multiplex RT-LAMP showed very strong correlation between the portable and benchtop analyzer for **(h)** HIV-1 and **(i)** RNase P Time to Positive (T_p).

3.3.8. Second generation analyzer performance using clinical HIV plasma samples

To further validate our analyzer, we examined its clinical sensitivity and specificity using 45 plasma samples. Each sample was divided into two equal aliquots of 50 µL. One sample was prepared and analyzed using typical laboratory protocol (centrifuge & qRT-PCR) (**Figure 3-11a**). The second aliquot was prepared and analyzed using our portable extraction methods and analyzed using our multiplex RT-LAMP analyzer (**Figure 3-11b**). These results are summarized in **Figure 3-11c** to provide qualitative analysis. Our PCR results indicated 21 and 24 positive and negative samples respectively. Initially, our RT-LAMP results identified 14 and 31 positive and negative samples, demonstrating a poor sensitivity (66.66%) with a high specificity (100%). However, when we consider the dual detection capability of our multiplex RT-LAMP assay we can remove invalid tests, samples where no RNase P is detected. Removing these samples reduced our PCR data set and results to 15 positive and 13 negative samples. As a result, our RT-LAMP performance greatly improves from 66.66% sensitivity to 93.33% as we identify 14 positive and 14 negative samples (**Figure 3-11d**). The specificity of our assay remained 100%. A strong agreement with PCR demonstrates the high-performance capabilities of quality control-based LAMP assays. With a sensitivity of 93.33% and 100% specificity, we demonstrate our analyzer's strong qualitative ability for classifying clinical samples.

To demonstrate semi-quantitative viral load monitoring, we classified each sample using qRT-PCR and our RT-LAMP. To achieve this, we used the clinically recommended threshold of 1000 cp/mL[122]–[127] to classify each sample using qRT-PCR C_q and RT-LAMP T_p. This was established using five reference concentrations for both PCR and RT-LAMP (dashed lines in

Figure 3-11a-b) to create two classes: ‘Above’ and ‘Below’. The classification is summarized in **Figure 3-11e**. Our analyzer identified 10 ‘above’ and 18 ‘below’ samples, whereas qRT-PCR classified 8 ‘above’ and 20 ‘below’. Comparing the analyzer’s T_p against the C_q from benchtop PCR (**Figure 3-11f**), we found our analyzer accuracy to be 86% and our overall quantitative ability showed 84% agreement with the benchtop device. These results are expected since our multiplex RT-LAMP assay shows an order of magnitude lower LOD than the typical qRT-PCR assay (1-10 cp/rxn). We expect that further improvements to this assay could boost its analytical sensitivity and therefore improve the overall accuracy for quantification. Currently, our analyzer boasts a 93.33% sensitivity and 100% specificity, showcasing the capability and need for quality-controlled RT-LAMP assays. With an accuracy of 86% and 84% agreement with benchtop qRT-PCR, we demonstrate our device is capable of semi-quantitative viral load monitoring. We believe that our work will spark innovation into point-of-care platforms that revolutionize viral load tests for patients with HIV.

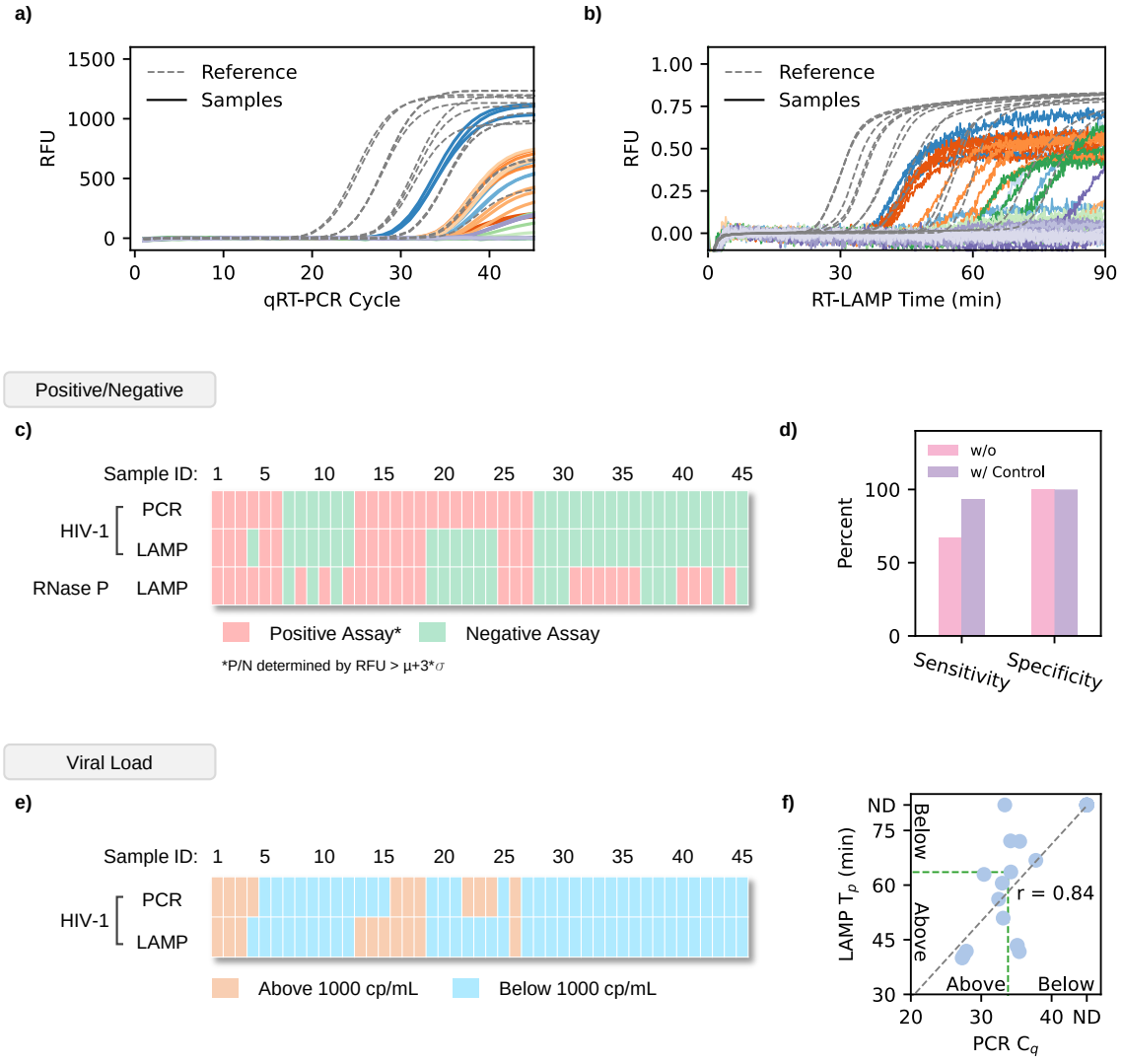

Figure 3-11. Clinical validation. **(a)** Amplification curves from 45 clinical samples using qRT-PCR as a benchmark. **(b)** Amplification curves from 45 clinical samples, analyzed using our multiplex LAMP assay on our portable analyzer. **(c)** Positive vs Negative comparison of qRT-PCR vs our multiplex LAMP output, displayed for all 45 samples. Positive assays are labeled in red. Negative assays are labeled in green. Positive/Negative was established using a RFU threshold of μ+3*σ. **(d)** Clinical sensitivity and specificity of our multiplex LAMP assay with and without an internal Control to eliminate invalid samples. **(e)** Viral load classification of qRT-PCR vs our multiplex LAMP assay for 45 clinical samples. The typical clinical threshold of 1000 cp/mL was used to define Above (>1000 cp/mL) and Below (<1000 cp/mL) classifications. **(f)** LAMP T_p vs PCR C_q for all valid samples, demonstrating a strong correlation in analysis between both methods.

3.4. Summary

In summary, we demonstrated the potential of a point-of-care HIV viral load self-testing device engineered to address current diagnostic challenges, particularly in low-resource settings. Our device, requiring 100 µL of finger-prick blood, offers a convenient, efficient, and non-invasive testing alternative, reducing the need for venous blood samples. With the integration of a smartphone interface, our tool provides real-time semiquantitative HIV viral load monitoring, achieving an accuracy of 95%. In overcoming common challenges associated with existing point-of-care tests, such as the need for complex laboratory infrastructure and accessibility issues, we successfully developed efficient absorption-based plasma separation methods that achieve an efficiency of 80 ± 2.3% (hematocrit is 40%), and our syringe-based RNA extraction method for on-site plasma processing yields a viral recovery efficiency of 86 ± 1.7% (VL = 25 copies/µL). These high-efficiency rates significantly enhance the robustness of the testing process. Additionally, we incorporated the use of lyophilized reagents, enhancing the longevity and practicality of our device. Furthermore, the results of our study underscore the importance and potential of using our device for regular self-monitoring of HIV viral load, thereby supporting effective management of antiretroviral therapy. We evaluated our device using clinical samples, achieving a 95% accuracy rate and 99% agreement with conventional RT-PCR methods. These findings suggest the device's potential for routine HIV viral load self-testing at home, enhancing ART treatment monitoring. This development may be a foundational step towards more user-friendly HIV self-testing solutions to improve patient care. Future work will focus on improving device efficiency, exploring ways to lower manufacturing costs, and conducting extensive field trials in various settings. As we move forward, we remain optimistic that our device will have implications for global health by providing a rapid, affordable, and easy-to-use solution to HIV viral load testing.

CHAPTER 4 Compact Multiplex PCR Device for HIV-1 and HIV-2 Viral Load Determination from Finger-Prick Whole Blood in Resource-Limited Settings

In this chapter, we report a multiplexed PCR device developed for simple and efficient quantification of HIV-1 or HIV-2 viral loads using finger-pricked whole blood from rural decentralized settings. This device is comprised of a previously developed RNA extraction module combined with an optimized real-time PCR amplification system. Together, these combine to simultaneously detect and differentiate HIV-1 & 2; as well are adopting a testing control of RNase P allowing for full diagnostic analysis from one sample. Our device also includes an intuitive user interface and is completely autonomous so it can serve individuals in remote areas who are unfamiliar with the field of medical testing. They get the results in a very short time of around 70 minutes and hence save on testing times without leaving accuracy behind. The efficiency and effectiveness of the device were validated through the analysis of 30 clinical samples, yielding a sensitivity of 100% for both HIV-1 and HIV-2. The specificity was found to be 100% for HIV-1 and 90.91% for HIV-2, demonstrating high diagnostic accuracy. One of the most attractive things about this device is that it comes in comparison to all other counterparts. Given that you can run the assay for less than $10, it could be an economically viable way to use this as a broadscale test in regions where healthcare budgets don't allow others. Hence it is quite a useful device to aid HIV management in resource-limited settings, where conventional laboratory facilities are out of reach due its simplicity and affordability with rapid output. The point-of-care test is an effective, low-cost, high quality diagnostic tool-promoting rapid testing for HIV-inexpensively overcoming the barriers to efficient control of and care in resource-limited settings.

4.1. Introduction

The Human Immunodeficiency Virus (HIV) remains an important public health issue worldwide with population-level effects that generate considerable social and economic burden [2], [128]. While the outcome of HIV infection is also greatly serious, an entirely different problem has arisen following the introduction and evolution of antiretroviral therapy (ART) in managing adults with HIV. However, what was once a death sentence, HIV is now a treatable chronic infection if the proper treatment protocols are followed [3]. The success of ART is largely dependent on the accurate and frequent monitoring of viral load (VL) levels in order to assess the efficacy of treatment and stop the progression towards AIDS [129]. The international community aims to reach the 95-95-95 goals by setting ambitious global health targets based upon the year 2025 [130]. Realizing these goals relies on regular, high-quality VL testing that is essential for both the patient-level care of HIV and population-wide measures to control its spread [131], [132].

HIV has added complexities due to multiple subtypes, with HIV-1 nearly exclusively in western countries where it is primarily found and a significant portion of Africa and Southeast Asia, including geographical hotspots as considered middle-lower-income [133]. These differences in prevalence and clinical behavior necessitate a versatile approach to antiretroviral therapy (ART) monitoring, adapted to the distinct treatment needs and resistance profiles of each subtype [134]. A previous study has shown that aggressive treatment strategies are crucial for patients infected with the rapid progressive HIV-1 [135]. HIV-2, which progresses very slowly and is often resistant to drugs that would be effective against HIV-1 (such as the non-nucleoside reverse transcriptase inhibitors NNRTIs), on the other hand requires different treatments [136]. This difference highlights the need for flexible ART regimens aimed to appropriately treat disease based on subtype-specific features [137]. Moreover, dual infection with HIV-1 and HIV-2 adds to the complexity of this field rendering accurate diagnosis and treatment essential [138]. This is a

condition that warrants the application of diagnostics technology for virus type which can detect and quantify both types at once [139]. Critical to ensuring treatments are matched appropriately for the viral subtype, maximizing patient outcomes and contributing to global public health initiatives in management and control of the HIV epidemic [140].

In developed nations, access to VL testing is generally straightforward due to robust healthcare infrastructure and frequent healthcare visits [141]. Facilities often feature both traditional central laboratory setups and commercial point-of-care (POC) devices, such as the PIMA device, which facilitate rapid and accessible testing [142]. Technologies like the GeneXpert HIV-1 Viral Load Test and Roche's Cobas Liat™ System utilize plasma samples in controlled laboratory settings, catering primarily to developed markets with options extending to healthcare facilities and home-based self-testing [143], [144]. Ongoing research and development efforts focus on enhancing these technologies in accuracy, accessibility, and speed [17], [44], [88]–[94], [145]–[153]. Despite these developments, their use is largely limited to developed areas, mainly because of challenges in processing whole blood samples and the lack of quantitative features in a single operation [17]–[22]. These urgent concerns underscore the essential need for creating a sophisticated HIV viral load monitoring device that functions from sample to result and is appropriate for point-of-care use.

However, in low- and middle-income countries (LMICs) there are a number of additional challenges which must be addressed for effective viral load (VL) testing beyond infrastructure-related barriers such as lack of reliable electricity [154]. A first problem is the scarcity of skilled clinicians by knowledgeable to handle the complex laboratory instrumentation necessary for VL tests, which curtails testing capabilities [155]. Price is also a significant hurdle. Tackling the high costs of involuntary testing infrastructure in LMICs implies that foreign aid represents a substantial

contraction, as these technologies are not maintained locally and require expensive investment [156]. Furthermore, problems managing the supply chain (i.e. access to necessary materials) are made more severe by a lack of pre-existing infrastructure and result in delays around key supplies and results [157]. Additionally, sophisticated VL testing technologies developed for settings with stable infrastructure are oftentimes ill-equipped to handle the challenging and fluctuating field conditions that prevail in many LMICs (i.e. extreme temperatures or high humidity), which can interfere with sensitive equipment functionality [78]. In LMICs, these factors highlight the dire need for more appropriate VL testing solutions and a demand for innovations that are cost-effective and environmentally stable enough to be efficiently deployed in local settings. This leaves a balkanized landscape for affordable, accessible and feasible VL testing solutions in these regions so that there is an urgent need of innovative HIV management technology.

Addressing this gap, our research introduces a novel multiplex PCR-based detection system specifically tailored for LMICs. This innovative device is battery-powered, catering to areas with unreliable electricity, and is capable of differentiating between HIV-1 and HIV-2. It includes a control test to verify accuracy and employs a three-channel detection system that accurately measures viral load, which is crucial for effectively monitoring disease progression and adjusting treatment plans. The device boasts an RNA extraction efficiency of 80% through a compact sample preparation unit, designed to collect and examine viral RNA accurately. Its semi-automated nature allows for the processing of multiple samples simultaneously, enhancing throughput and minimizing human error, thereby ensuring consistent results. Our system not only measures HIV-1 and HIV-2 viral loads simultaneously with a 96% accuracy rate but also demonstrates over HIV

100% for HIV-1, 100% for HIV-2 sensitivity and 100% for HIV-1 and 90.91% for HIV-2 specificity in assays. These performance metrics confirm the device’s capability to reliably detect

HIV-1 as well as HIV-2 at various stages of infection, providing an essential tool in closing the significant gap in VL testing solutions for LMICs. This advancement is particularly vital as regular and precise VL testing is indispensable for effective global HIV control and prevention, with the added capability to manage co-infections of HIV-1 and HIV-2, underscoring its importance in the evolution of HIV management technologies.

4.2. Methods

4.2.1. Materials and chemicals.

Materials for this study were procured from various suppliers. RNA extraction kits, specifically the QIAamp Viral RNA Mini Kit, catalog number 52904, were sourced as detailed in **Figure 4-2**. Electronic and optical components for the HIV analyzer were purchased from DigiKey, as listed in **Figure 4-1**. RT-PCR primers and probes were supplied by IDT, while essential reagents and chemicals were acquired from Sigma-Aldrich and Thermo Fisher Scientific. The Bio-Rad CFX96 system was employed for assay validation. Viral RNAs for HIV-1, HIV-2, and RNase P, with catalog numbers VR-3245SD, VR-3266SD, and 1006626 respectively, were obtained from ATCC. Clinical HIV samples were provided by the Penn State Hershey Medical Center. All materials were used as received and stored according to the manufacturers' guidelines.

Table 4-1. Bill of materials of the analyzer

System	Description	Part#	Function	Unit Cost ($)	Unit Qty.	Ext. Cost ($)
Electronics	Arduino Nano	7630049200173	Microcontroller	6.00	1	6.00
Electronics	Adafruit Bluefruit LE SPI	2633	Bluetooth Low Energy	14.00	1	14.00
Electronics	Capacitor 10uF	P10425CT	Power stabilizing	0.147	1	0.15
Electronics	DC Barrel Power Jack/Connector	PRT-00119	Power Connector	1.25	1	1.25

Electronics	36-pin stripe male header	392	Headpins	4.95	0.1	0.50
Thermal	Aluminum CNC block	CP-0.91-0.91	Heating Stage	5.75	0.25	1.44
Thermal	2Ω Power Resistor	MP725-2.00-FCT	Heater	7.01	1	7.01
Thermal	SMD Resistor, 1kΩ	311-1.00KHRCT	Temperature/EM control	0.0072	1	0.01
Thermal	Thermistor	235-1057	Temperature sensing	3.5	1	3.50
Thermal	SMD Resistor, 10kΩ	RNCP0603FTD10K0CT	Temperature control	0.1	1	0.10
Thermal	N Channel Power MOSFET	DMN1019USN-7DICT	Switch for heater and fan	0.354	2	0.70
Thermal	FAN AXIAL 40X15MM 12VDC	603-1006-ND	Fan for colling	8.86	1	8.86
Optics	Res Cermet Trimmer 500K ohm	3296W-1-501RLF	Adjust LED intensity	0.6	3	1.80
Optics	SMD Resistor, 1kΩ	RNCP0805FTD1K0CT	Optical module	0.0277	3	0.08
Optics	SMD Resistor, 10kΩ	RNCP0805FTD10K0CT	Optical module	0.0277	8	0.22
Optics	IC Color Sensor	AS7341	Optical detection	3.00	3	9.00
Optics	SMD LED, Blue	1497-1138-1	Fluorescence excitation	0.528	3	1.58
Optics	Capacitor 10uF	P10425CT	Power stabilizing	0.147	3	0.44
Optics	Capacitor 0.1uF	P01425CT	Power stabilizing	0.147	1	0.15
Optics	Voltage Regulator	AP7312-3.3/1.8	Power supplier	0.8	1	0.80
Optics	I2C Multiplexer	TCA9548A	I2C expender for sensor	1.10	1	1.10
Enclosure	ABS Filament (Black)	-	3D platform material	69.00	0.05	3.45
Enclosure	Screws (M2 cap screw)	91290A015	Assembly	0.14	10	1.40
			Total Cost			**$63.54**

Table 4-2. Cost per test

Reagents	**Vendor**	**Function**	**Stock Vol (mL)**	**Unit Cost ($)**	**Volume (μL)/rxn**	**Ext Cost/rxn**
RT-LAMP Mixes	Meridian Life Science	LAMP master mix	5	198	6.25	0.2475
HIV-1 Forward	IDT	PCR master mix	0.856	12.05	0.4	0.00563
HIV-1 Reverse	IDT	PCR master mix	0.67	9.15	0.4	0.00546
HIV-1Probe	IDT	PCR master mix	0.185	381	0.4	0.82378
HIV-2 Forward	IDT	PCR master mix	0.697	9.64	0.4	0.00553
HIV-2 Reverse	IDT	PCR master mix	0.87	10.60	0.4	0.00487
HIV-2Probe	IDT	PCR master mix	0.201	311	0.4	0.61891
RnaseP Forward	IDT	PCR master mix	0.763	9.15	0.4	0.0048
RnaseP Reverse	IDT	PCR master mix	0.68	9.64	0.4	0.00567
RnaseP Probe	IDT	PCR master mix	0.231	284	0.4	0.49177
Lysis Buffer	Invitrogen	Sample Prep.	25	6	200	0.02
Wash Buffer	Invitrogen	Sample Prep.	37.5	54	500	0.12
Elution Buffer	Invitrogen	Sample Prep.	11	35	30	0.1

Ethanol	Sigma-Aldrich	Sample Prep.	100	10	200	0.02
Material	**Vendor**	**Function**	**Stock Vol (sq. m.)**	**Unit Cost ($)**	**Volume (sq. mm)/rxn**	**Ext Cost/rxn**
Vivid PSM-GR	Pall Corporation	PSM card	0.06	30.00	200	0.30
Silica column	Qiagen	RNA extraction		2.00	1	2.00
PCR tube		Fisher scientific		0.01	1	0.01
					Total	**$4.28**

4.2.2. Portable PCR analyzer instrumentation

The complete design of the device was developed using PTC Creo software, with the casing produced through 3D printing on a METHOD X, MakerBot printer. The printed circuit board (PCB) was designed using Autodesk Eagle and manufactured by OSH Park. Assembly of the electronic components and the microcontroller unit on the PCB was performed manually in our laboratory. A resistive heating element (PWR263S-20-2R00J, sourced from Digi-Key) was affixed to the underside of a specially fabricated aluminum heating plate with thermal paste (AATA-5G, Artic Alumina). For accurate temperature control, a thermistor (95C0606, Digi-Key) was integrated at the center of the heating plate, facilitating real-time temperature monitoring. Temperature regulation during nucleic acid testing was achieved through a negative thermal feedback mechanism using an N-channel power MOSFET (63J7706, Digi-Key). The control software for the graphical user interface (GUI) was developed in Android IDE, enabling device management and data exchange via Bluetooth connectivity.

4.2.3. Multiplex RT-PCR reaction

In this study, we employed a dual-enzyme, one-step RT-PCR method for detecting HIV-1. The reaction mixture, with a total volume of 20 µL, consisted of 5 µL of TaqMan Fast Virus 1-Step Master Mix, paired with forward and reverse primers (each at a 1 µM concentration), a probe (1 µM), 1 µL of RNA templates, and 11 µL of PCR-grade water. We used a verified set of HIV-1 RT-PCR primers for this assay. The RT-PCR protocol followed specific thermal conditions, beginning with a single reverse transcription step at 50 ℃ for five minutes to convert HIV-1 RNA into cDNA. This step was immediately followed by a denaturation phase at 95 ℃ for 20 seconds, and then 40 cycles of amplification. Each amplification cycle consisted of a 3-second denaturation at 95 ℃ and a 30-second annealing and extension phase at 60 ℃. The details of the primers and probes are listed in **Table 4-5, Table 4-6, Table 4-7**. In our experiment, the reporters used were ATTO425, HEX, and Cy5.

4.2.4. Statistical analysis

For this study, all statistical analyses and regression modeling were executed utilizing MATLAB R2020 software (Natick, MA). Data visualization, including all figures and plots, was also primarily performed with MATLAB, supplemented by Microsoft PowerPoint for layout adjustments and final presentations. Each plot displayed in the results represents the average value (mean) accompanied by three standard deviations. These measurements were consistently derived from three separate tests (triplicates) to ensure reliability unless otherwise indicated. This standard approach was maintained across all experimental conditions to facilitate accurate comparison and reproducibility of the data. The use of MATLAB was integral not only for the initial data processing

but also for the subsequent analysis stages, ensuring a seamless workflow from data collection to visualization.

4.3. Results and discussion

4.3.1. Overall workflow

Figure 4-1a illustrates the complete workflow of our multiplex viral load testing PCR-Based approach for detecting HIV-1 and HIV-2 viral loads. **Figure 4-1b** details all necessary materials required for the workflow. The steps are as follows: Step 1 - Activation of the application on an Android smartphone with step-by-step instructions. Step 2: The user collects around 100 µL of blood using a disposable pipette through a finger prick. Blood is collected and processed using a plasma separation card apparatus [146]. The separation of plasma on filter paper as the blood passes through the card. In the datasheet for Vivid™ Plasma Separation GR, a wait time of 1 minute is indicated to achieve full filtration. After separation from the rest of the whole blood specimen, plasma is ready for diagnostic or research use. Step 3 - Transfer the absorbent paper with plasma to a collection tube. The RNA are then purified using a centrifuge-based portable RNA extraction device that we previously developed [150], [158]. The collected RNA is then added into a test tube that contains RT-PCR reagents. The portability and user-friendliness of this on-site sample preparation solution, that can be done in under 10 minutes without the need for carrier RNA or cold storage highlights how versatile & practical the device is, especially in resource-limited settings. Step 4 : At this point, the test tube is inserted into the machine and placed in front of a device to start testing. Step 5: The application shows the end results after 70 minutes. All of this can be done at home by the user, without requiring professional staff or laboratory facilities. This capacity

would allow simultaneous testing for HIV viral load from multiple samples in low- and middle-income countries (LMICs).

Detailed mechanistic steps for the reaction mechanism used in this study are outlined pictorially in **Figure 4-1c**. The process begins by using a custom plasma separation card that separates the red blood cells so as to isolate virus particles i.e., HIV-1, HIV-2 and RNase P in the sample. Following this, Step 2 continues by isolating the viral-imparted RNA with a portable centrifuge-based reagent that streamlines rapid and efficient preparation of the extracted RNA for analysis. The third step of the mechanism is for this extracted RNA to be amplified by a usable, mobile PCR device expressing a fluorescence signal in the presence of viral RNA. In this step we use the state of art multiplex RT-PCR technology which involves a reverse transcriptase enzyme to convert RNA into complementary DNA(cDNA) first. This cDNA is then subjected to TaqMan PCR detection, an extremely specific and sensitive technique that uses a double-labeled probe system for amplification. The multiplex RT-PCR assay detected simultaneously with differentiating and relayed results for HIV: ATTO425, HEX and Cy5 channels targeted HIV-1, HIV-2, RNase P, respectively. Each probe has been engineered with high specificity for one of three targets, providing real-time PCR detection by unique fluorescent labeling [159]. Such multiplex detection capabilities are essential for the robust surveillance and precise diagnosis of viruses [160]. Interpretation of the test results is the final step in analysis, with whether or not a sample tested positive determined from fluorescent signals and how many PCR cycles were needed to reach significant levels. The advantage of this is for quantitative analysis with high level of specificity to accurately detect viral load in the sample which can be helpful in determining whether a patient is still infected or drug treatment was successfully applied.

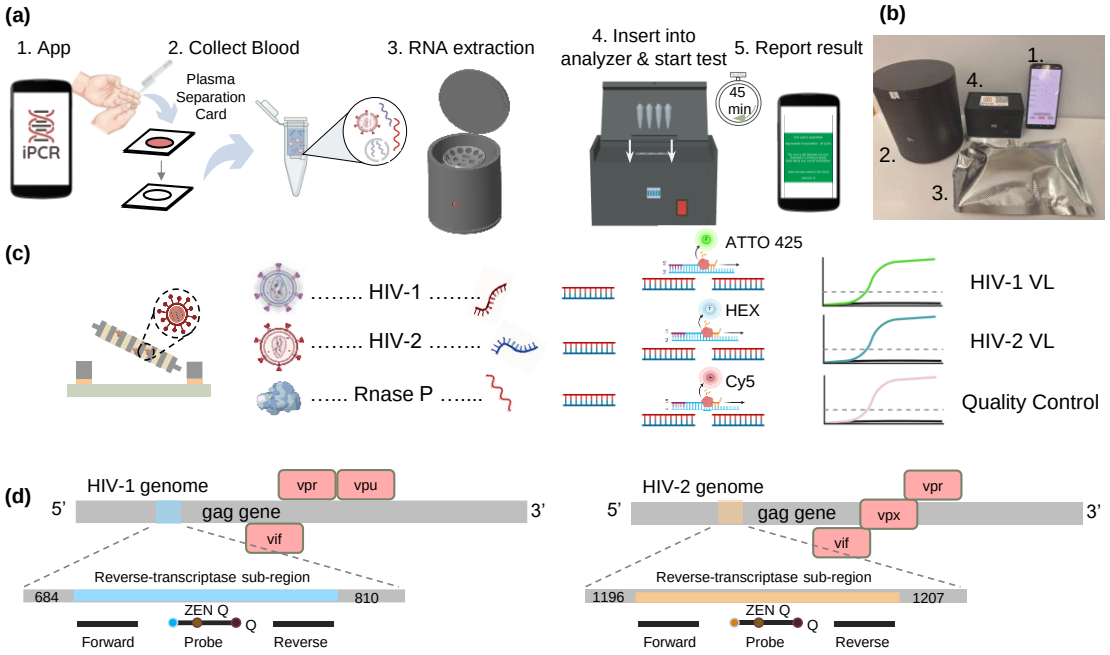

Figure 4-1. Overall Device Workflow and Assay Design. **(a)** Outline of the procedure as detailed in the mobile application: the user starts the app, collects a blood sample using a disposable pipette and a plasma separation card, places the card into a centrifuge-based portable RNA extraction device for RNA extraction, inputs the extracted RNA with water into the test tube, and receives results via the app after 40 minutes. **(b)** Depiction of the device components, including: 1. An Android smartphone, 2. A centrifuge-based portable RNA extraction device, 3. Reagents and materials for testing, 4. A portable PCR analyzer. **(c)** Schematic illustrating the reaction mechanism: Step one involves separating plasma and red blood cells using a plasma separation card, which contains viruses (HIV-1, HIV-2, and RNase P). Step two extracts the viral RNA using the centrifuge-based portable RNA extraction device. Step three amplifies the RNA through portable PCR, generating a fluorescent signal. The final step determines the test results based on the fluorescent signal and cycle number. **(d)** Primer design for HIV-1 and HIV-2, featuring two RT-PCR primers and one probe for each virus targeting the beginning of the gag gene.

4.3.2. Multiplex PCR assay performance

Specific primer-probe sets for each human target were designed in the multiplexed assay targeting HIV-1, HIV-2 and RNase P. This assay also employs two reverse transcription PCR (RT-PCR) primers and one fluorescent probe per viral type, targeting the first part of gag gene (**Figure 4-1d**). Both the Reverse-transcriptase sub-region targeting HIV-1 and its corresponding region for targeting HIV-2 are depicted in **Table 4-3 & Table 4-4**. This region was chosen because it is well

conserved among various strains mnemonic, making short for better detection per wear [96], [161]. RNase P was used as an internal control to confirm RNA extraction and general assay effectiveness, for which a unique set of primers along with a probe were designed [162]. For detecting samples with each primer and probe set, amplification reaction mixtures were prepared that contained all combinations of primers/probes at the same concentration under a common thermal cycling protocol. We sought a strategy by which we could detect only the desired RNA targets, and limit signal for any target to their respective optical channel as much in order not need separate runs. This specificity is likely to be important in limiting cross-reactivity between the targets and ultimately improving diagnosis using our approach. Benefits of this multiplex method are increased efficiency and require less time and costs for HIV infection diagnosis. Primer and probe design were conducted with 6 primers and 3 probes, respectively for the PCR (**Table 4-5, Table 4-6, Table 4-7**).

Table 4-3. Reverse-transcriptase sub-region targeting HIV-1

Sequence (5' → 3')
tctcgacgcaggactcggcttgctgaagcgcgcacggcaagaggcgaggggcggcgactggtgagtacgccaaaaattttgactagc ggaggctagaaggagagagatgggtgcgagagcgtcagta

Table 4-4. Reverse-transcriptase sub-region targeting HIV-2

Sequence (5' → 3')
gcgcgagaaactccgtcttgcgagggaaaaaagcagatgaattagaaacaattaggttacggcccggcgggaagaaaaagtacagac taaaacatattgtgtgggcagcgaa

Table 4-5. RT-qPCR primer set targeting HIV-1

Primer	**Sequence (5' → 3')**
Forward	TACTGACGCTCTCGCACC
Reverse	TCTCGACGCAGGACTCG

Probe	ATTO425-CTCTCTCCTTCTAGCCTC

Table 4-6. RT-qPCR primer set targeting HIV-2

Primer	**Sequence (5' → 3')**
Forward	GCGCGAGAAACTCCGTCTTG
Reverse	TTCGCTGCCCACACAATATGTT
Probe	HEX-TAGGTTACGGCCCGGCGGAAAGA

Table 4-7. RT-qPCR primer set targeting Rnase P

Primer	**Sequence (5' → 3')**
Forward	AGATTTGGACCTGCGAGCG
Reverse	GAGCGGCTGTCTCCACAAGT
Probe	Cy5-TTCTGACCTGAAGGCTCTGCGCG

Specificity of our multiplex RT-PCR assay is an essential parameter, directly related to the accuracy at which we can detect. It was critical that our assay had a clean and distinct signal for differentiation of HIV-1, HIV-2, and RNase P with little to no cross reactivity between them in order as an effective diagnostic tool. To determine the specificity and multiplexing ability of our assay, we performed a well-thought-out set of experiments. An ordered list of eight experimental biotin samples were systematically created. They include synthetic RNA of HIV-1, HIV-2 and RNase P per sample; specific samples with the presence or absence of these added RNA sequences were classified as either positive or negative for that respective marker. The RNA content in these samples was at concentrations of either 0 or 1000 copies per reaction thus serving as a serial dilution of target (RNA) concentration for assay evaluation. This pattern was quantitatively reflected in how

each sample looked visually (

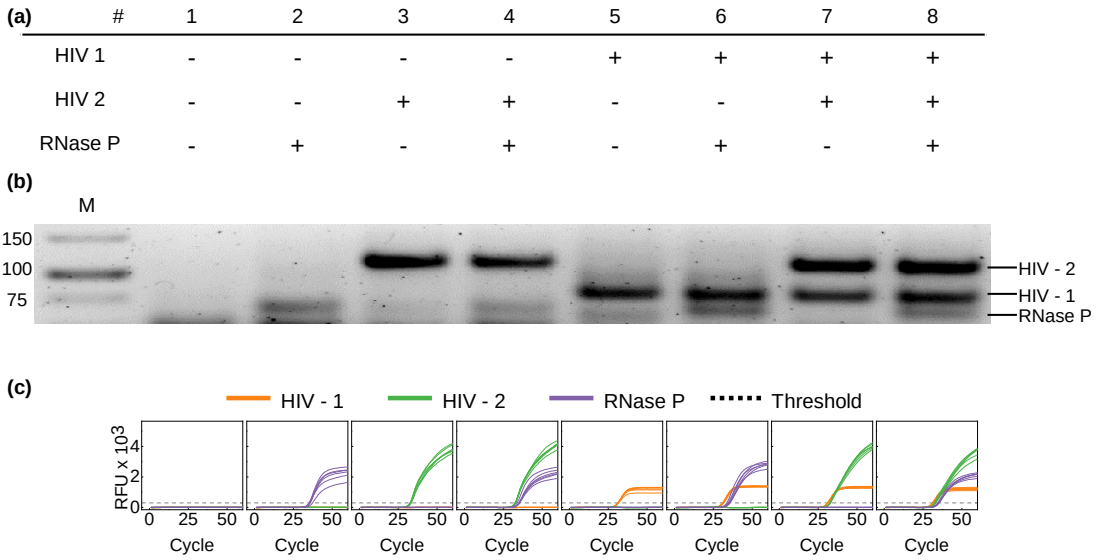

Figure 4-2a).

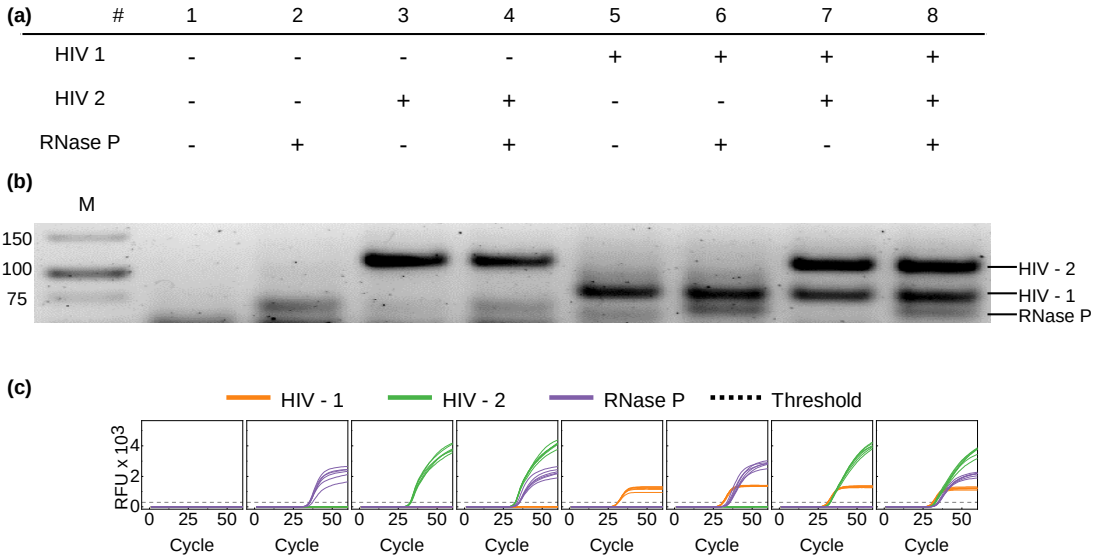

Figure 4-2. Validation of the specificity of the multiplex RT-PCR assay. **(a)** Samples 1 through 8 were created by mixing synthetic RNA of HIV-1, HIV-2, and RNase P, each positive or negative marked with "+/-" sign. The concentration of each viral RNA in the samples ranged from 0 or 1000 copies per reaction. **(b)** Agarose gel electrophoresis was used to analyze the RT-PCR products, displaying the amplification profiles for Samples 1 to 8. Each sample was tested six times. **(c)** Results from real-time multiplex RT-PCR amplification obtained from Bio-Rad bench top PCR analyzer for Samples 1 to 8 are presented. Optical signals for HIV-1, HIV-2, and RNase P from three different optical channels are combined into a single figure.

PCR amplification was performed on the samples (followed by agarose gel electrophoresis analysis as presented in

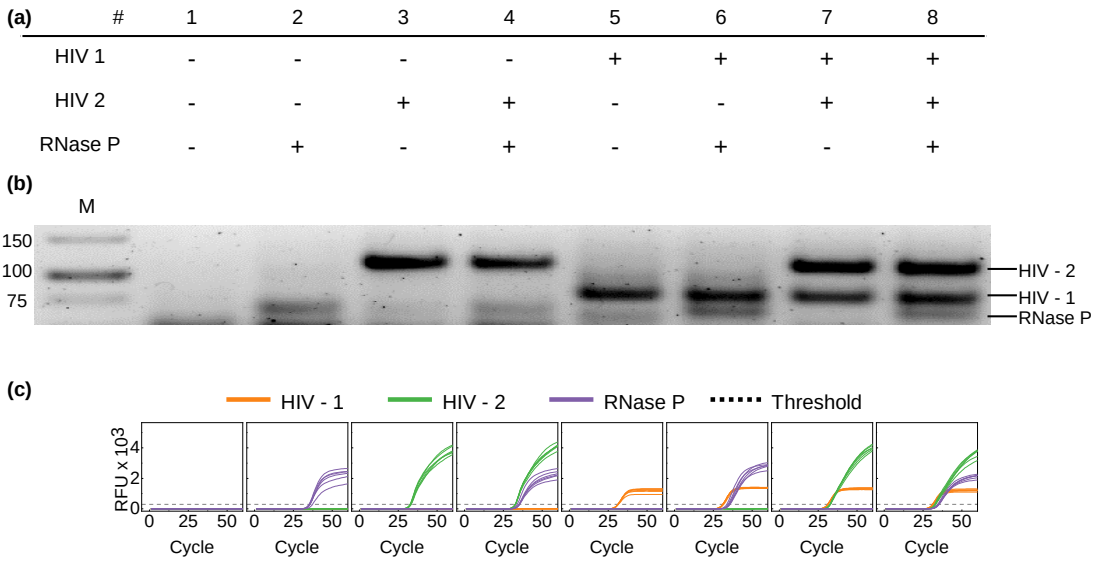

Figure 4-2b: after running through a final total of 60 cycles, clear-visible bands at different base pair lengths indicated presence of amplified genetic material at desired length ranges for all analyzed cases. Lanes 2, 3 and 5 in particular showed single bands corresponding to individual target amplifications (HIV-1, HIV-2 and RNase P respectively) By contrast, lanes 4, lane 6 and lane 7 showed dual bands reflecting co-amplification of two different targets per sample. Lane 8 was of particular interest because it displayed multiple bands specific to all three targets resulting from efficient multiplex amplification, validating the ability and sensitivity of our assay for detecting more than one pathogen. No amplification was observed for NTC in lane 1, confirming the absence of contamination and non-specific amplifications. To validate the gel electrophoresis data, we quantitated selected samples to real-time PCR for 60 cycles. Fluorescence detection

results, where

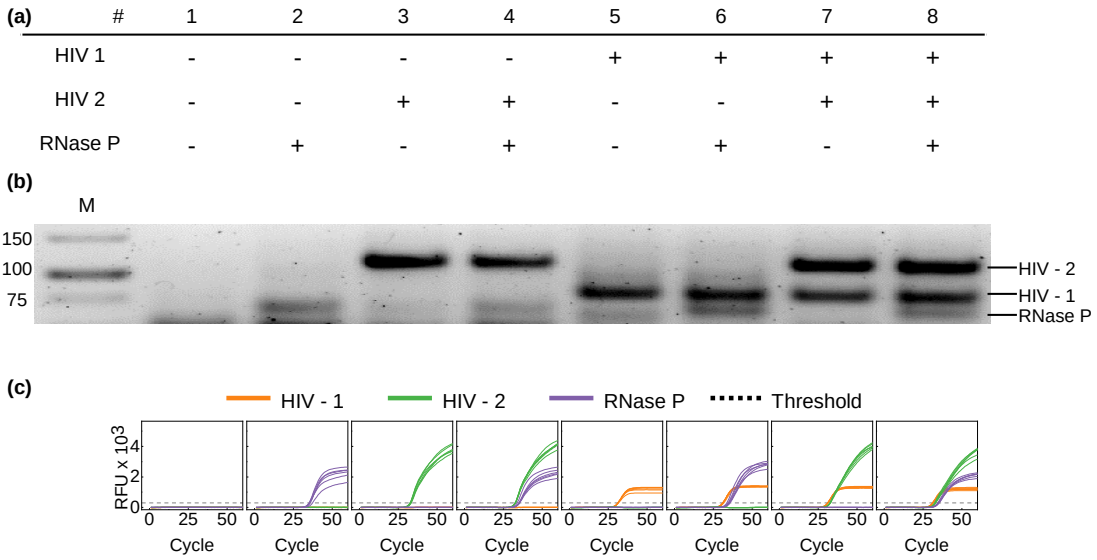

Figure 4-2c shows fluorescence and all experimental samples show a signal above the background threshold representing successful RNA amplification in target selection. This cross-validation not only confirms the accuracy of the gel electrophoresis data but also demonstrates the reliability of the assay under dynamic conditions. Taken together, our results from both basic and advanced analyses strongly indicated that the PCR assay is highly specific with high multiplexing capability, rendering it ideal as a candidate for external integration into portable diagnostic platforms developed against rapid diagnosis of infectious diseases in point-of-care testing formats. This simplification of this assay is a major step forward in molecular diagnostics especially when simultaneous comprehensive detection for multiple viral targets uses to be performed at resource-limited settings.

4.3.3. Analyzer development and sub-module validation

Next, we developed a portable analyzer prototype capable of multiplex RT-PCR amplification and fluorescent signal quantification. **Figure 4-3a** presents the disassembled views of the device. This

portable unit is loaded with an internal lithium-ion battery and Bluetooth wireless technology, bringing together electronic, optical and thermal cycling components at the small lab scale. **Figure 4-4** illustrates a simple block diagram of the entire device as well as a complete flowchart explaining about developing an android GUI. More detailed information on the materials and fabrication processes of the each type of analyzer can be seen in **Table 4-1**. It orients the devices perpendicularly and employs custom-designed circuit boards for heat control & fluorescence. Task results can also be viewed via a custom GUI on mobile phone supporting Bluetooth.

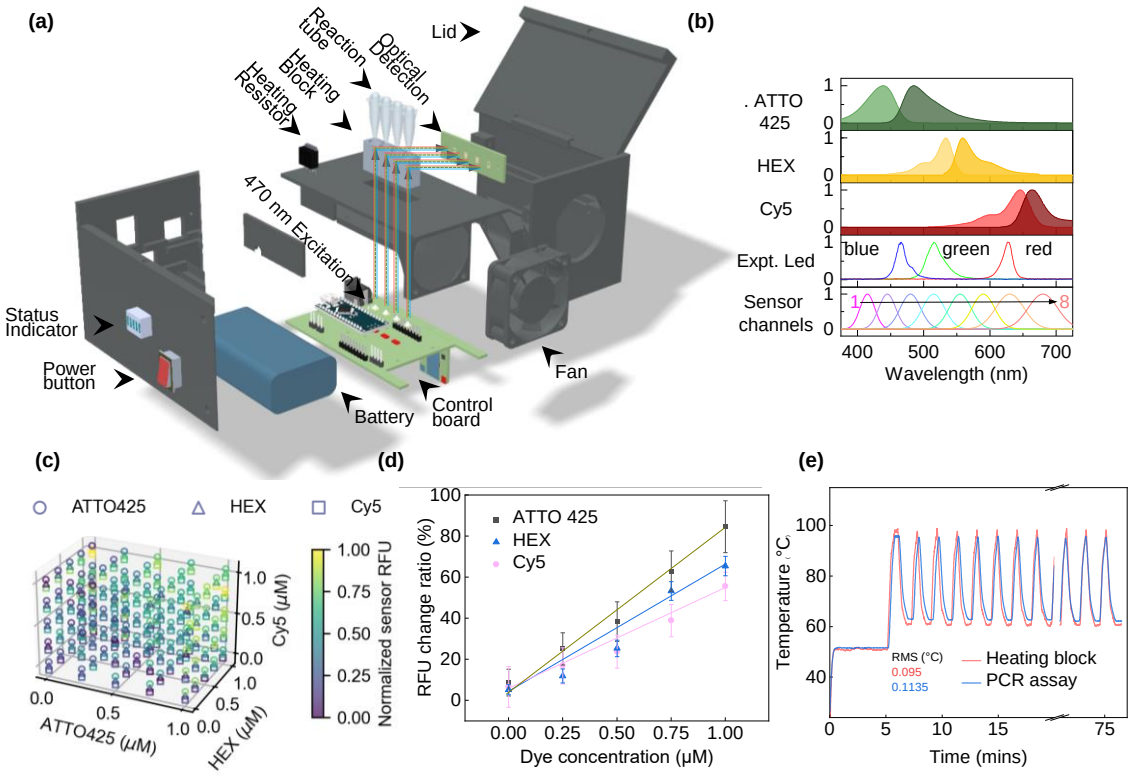

Figure 4-3. The probable PCR analyzer design and its sub module validation. **(a)** Illustrations depict a fully enclosed analyzer and a partial exploded view. The unit features Bluetooth connectivity for wireless data transmission and incorporates integrated optical and thermal cycling subsystems for efficient nucleic acid analysis. It operates on an internal rechargeable battery. **(b)** Presented are the theoretical excitation and emission spectra for three selected fluorophores—ATTO425, HEX, and Cy5—alongside the RGB excitation sources and the sensor's eight distinct detection channels. The blue, green, and red light sources are optimally matched with the excitation spectra of ATTO425, HEX, and Cy5, respectively, while the detection channels 4, 6, and 8 correspond closely with their emission spectra. **(c)** A 3D scatter plot shows normalized sensor RFU

responses to varying concentrations of mixed fluorophores. The plot uses the optimal excitation sources and detection channels noted in (a), with 125 unique combinations of ATTO425, HEX, and Cy5 tested at five concentrations (0, 0.25, 0.5, 0.75, and 1 µM). The visualization highlights the increasing RFU trends correlated with rising fluorophore concentrations, independent of the levels of the other two fluorophores. **(d)** Evaluation of the optical sensor's response to different fluorophores. Each sensor channel demonstrated a linear response across fluorophore concentrations ranging from 0 to 1 µM. Measurements were conducted using a 256X gain, a 154 ms integration time, and 80% PWM for the RGB LED excitation control. **(e)** Temperature profile for the PCR assay's heating block, detailing the stages of heating, incubation, and cooling throughout the PCR cycle.

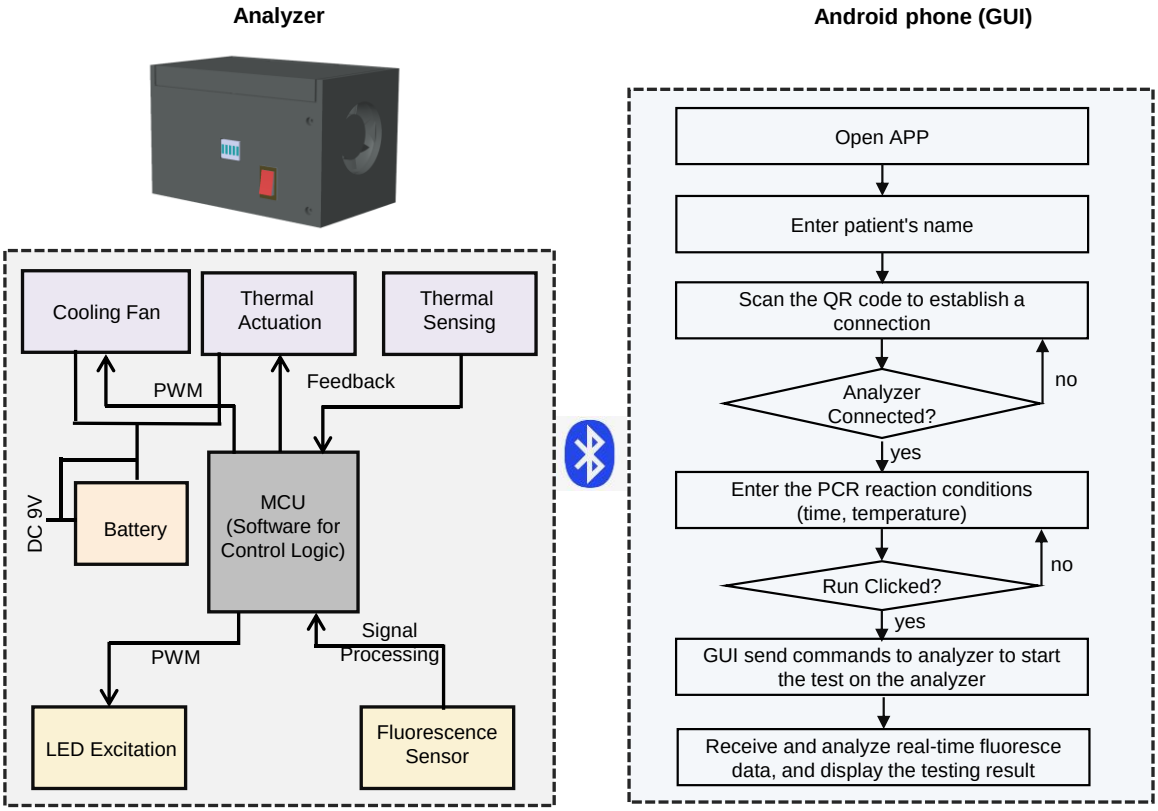

Figure 4-4. A streamlined block diagram illustrates all components of the device. Outputs or actuators include a fan, a resistive heater, an LED for excitation, and a status LED bar. Inputs for feedback comprise a thermistor and an RGB color sensor. At the heart of the system, an Arduino Nano orchestrates the interactions among these modules. The device interfaces with an Android phone through a Bluetooth module, managed via the Arduino IDE. Amplification data is captured in real time, then processed and analyzed offline. This setup has the potential to be integrated with a specifically designed graphical user interface (GUI) for Android, alongside the development process for the Android GUI.

In developing our portable PCR analyzer, achieving precise temperature control and rapid heating and cooling is crucial. We engineered a temperature control module featuring an aluminum heating block with a hollow design to reduce mass and enhance the speed of temperature changes. A 2 Ω power resistor heats the block swiftly, while a fan, paired with ducting and a heat sink, cools it efficiently. The schematic of the thermal module is shown in **Figure 4-5a&b**. Both fan and resistor are controlled via a PID temperature function on an Arduino Nano, powered by a 9V source. **Figure 4-3e** displays the temperature fluctuations throughout the test cycle, monitoring both the block and the fluid temperatures in the PCR assay. Completing the cycle, including reverse transcription, initial denaturation, denaturing, annealing/extending, and 40 cycles, takes about 70 minutes. Our thermal cycling module achieves a maximum heating rate of 1.82°C/second and a cooling rate of 1.31 °C/s, approximately 15 minutes slower than a Bio-Rad benchtop PCR [163]. The RMS for the heating block and PCR assay fluid temperatures are 0.095 and 0.1135, respectively. **Figure 4-5c** illustrates the power profile over a 77-minute test cycle, with a peak power of approximately 30W. The entire test consumes 14.2 Wh of energy, and it can be powered by a 20 Wh EBL rechargeable lithium battery (**Figure 4-5d**). Despite being slower than the Bio-Rad benchtop PCR, our device's simple structure, compact size, and battery operability meet the temperature standards required for PCR reactions, making it valuable in resource-limited settings, particularly in LMICs [112].

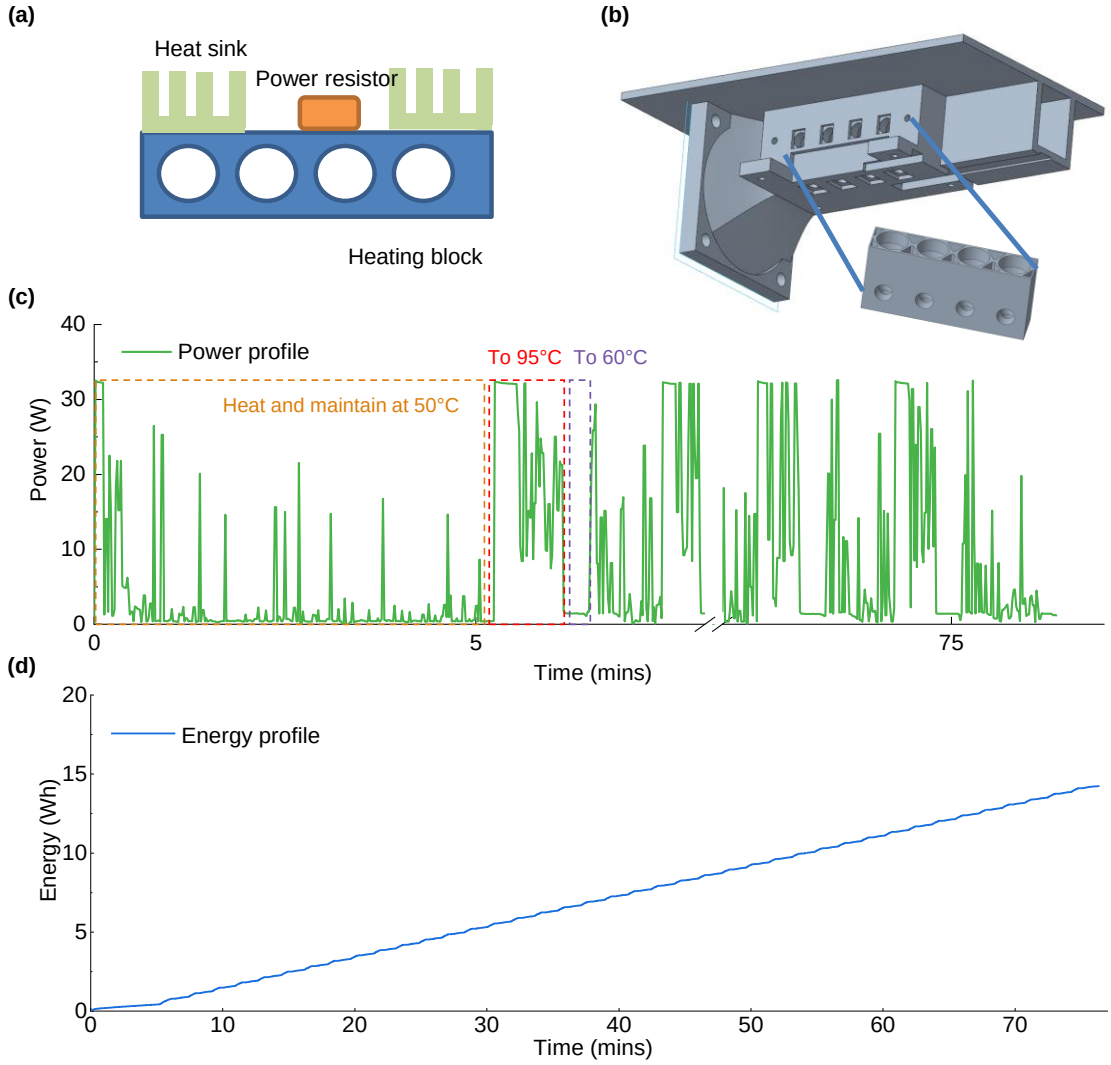

Figure 4-5. (a) Schematic of the thermal module. The thermal module consists of a power resistor as the heat source, a thermistor for temperature feedback, and a CNC-machined aluminum plate designed with hollow sections to reduce weight and enhance heating and cooling efficiency. **(b)** The heating block within the thermal module is positioned in a duct made from ABS plastic, with a fan installed at one end of the duct. The combination of the fan, duct, and power resistor enables rapid heating and cooling. **(c)** Power profile during a 77-minute test cycle. The profile is divided into three sections: the first (yellow) section shows heating from room temperature to 50°C and maintaining this for 5 minutes, the second (red) section represents heating from 50°C to 95°C, and the third (purple) section details cooling from 95°C to 60°C. This is followed by repeated heating and cooling cycles between 95°C and 60°C. **(d)** Energy consumption profile for the entire 77-minute test cycle.

4.3.4. Analyzer analytical evaluation

In order to evaluate the performance of our assay in identifying viral presence over a wide range of clinical and field scenarios, we carried out an extended sensitivity comparison versus standard benchtop PCR utilizing multiplexed HIV-1, HIV-2 detection with RNase P on portable analyzer. The initial phase involved assessing the assay's aptitude to quantify precise RNA levels across a wide range of concentrations, from 1 to 10^5 copies/rnx. As illustrated in **Figure 4-6a**, real-time multiplex RT-PCR trials were conducted on a Bio-Rad desktop PCR analyzer with serial dilutions of synthetic RNA standards, spanning from 10^5 to 0 copies/rnx, each replicated six times across three independent optical channels. This benchmark utilized the Bio-Rad instrument to establish the detection thresholds for each virus, found to be 5 copies/µL for both HIV-1, HIV-2, and the RNase P reference gene. The precision of these conclusions was corroborated by additional analyses. These insights are detailed expansively in **Figure 4-6b**, exhibiting the highly quantitative capabilities of our approach.

To additionally validate the absolute quantification of our portable analyzer systemically, we performed validation measurements across a real-time RT-PCR array panel from various serially diluted RNA samples (**Figure 4-6c**). All concentrations of RNA were performed in triplicate to demonstrate reproducibility (from 10^5 to 0 copies/rnx). Comparative analysis between our portable device and traditional Bio-Rad analyzer demonstrated the amplification curves generated by testing each of RNA type with two systems were identical. Comparing the results (**Figure 4-6d**) gave a correlation coefficient of between 0.96 and 0.99. Meanwhile, the combination of a portable PCR analyzer with an in-house multiplex RT-PCR assay can achieve detection limit up to 10 copies per reaction. These results are evidence of the validity and applicability of our portable PCR with respect to conventional laboratory devices. These results highlight the utility of this analyzer for viral loads in quantitative analysis. Collectively, these findings underscore the superior

performance of our multiplex assay when deployed on our portable analyzer, confirming its suitability for use in a variety of settings, including those with limited resources. The assay's ability to deliver sensitive, specific, and reliable results in a portable format presents significant advantages for on-site diagnostics and real-time monitoring of viral loads. This makes our portable analyzer a crucial tool in the global effort to control and manage HIV, especially in regions where access to traditional lab facilities is constrained.

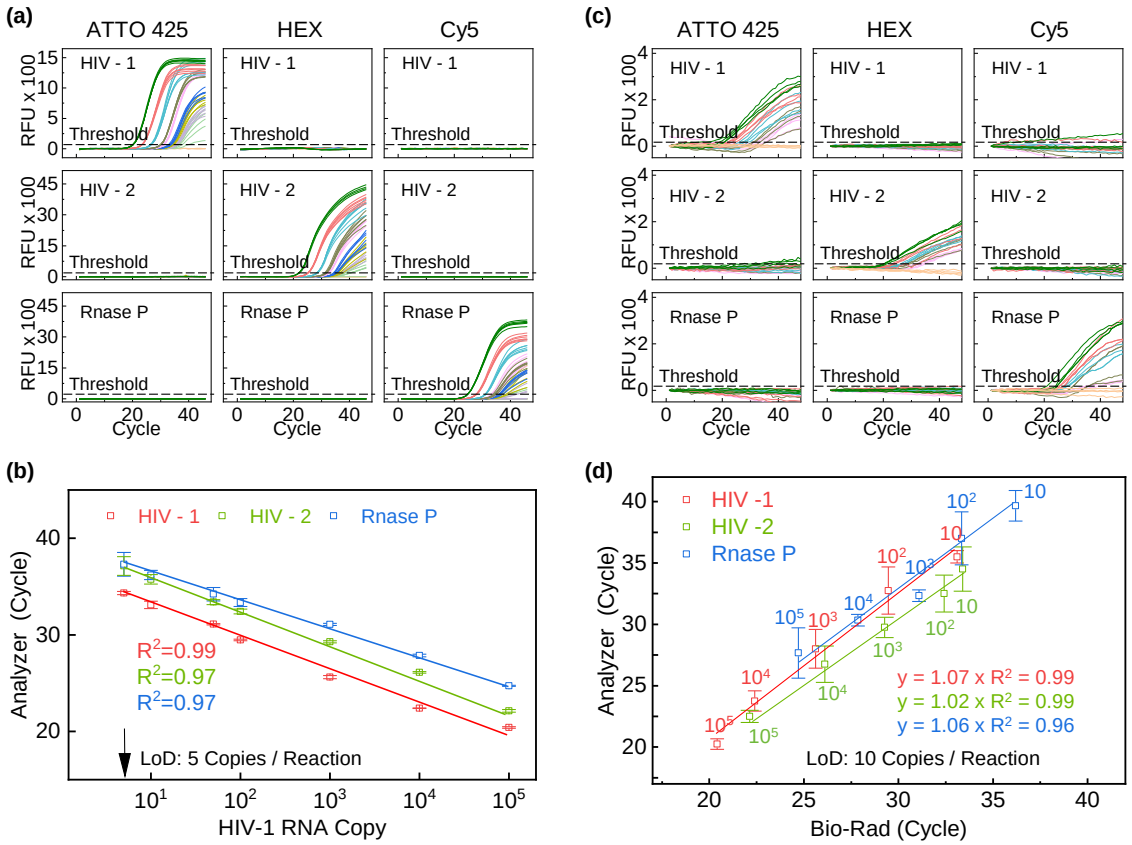

Figure 4-6. Evaluation of Sensitivity and Quantitative Performance of Multiplex RT-PCR Assays Using Bio-Rad Equipment and a Portable PCR Analyzer. **(a)** This figure illustrates the results from real-time multiplex RT-PCR using a Bio-Rad benchtop PCR analyzer with serially diluted RNA standards at concentrations ranging from 10^5 to 0 copies per reaction, replicated six times. Optical detection for HIV-1, HIV-2, and RNase P across three distinct optical channels is shown in three separate columns. **(b)** The graph displays the cycle threshold (Ct) values at varying RNA concentrations for each target. The "Cq values" is marked by the duration required for relative fluorescence units (RFU) to exceed a threshold of 100 (indicated by a dashed line in the plot). **(c)** A panel displaying real-time RT-PCR data from tests on serially diluted RNA, with HIV concentrations from 105 to 0 copies per reaction, each tested in triplicate. Optical signals for the

three targets are again split into three columns. **(d)** A comparative plot shows the Ct values obtained with both the Bio-Rad benchtop PCR analyzer and our portable analyzer for all three targets.

4.3.5. Diagnostic performance from sample to answer

To show the clinical utility of our HIV VL PCR instrument, we subjected a total of 30 archived samples that have been extracted from HIV positive symptomatic subscribers who had already enrolled into one or two programs within Penn State Hershey Medical Center's infectious diseases and consultative services. Multimodal plasma samples of 13 positive HIV-1-negative/2negative individuals at various viral load (VL) levels. Seventeen healthy blood donors were identified as confirmed HIV-1 and HIV-2 negative by Roche COBAS® AmpliPrep. Given the lack of clinical samples from HIV-2-infected patients, we spiked extracted RNA with synthetic HIV-2 RNA to mimic the setting in which such infections could occur and reproduce this challenging situation within our study.

We compared our HIV VL PCR device with a conventional benchtop RT-PCR by testing two identical samples with both methods to evaluate consistency. Further, traditional centrifugation methods were employed for RNA extraction, followed by RT-PCR testing on these samples to assess our device's performance agreement with the benchtop RT-PCR. Each analysis utilized an identical volume of 25 µL, though the benchtop RT-PCR employed a column-based extraction method. **Figure 4-7** displays the real-time RT-PCR results of these clinical samples alongside six concentration references for quantification. This figure also includes a calibration curve, illustrating the robustness of our testing approach. **Figure 4-9&Figure 4-10** display the optical signals obtained from 30 clinical samples processed through our portable centrifuge RNA extraction module, as detected in the HIV VL PCR device. The signals for HIV-1, HIV-2, and RNase P, derived from three distinct optical channels, are consolidated into a unified figure. Additionally,

Figure 4-11 features RT-PCR analysis results from our HIV VL PCR device for a cohort of 30 clinical samples, encompassing both positive and negative outcomes. **Figure 4-8a** presents a detailed qualitative and quantitative analysis of HIV-1, HIV-2, and RNase P results from both the benchtop RT-PCR and our device. White boxes highlight samples from uninfected individuals or those successfully undergoing antiretroviral therapy (ART) with a fully suppressed viral load within the safe threshold (Low: 0 - 1,000). Light red or green boxes denote samples with viral loads exceeding safe limits, indicating a need for enhanced medical oversight(Medium: 1,000 - 20,000). Dark red or blue boxes reveal a significantly higher viral load, signaling potential treatment failure and a risk of viral rebound despite ongoing ART(High: > 20,000 copies/mL)[113], [114]. A heatmap on the right side of the figure provides reference values to further guide interpretation.

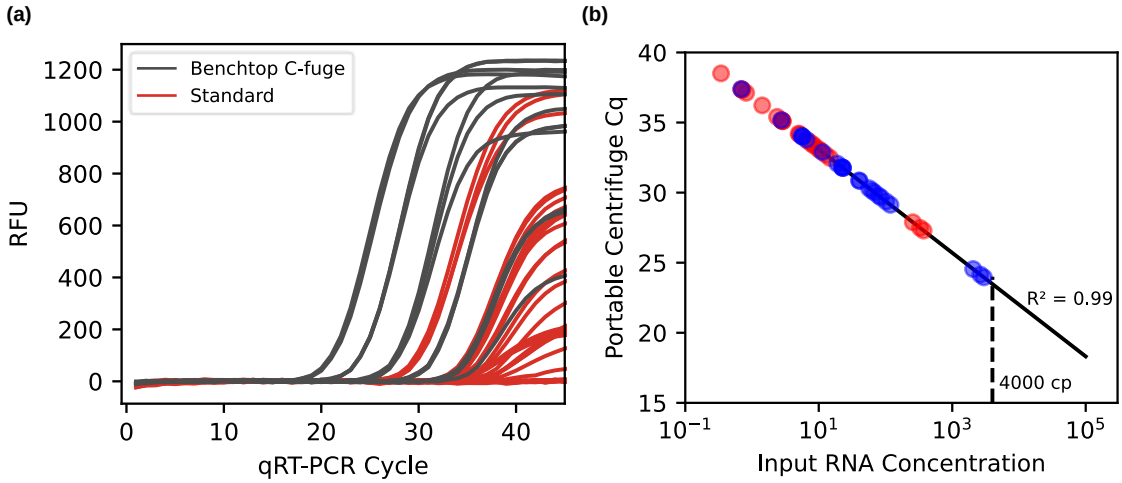

Figure 4-7. (a) Data from real-time HIV-1 RT-qPCR amplification is presented. The solid line represents the reference reaction with known copy numbers, while the dashed line signifies RNA extracted using the lab-based protocol. **(b)** RT-PCR fitted reference line was generated to quantify the copy numbers of extracted RNA. The blue dots indicate the reference reaction with known copy numbers. The red dots represent RNA extracted using the lab-based protocol.

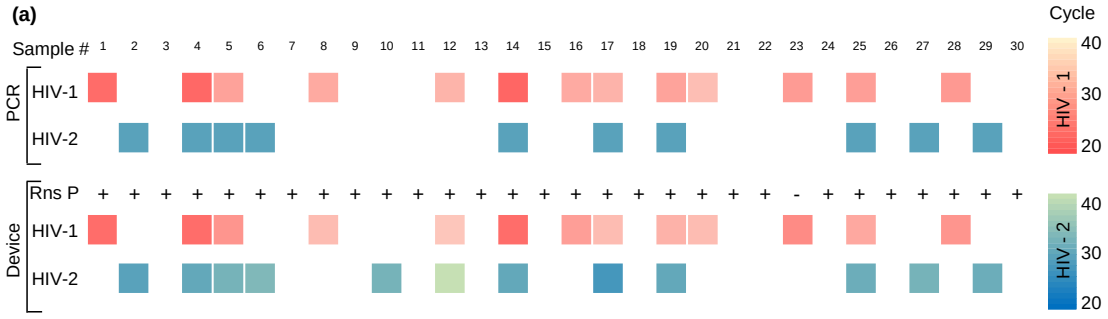

(b)

	Sensitivity	Specificity	Accuracy	Valid Rate
HIV - 1	100 %	100 %	100 %	96.0 %
HIV - 2	100 %	90.91%	93.75 %	

Figure 4-8. Evaluation of Clinical Samples with Our Device. **(a)** Validation with Constructed Clinical Samples in a Blind Test. RNA from HIV-1 and RNase P was extracted from the plasma of 30 patients utilizing our centrifuge-based portable RNA extraction device. After sample preparation, HIV-2 RNA was introduced to the extracted RNA. Qualitative analysis for RNase P and quantitative analyses for HIV-1 and HIV-2 were performed using our device and a Bio-Rad benchtop PCR system. A heat map displays the Ct values from the quantitative analyses of HIV-1 and HIV-2. **(b)** Diagnostic Performance Overview: This table displays the performance metrics of our system, including Sensitivity, Specificity, Accuracy and Valid Rate for HIV-1, HIV-2, and RNase P.

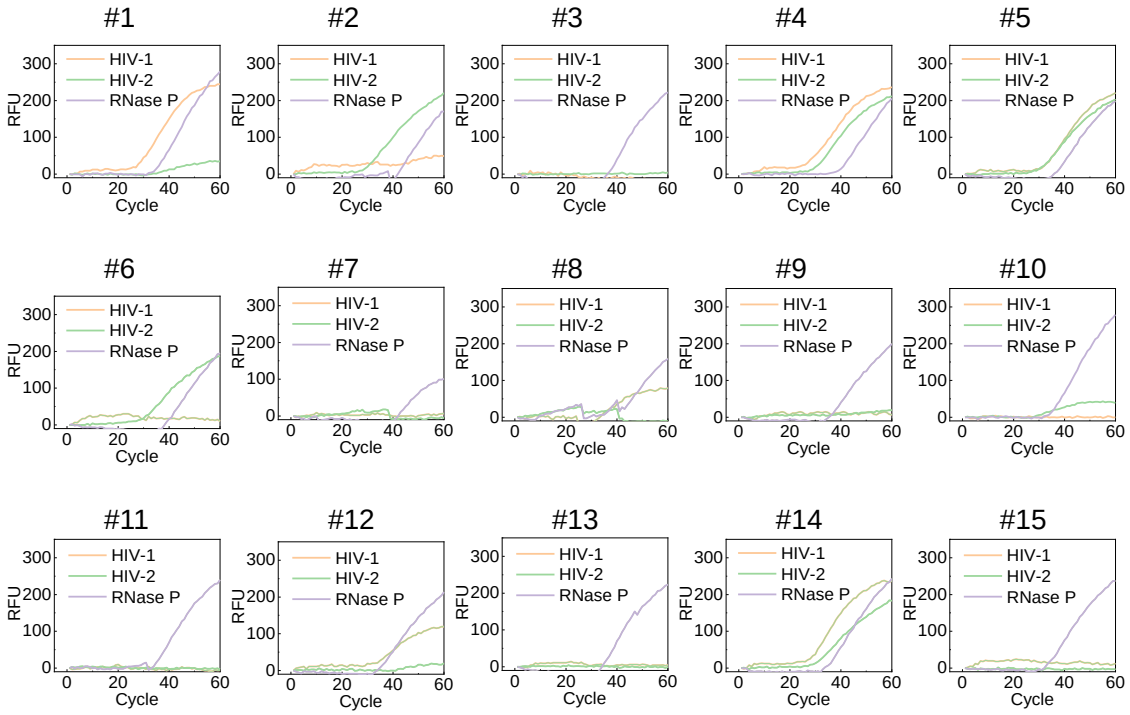

Figure 4-9. The real-time RT-PCR curves for first 15 of 30 clinical samples tested with our device

are presented. Each set includes curves for HIV-1, HIV-2, and RNase P from three separate optical channels.

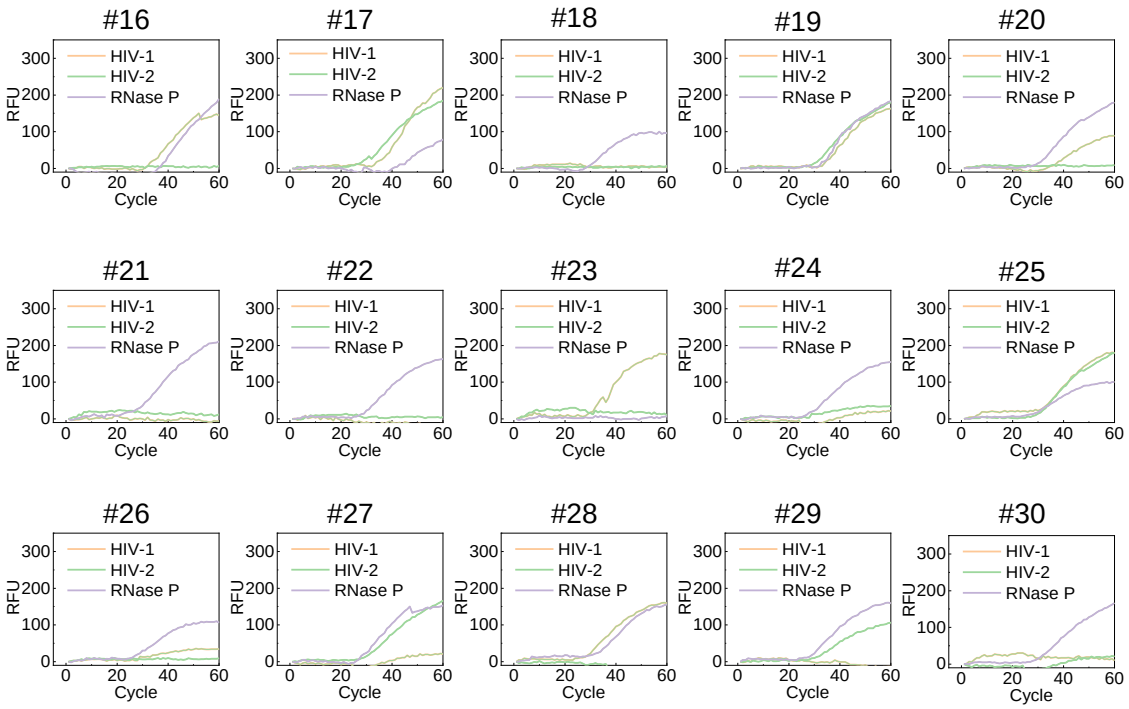

Figure 4-10. The real-time RT-PCR curves for second 15 of 30 clinical samples tested with our device are presented. Each set includes curves for HIV-1, HIV-2, and RNase P from three separate optical channels.

	#1	#2	#3	#4	#5	#6	#7	#8	#9	#10
Expect (Cycles) or (P/N)										
HIV-1	27.88	N	N	27.48	33.35	N	N	34.17	N	N
HIV-2	N	29	N	29	29	29	N	N	N	N
Rnase P	P	P	P	P	P	P	P	P	P	P
Resule (Cycles) or (P/N)										
HIV-1	28	N	N	28	32	N	N	36	N	N
HIV-2	N	29	N	30	32	33	N	N	N	32
Rnase P	P	P	P	P	P	P	P	P	P	P

	#11	#12	#13	#14	#15	#16	#17	#18	#19	#20
Expect (Cycles) or (P/N)										
HIV-1	N	35.17	N	27.29	N	34.21	35.09	N	33.48	36.23
HIV-2	N	N	N	29	N	N	29	N	29	N
Rnase P	P	P	P	P	P	P	P	P	P	P
Resule (Cycles) or (P/N)										
HIV-1	N	37	N	28	N	33	36	N	35	36
HIV-2	N	49	N	30	N	N	27	N	30	N
Rnase P	P	P	P	P	P	P	P	P	P	P

	#21	#22	#23	#24	#25	#26	#27	#28	#29	#30
Expect (Cycles) or (P/N)										
HIV-1	N	N	32.7	N	32.99	N	N	32.47	N	N
HIV-2	N	N	N	N	29	N	29	N	29	N
Rnase P	P	P	P	P	P	P	P	P	P	P
Resule (Cycles) or (P/N)										
HIV-1	N	N	31	N	34	N	N	32	N	N
HIV-2	N	N	N	N	31	N	32	N	31	N
Rnase P	P	P	N	P	P	P	P	P	P	P

Figure 4-11. The quantification cycle (Cq) values for HIV-1 and HIV-2 from **Figure 4-6**, obtained using benchtop PCR, are presented as expected cycles. The clinical samples also contain RNase P, indicated as positive ("P") in the expected positive/negative (P/N) values. The data from **Figure 4-9** & **Figure 4-10** are used to convert these findings into Cq values for HIV-1, HIV-2, along with their respective positive or negative conclusions for RNase P.

Figure 4-8b, which serves as a table, summarizes the Diagnostic Performance of our device. We carefully compared the Cq values from our device with those from the benchtop PCR to evaluate our analyzer's capabilities in quantitative viral load analysis. Our device incorporates a quality control method to eliminate invalid tests, achieving a high testing validity rate of 96%. For HIV-1 and HIV-2, the sensitivity was 100% and 100%, specificity was 100% and 90.91%, and accuracy was 100% and 93.75% respectively, confirming that our device performs on par with traditional laboratory protocols using benchtop RT-PCR. These findings robustly support the implementation

of our innovative point-of-care platform in settings where precise and reliable HIV viral load testing is essential.

4.4. Summary

In conclusion, our research introduces a pioneering multiplex PCR-based device specifically engineered for effective HIV-1 and HIV-2 viral load testing in resource-limited settings. This portable and battery-operated system overcomes significant logistical and technical challenges by offering high levels of sensitivity and specificity, essential for managing HIV effectively. Demonstrating a sensitivity of 100% for both HIV-1 and HIV-2, and a specificity of 100% for HIV-1 and 90.91% for HIV-2, our device sets a new benchmark in the field of HIV diagnostics. Furthermore, the device successfully achieved a diagnostic accuracy of 100% for HIV-1 and 93.75% for HIV-2, confirming its reliability and effectiveness in a range of testing environments. The entire testing process can be completed in approximately 60 minutes, offering a significant time advantage over traditional lab-based tests. Moreover, the cost per test has been reduced to under $10, making it financially accessible for widespread deployment in low-resource settings. These performance metrics and cost-efficiency are critical for enhancing access to vital health metrics, supporting ongoing treatment efforts, and aligning with global health initiatives like the 95-95-95 targets set by the World Health Organization. The device's ability to deliver rapid, robust, and accurate viral load results directly at the point-of-care marks a substantial advancement in HIV management, particularly in low-resource settings where traditional testing facilities are not readily accessible. The potential of this technology to transform HIV diagnostics and treatment in these regions is immense, underscoring the vital role of innovative diagnostic solutions in combating the global HIV/AIDS epidemic.

CHAPTER 5 Portable Multiplex Rapid PCR Device for Simultaneous Self-Testing Detection of HIV and HCV Viral Loads

5.1. Introduction

Human Immunodeficiency Virus (HIV) and Hepatitis C Virus (HCV) are both global public health challenges with significant implications for individual and community health [164]–[166]. While both conditions are manageable with modern medicine—HIV through Antiretroviral Therapy (ART) and HCV through Direct-Acting Antivirals (DAAs)—effective management critically depends on accurate and timely viral load (VL) testing [3], [167]. Such testing is integral not only for initiating treatment but also for monitoring disease progression and treatment efficacy [129], [168]. For HIV, the global health community has set ambitious targets known as the 95-95-95 goals, which aim to diagnose 95% of all HIV-positive individuals, provide ART for 95% of those diagnosed, and achieve viral suppression for 95% of those treated by 2030 [130]. Goals for HCV elimination include a 90% reduction in new cases and a 65% reduction in deaths by 2030, underscoring the need for widespread access to effective diagnostic tools [169].

The intersection of HIV and HCV infections is particularly problematic due to the frequency of co-infections, which complicate treatment and disease management strategies significantly [170]. Indeed, individuals can be co-infected with HIV (Human Immunodeficiency Virus) and HCV (Hepatitis C Virus), a situation known as co-infection, which is relatively common among certain populations, especially among those who inject drugs [171]. Both viruses can be transmitted via blood, which is why this group is particularly at risk [172]. Additionally, co-infection can also occur among HIV-positive individuals who engage in unprotected sexual activities or those who

have been exposed to infected blood through other means [173]. The common routes of transmission for both viruses mean that co-infections are not rare, and their management requires well understanding and approaches [174]. The health impacts of co-infection are more severe because HIV weakens the immune system while HCV primarily affects the liver [175]. The presence of HIV can accelerate the progression of liver disease caused by HCV, increasing the risk of cirrhosis and liver cancer [176]. Therefore, managing co-infection requires special monitoring and treatment strategies to control the impact of both viruses while minimizing their damage to the body [177]. Simultaneous testing for HIV and HCV viral loads is important because coinfection with these viruses is common in high-risk populations, and coinfection can exacerbate disease progression and complications. By testing both viruses simultaneously, healthcare providers can better select and adjust treatment regimens, monitor treatment efficacy, and prevent the development of viral resistance. This approach also enhances public health control measures, leading to more comprehensive management of patient health. Typically, this approach requires patients to visit hospitals or healthcare facilities to collect samples, which are then sent to a central lab equipped with complex machinery and specialized personnel [78]. The traditional approach has significant drawbacks, including long feedback times that do not meet the need for timely results. In many resource-limited areas, the absence of reliable electricity makes it impossible to deploy central labs with complex machinery. Additionally, privacy concerns lead people to prefer home testing over hospital visits. Therefore, developing methods for rapid viral load measurement based on self-testing in resource-limited areas is a significant problem that needs addressing.

POCT devices, especially those using PCR for their accuracy and reliability, can play a critical role in various environments, enhancing the efficiency of immediate health surveillance and management, addressing issues of long feedback times, lack of infrastructure in resource-limited

areas, and privacy concerns with home testing [16]. Devices must be economical, sensitive, specific, user-friendly, and operable by non-professionals, as well as adaptable, compact, portable, and independent of complex power sources, handling varying power in clinics and using rechargeable batteries for home testing [23]–[27]. Although there are existing commercial point-of-care (POC) devices, such as the Combiquic device [178], that provide rapid and accessible testing solutions, there are also technologies like the Triplex HIV/HCV/HBsAg self-test by Biosynex [179]. Originally designed for professional use, this test has been adapted for individual self-testing. Concurrently, research into the development of POC testing for HIV and HCV viral load measurement is ongoing [17], [44], [88]–[94], [145]–[153]. However, the utilization of these devices is hindered by several factors: the complexities involved in processing whole blood samples, the lack of capability for conducting quantitative analysis in a single step, and difficulties in detecting HIV and HCV infections concurrently, as well as incorporating quality control measures in the testing process [17]–[22]. Consequently, developing point-of-care testing devices that can simultaneously measure HIV and HCV viral loads for self-testing which can be used by lay person in resource-limited settings is crucial for filling a significant gap in current healthcare surveillance technologies.

In this work, we have developed a novel, battery-operated multiplex PCR system, integrated with our previously developed portable sample preparation module, specifically optimized for home self-testing to simultaneously determine the viral loads of HIV and HCV. It incorporates a control test to ensure accuracy and features a three-channel detection system that precisely measures viral loads—essential for monitoring disease progression and tailoring treatment strategies effectively. The device achieves an RNA extraction efficiency of 80% using a compact sample preparation unit that accurately processes viral RNA. Its semi-automated capabilities allow it to handle multiple samples at once, increasing efficiency while reducing human error, thus

delivering consistent results. Our system provides concurrent measurements of viral loads for HIV and HCV. The novel portable PCR system, when compared to the Bio-Rad benchtop PCR, demonstrates correlation coefficients between 0.96 and 0.99. This highlights the accurate and reliable performance of our portable system in comparison to the traditional benchtop equipment. These performance figures underscore the device's reliability in detecting both HIV and HCV across different infection stages, making it a critical tool in bridging the current gap in VL testing options for home-based self-testing. This breakthrough is crucial for the effective management and prevention of HIV and HCV globally, including handling co-infections, thereby marking a significant step forward in the development of technologies for managing sexually transmitted diseases.

5.2. Methods

5.2.1. Materials and chemicals

Materials for this study were obtained from several suppliers. The RNA extraction kits, particularly the QIAamp Viral RNA Mini Kit (catalog number 52904), are detailed in **Table 5-1** Components for the HIV analyzer, including electronic and optical parts, were purchased from DigiKey, as noted in **Table 5-2** RT-PCR primers and probes were procured from IDT, while necessary reagents and chemicals were sourced from Sigma-Aldrich and Thermo Fisher Scientific. Assay validation was conducted using the Bio-Rad CFX96 system. Viral RNAs for HIV-1, HCV, and RNase P, with catalog numbers VR-3245SD, VR-3233SD, and 1006626 respectively, were supplied by ATCC. Clinical HIV samples came from the Penn State Hershey Medical Center. All materials were used as received and stored following the manufacturers' instructions.

Table 5-1. Bill of materials of the analyzer

System	Description	Part#	Function	Unit Cost ($)	Unit Qty.	Ext. Cost ($)
Electronics	Arduino Nano	7630049200173	Microcontroller	6.00	1	6.00
Electronics	Adafruit Bluefruit LE SPI	2633	Bluetooth Low Energy	14.00	1	14.00
Electronics	Capacitor 10uF	P10425CT	Power stabilizing	0.147	1	0.15
Electronics	DC Barrel Power Jack/Connector	PRT-00119	Power Connector	1.25	1	1.25
Electronics	36-pin stripe male header	392	Headpins	4.95	0.1	0.50
Thermal	Aluminum CNC block	CP-0.91-0.91	Heating Stage	5.75	0.25	1.44
Thermal	2Ω Power Resistor	MP725-2.00-FCT	Heater	7.01	1	7.01
Thermal	SMD Resistor, 1kΩ	311-1.00KHRCT	Temperature/EM control	0.0072	1	0.01
Thermal	Thermistor	235-1057	Temperature sensing	3.5	1	3.50
Thermal	SMD Resistor, 10kΩ	RNCP0603FTD10K0CT	Temperature control	0.1	1	0.10
Thermal	N Channel Power MOSFET	DMN1019USN-7DICT	Switch for heater and fan	0.354	2	0.70
Thermal	FAN AXIAL 40X15MM 12VDC	603-1006-ND	Fan for colling	8.86	1	8.86
Optics	Res Cermet Trimmer 500K ohm	3296W-1-501RLF	Adjust LED intensity	0.6	3	1.80
Optics	SMD Resistor, 1kΩ	RNCP0805FTD1K0CT	Optical module	0.0277	3	0.08
Optics	SMD Resistor, 10kΩ	RNCP0805FTD10K0CT	Optical module	0.0277	8	0.22
Optics	IC Color Sensor	AS7341	Optical detection	3.00	3	9.00
Optics	SMD LED, Blue	1497-1138-1	Fluorescence excitation	0.528	3	1.58
Optics	Capacitor 10uF	P10425CT	Power stabilizing	0.147	3	0.44
Optics	Capacitor 0.1uF	P01425CT	Power stabilizing	0.147	1	0.15
Optics	Voltage Regulator	AP7312-3.3/1.8	Power supplier	0.8	1	0.80
Optics	I2C Multiplexer	TCA9548A	I2C expender for sensor	1.10	1	1.10
Enclosure	ABS Filament (Black)	-	3D platform material	69.00	0.05	3.45
Enclosure	Screws (M2 cap screw)	91290A015	Assembly	0.14	10	1.40
			Total Cost			**$63.54**

Table 5-2. Cost per test

Reagents	Vendor	Function	Stock Vol (mL)	Unit Cost ($)	Volume (μL)/rxn	Ext Cost/rxn
RT-LAMP Mixes	Meridian Life Science	LAMP master mix	5	198	6.25	0.2475
HIV-1 Forward	IDT	PCR master mix	0.856	12.05	0.4	0.00563
HIV-1 Reverse	IDT	PCR master mix	0.67	9.15	0.4	0.00546
HIV-1 Probe	IDT	PCR master mix	0.185	381	0.4	0.82378
HCV Forward	IDT	PCR master mix	0.697	9.64	0.4	0.00553
HCV Reverse	IDT	PCR master mix	0.87	10.60	0.4	0.00487
HCV Probe	IDT	PCR master mix	0.201	311	0.4	0.61891
RnaseP Forward	IDT	PCR master mix	0.763	9.15	0.4	0.0048
RnaseP Reverse	IDT	PCR master mix	0.68	9.64	0.4	0.00567
RnaseP Probe	IDT	PCR master mix	0.231	284	0.4	0.49177

Lysis Buffer	Invitrogen	Sample Prep.	25	6	200	0.02
Wash Buffer	Invitrogen	Sample Prep.	37.5	54	500	0.12
Elution Buffer	Invitrogen	Sample Prep.	11	35	30	0.1
Ethanol	Sigma-Aldrich	Sample Prep.	100	10	200	0.02
Material	**Vendor**	**Function**	**Stock Vol (sq. m.)**	**Unit Cost ($)**	**Volume (sq. mm)/rxn**	**Ext Cost/rxn**
Vivid PSM-GR	Pall Corporation	PSM card	0.06	30.00	200	0.30
Silica column	Qiagen	RNA extraction		2.00	1	2.00
PCR tube		Fisher scientific		0.01	1	0.01
					Total	**$4.28**

5.2.2. Multiplex RT-PCR reaction

In this research, we utilized a dual-enzyme, one-step RT-PCR technique to detect HIV-1. The reaction mixture, totaling 20 µL, included 5 µL of TaqMan Fast Virus 1-Step Master Mix, forward and reverse primers (each at a 1 µM concentration), a probe (1 µM), 1 µL of RNA templates, and 11 µL of PCR-grade water. The assay employed a validated set of HIV-1 RT-PCR primers. The RT-PCR protocol involved specific thermal conditions: an initial reverse transcription step at 50 ℃ for five minutes to convert HIV-1 RNA into cDNA, followed by a denaturation phase at 95 ℃ for 20 seconds, and then 40 cycles of amplification. Each amplification cycle comprised a 3-second denaturation at 95 ℃ and a 30-second annealing and extension at 60 ℃. Details of the primers and probes are provided in **Table 5-5, Table 5-6, Table 5-7**. The reporters used in our experiment were ATTO425, HEX, and Cy5.

5.2.3. Statistical analysis

For this study, all statistical analyses and regression modeling were executed utilizing MATLAB R2020 software (Natick, MA). Data visualization, including all figures and plots, was also primarily performed with MATLAB, supplemented by Microsoft PowerPoint for layout adjustments and final presentations. Each plot displayed in the results represents the average value (mean) accompanied by three standard deviations. These measurements were consistently derived from three separate tests (triplicates) to ensure reliability unless otherwise indicated. This standard approach was maintained across all experimental conditions to facilitate accurate comparison and reproducibility of the data. The use of MATLAB was integral not only for the initial data processing but also for the subsequent analysis stages, ensuring a seamless workflow from data collection to visualization.

5.3. Results and discussion

Overall workflow **Figure 4-1a** shows the comprehensive diagnostic procedure for measuring viral loads of HIV and HCV. This process is divided into two main stages: sample preparation and RNA detection. Initially, RNA is extracted using a portable centrifuge and a plasma separation module we previously developed. Subsequently, the extracted RNA is transferred into a test tube filled with RT-PCR reagents for amplification and detection. This step is vital for determining the viral load and infection status based on the quantification cycle (Cq) values. A notable innovation in this protocol is the substantial reduction in time required for point-of-care (POC) self-testing applications. Traditional protocols typically take 70 minutes, but our enhanced ultrafast protocol completes the PCR amplification in just 45 minutes. This acceleration is achieved by reducing the reverse transcription time from 5 to 3 minutes, the qPCR activation phase from 3 minutes to 1

minute, and shortening the denaturation and extension phases from 3 seconds and 30 seconds to 1 second each, respectively. The streamlined and rapid workflow of this portable PCR device underscores its potential for wide application in various settings, particularly in resource-limited environments. By enabling accurate, rapid, and user-friendly self-testing, the device addresses the critical need for effective point-of-care diagnostics, enhancing the management and monitoring of HIV and HCV infections globally.

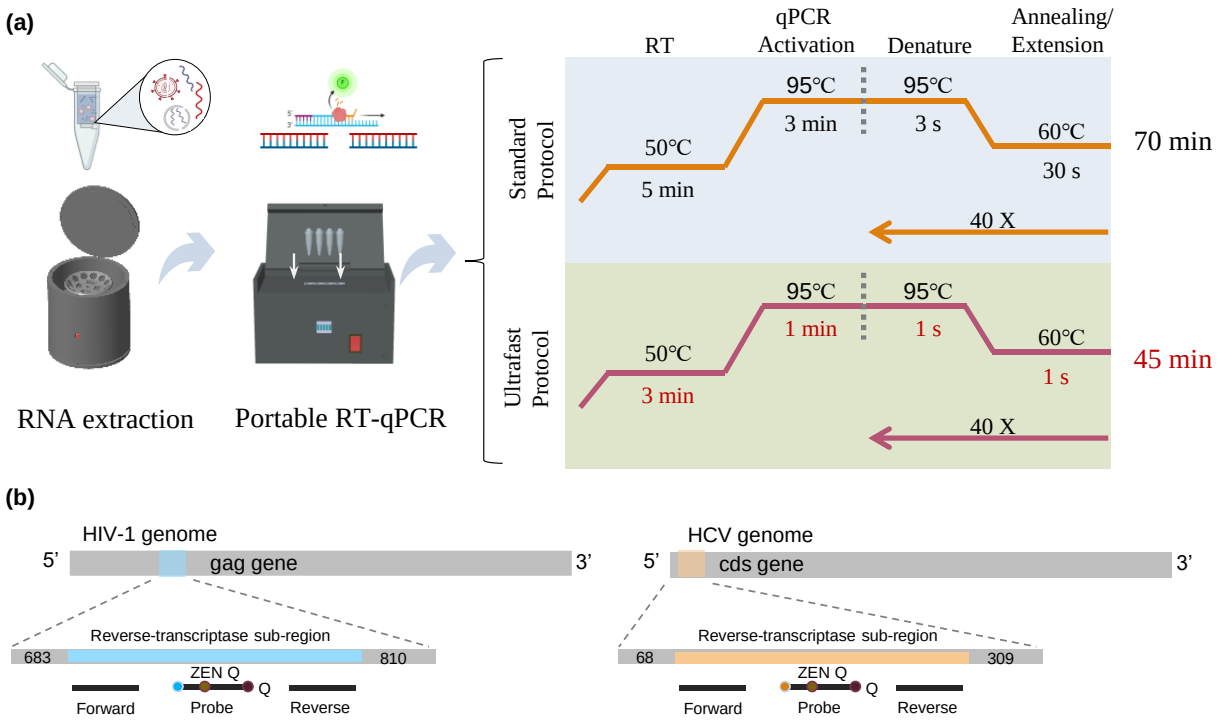

Figure 5-1. Overall Device Workflow and Assay Design. **(a)** Overview of the workflow for the portable rapid qRT-PCR, juxtaposed with the conventional qRT-PCR process for detecting HIV and HCV, starting from plasma samples to final results. **(b)** Primer design for HIV-1 and HCV, incorporating two RT-PCR primers and a single probe per virus, specifically targeting the initial segment of the gag gene in HIV-1 and the cds gene in HCV.

5.3.1. Multiplex PCR assay specificity

For the multiplex assay designed to detect HIV-1, HCV, and RNase P, we crafted specific primer-probe sets for each target. The assay employs two reverse transcription PCR (RT-PCR) primers and a single fluorescent probe for each virus, targeting the initial segments of the HIV gag gene and the HCV cds gene as shown in **Figure 4-1b**. The primer-probe sets for HIV-1 and HCV target highly conserved regions within the reverse-transcriptase sub-regions, as detailed in **Table 5-3** & **Table 5-4**. These regions were chosen for their high conservation across various strains, ensuring broad detection capabilities. Additionally, a distinct set of primers and a probe for RNase P were developed to serve as an internal control, confirming the efficacy of the RNA extraction and the overall reliability of the assay. The primer and probe sets were meticulously optimized to operate under identical thermal cycling conditions, enabling simultaneous amplification and detection in a unified reaction mixture. To enhance the specificity and accuracy of our assay, it was engineered to produce target-specific signals confined to distinct optical channels. This specificity is crucial for minimizing cross-reactivity among the targets, thus significantly improving the diagnostic precision of our method. This multiplex technique not only boosts efficiency but also reduces the time and costs associated with diagnosing HIV infections. The PCR assay employs 6 primers and 3 probes, with the design specifics detailed in **Table 5-5, Table 5-6, Table 5-7**.

Table 5-3. Reverse-transcriptase sub-region targeting HIV-1

Sequence (5' → 3')
tctcgacgcaggactcggcttgctgaagcgcgcacggcaagaggcgaggggcggcgactggtgagtacgccaaaaattttgactagc ggaggctagaaggagagagatgggtgcgagagcgtcagta

Table 5-4. Reverse-transcriptase sub-region targeting HCV

Sequence (5' → 3')

gcagaaagcgtctagccatggcgttagtatgagtgtcgtgcagcctccaggacccccccctcccgggagagccatagtggtctgcggaa
ccggtgagtacaccggaattgccaggacgaccgggtcctttcttggataaaacccgctcaatgcctggagatttgggcgtgcccccgca
agactgctagccgagtagtgttgggtcgcgaaaggccttgtggtactgcctgatagggtgcttgcg

Table 5-5. RT-qPCR primer set targeting HIV-1

Primer	**Sequence (5' → 3')**
Forward	TACTGACGCTCTCGCACC
Reverse	TCTCGACGCAGGACTCG
Probe	ATTO425-CTCTCTCCTTCTAGCCTC

Table 5-6. RT-qPCR primer set targeting HCV

Primer	**Sequence (5' → 3')**
Forward	GCAGAAAGCGTCTAGCCATG
Reverse	CGCAAGCACCCTATCAGG
Probe	HEX-CATAGTGGTCTGCGGAACCG

Table 5-7. RT-qPCR primer set targeting Rnase P

Primer	**Sequence (5' → 3')**
Forward	AGATTTGGACCTGCGAGCG
Reverse	GAGCGGCTGTCTCCACAAGT
Probe	Cy5-TTCTGACCTGAAGGCTCTGCGCG

To test the specificity and multiplexing abilities, we conducted a series of experiments with eight synthetic RNA samples representing HIV-1, HIV-2, and RNase P. These samples varied in RNA concentration from none to 1000 copies per reaction, arranged in a serial dilution to methodically assess the assay's performance, as depicted in **Figure 5-2a** Post-amplification, the samples were analyzed through agarose gel electrophoresis, with results shown in **Figure 5-2b** After 60 PCR

cycles, clear bands at specific base pair lengths indicated successful amplification. Lanes 2, 3, and 5 showed single bands for each target respectively, whereas lanes 4, 6, and 7 displayed dual bands, confirming co-amplification of targets. Lane 8 was notable for showing multiple bands, demonstrating the assay's capability for multiplex detection. Lane 1, the no-template control, confirmed no contamination. These results were further validated by real-time PCR analysis over 60 cycles, shown in **Figure 5-2c**, where all samples except the no-template control displayed fluorescence intensities indicating successful RNA amplification. This dual-validation emphasizes the reliability and dynamic capabilities of our assay. The comprehensive data supports the assay's high specificity and effective multiplexing, making it an excellent choice for integration into portable diagnostic platforms for quick and precise detection in resource-limited environments.

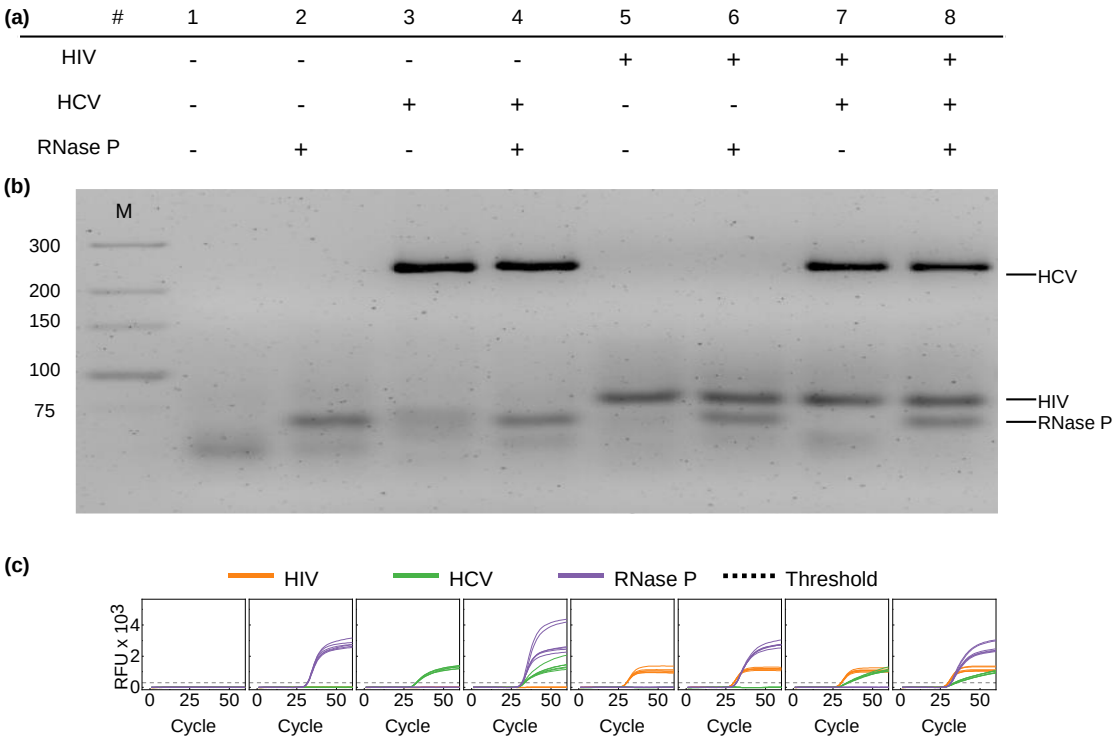

Figure 5-2. Evaluation of the specificity for a multiplex RT-PCR protocol. **(a)** Samples numbered 1 to 8 were prepared using synthetic RNA sequences of HIV, HCV, and RNase P, with each marked as positive or negative ("+" or "-"). The viral RNA concentrations in these samples varied from 0 to 1000 copies per reaction. **(b)** The RT-PCR outputs were examined via agarose gel electrophoresis, showing the amplification patterns for Samples 1 through 8. Each sample

underwent six rounds of testing. **(c)** The data from real-time multiplex RT-PCR, performed using a Bio-Rad desktop PCR analyzer for Samples 1 to 8, are shown. Optical readings for HIV, HCV, and RNase P were captured from three separate optical channels and consolidated into a composite image.

5.3.2. Rapid PCR speed limitation

To further refine our investigation of the rapid PCR speed limit, we hypothesized that the duration of incubation significantly impacts reaction efficiency. Enzymatic kinetics, particularly for reverse transcriptase and DNA polymerase, are highly sensitive to both time and temperature. Shortening RT and qPCR activation times could risk incomplete template synthesis and primer annealing, potentially compromising amplification efficacy.

To address these concerns and validate our hypothesis, we explored the impact of thermal speed on PCR efficiency by systematically varying the incubation times for RT, qPCR activation, and denaturation and extension phases. We conducted three sets of experiments: In the first set, we fixed the RT time at 5 minutes and qPCR activation at 3 minutes, varying the denaturation and extension times from 3s/3s to 2s/2s, and finally to 1s/1s. In the second set, we controlled the qPCR activation and denaturation/extension parameters, varying the RT times to find the fastest possible value. In the third set, we fixed the RT and qPCR activation parameters to determine the fastest qPCR activation time. In this study, we added 1000 copies of RNA to each reaction, with each set of experiments repeated three times. **Figure 5-3** shows the amplification curves for HIV-1, HCV, and RNase P under different conditions. Each curve varies one parameter—RT time, qPCR activation time, or denaturation and extension durations—while keeping the others constant. The integrated signals from three optical channels highlight which combinations achieve effective target detection. As shown in **Figure 5-4**, the results from these experiments were integrated into our original findings. We observed that the limits of RT and qPCR activation times could be pushed

slightly further—down to 3 minutes and 1 minute, respectively, without losing target detectability for HIV-1 and RNase P. However, HCV remained the limiting factor, likely due to its lower replication efficiency under accelerated conditions. These findings underscore the trade-offs between speed and accuracy in the development of rapid PCR protocols. While our optimized conditions (RT of 3 minutes, qPCR activation of 2 minutes, and denaturation and extension phases of 1s/1s) represent the fastest settings feasible without compromising diagnostic accuracy, the experiments with high-efficiency enzymes and rapid thermal cyclers suggest potential areas for further improvement. In conclusion, our study identifies the practical limits for rapid PCR cycling. These insights are essential for developing next-generation rapid PCR technologies that meet the stringent requirements of point-of-care diagnostics. The combination of speed and accuracy is crucial for rapid disease detection, significantly influencing clinical outcomes and public health interventions.

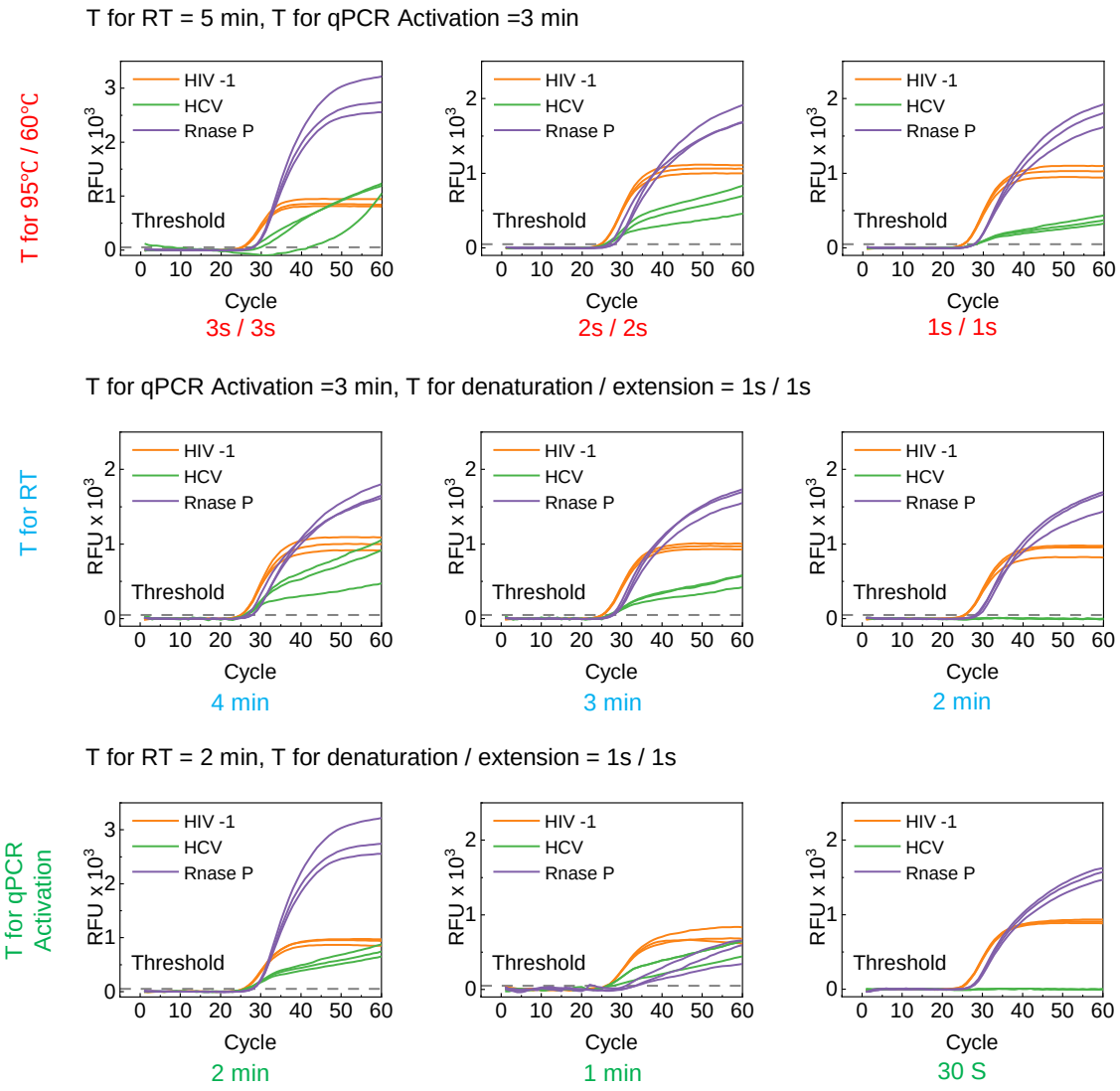

Figure 5-3. This figure illustrates the integrated amplification curves for HIV-1, HCV, and RNase P across different experimental conditions. Each curve represents the result of varying one of three parameters—RT time, qPCR activation time, or denaturation and extension durations—while holding the other two constant. The signal integration from three optical channels allows for a comprehensive visualization of the comparative efficiencies under each test condition, showcasing which combinations result in sufficient target detection.

T for RT = 5 min, T for qPCR Activation =3 min

T for denaturation / extension	HIV - 1	HCV	RNase P
3s / 3s	3/3	3/3	3/3
2s / 2s	3/3	3/3	3/3
* 1s / 1s *	3/3	3/3	3/3

T for qPCR Activation =3 min, T for denaturation / extension = 1s / 1s

T for RT	HIV - 1	HCV	RNase P
4 min	3/3	3/3	3/3
* 3 min *	3/3	3/3	3/3
2 min	3/3	0/3	3/3

T for RT = 2 min, T for denaturation / extension = 1s / 1s

T for qPCR Activation	HIV - 1	HCV	RNase P
2 min	3/3	3/3	3/3
* 1 min *	3/3	3/3	3/3
30 s	3/3	0/3	3/3

Figure 5-4. This table provides detailed statistical outcomes from the experiments, organized into three sets based on the variable parameter. Set 1 varies denaturation and extension times while fixing RT and qPCR activation times; Set 2 varies RT time with fixed qPCR activation and denaturation/extension times; Set 3 varies qPCR activation time with other conditions constant. The table lists detection successes and failures for HIV-1, HCV, and RNase P, indicating the minimal operational standards for each parameter set. Highlighted results pinpoint the RT time of 3 minutes, qPCR activation time of 1 minutes, and denaturation/extension times of 1s/1s as the optimal conditions for rapid PCR diagnostics, ensuring accuracy while reducing processing time.

5.3.3. Rapid PCR assay performance validation

To further assess the analytical precision of our multiplex PCR assay, we conducted a meticulous sensitivity analysis, comparing it to a traditional benchtop PCR system using a multiplex assay designed for the concurrent detection of HIV-1, HCV, and RNase P. This endeavor aimed to evaluate the assay's efficacy in accurately detecting diverse viral loads, thereby facilitating its deployment across varied clinical and field settings that demand robust and flexible diagnostic solutions.

The examination began by assessing the assay's capability to accurately quantify specific RNA levels across a significant concentration range, from 1 to 10^5 copies/rxn. The results were gathered through real-time multiplex RT-PCR experiments conducted using a Bio-Rad desktop PCR analyzer. These experiments involved serial dilutions of synthetic RNA standards ranging from 10^5 to 0 copies/rxn, each performed in six replicates to ensure statistical reliability. **Figure 5-5a** illustrates the detection capabilities for HIV-1, HCV, and RNase P across three separate optical channels, allowing clear observation of the assay's performance across the spectrum of tested concentrations.

The limits of detection for each virus were established at 5 copies/µL, corroborated by a compelling linear correlation between the known RNA concentrations and those detected by the assay. This correlation produced coefficients (R^2) between 0.98 and 0.99, signifying a highly accurate quantitative capability of the multiplex assay. **Figure 5-5b** illustrates the cycle threshold (Cq) values corresponding to various RNA concentrations for each analyzed target. The Cq values are determined by the time it takes for the relative fluorescence units (RFU) to surpass a set threshold of 100, depicted by a dashed line on the graph, demonstrating the assay's powerful quantitative precision and the reliability of the data generated by the desktop PCR system. In conclusion, our study shows that the multiplex PCR assay achieves high accuracy and sensitivity across a wide range of RNA concentrations, making it suitable for rapid and reliable diagnostics. Its robust performance, especially in detecting low viral loads, highlights its potential for diverse clinical settings. These findings support further advancements in PCR technology, aiming to combine speed and precision for point-of-care diagnostics and improved patient outcomes.

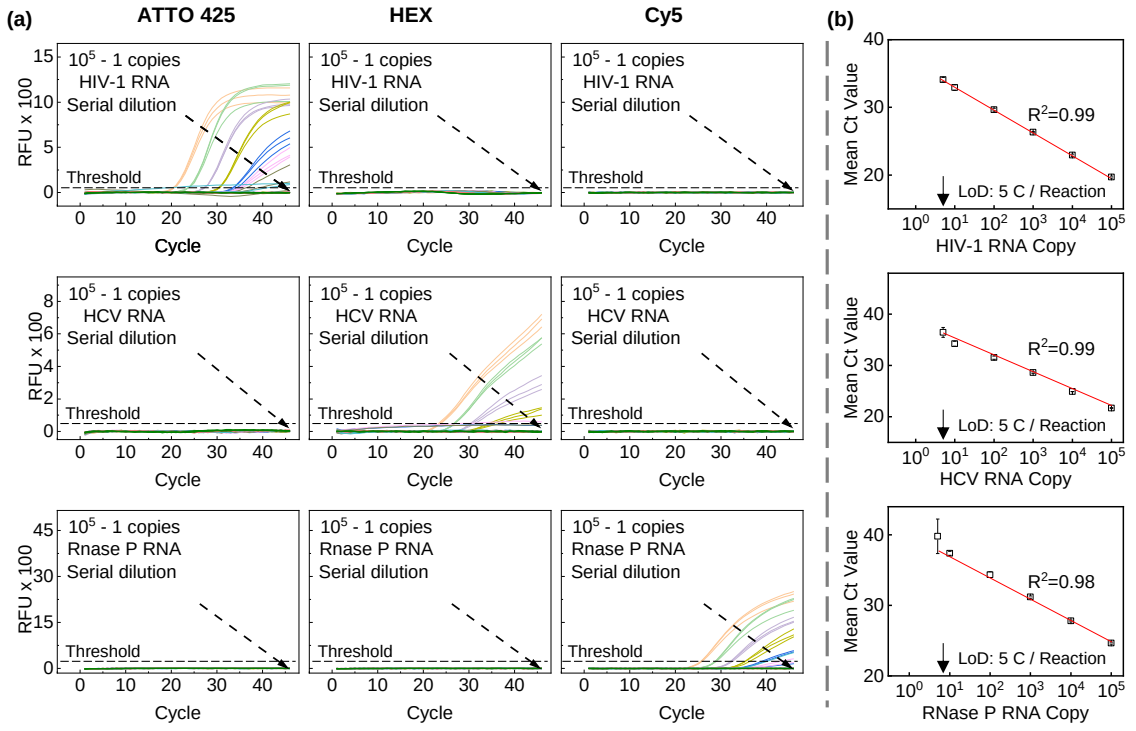

Figure 5-5. Evaluation of the Sensitivity and Quantitative Accuracy of Multiplex RT-PCR Tests Using Bio-Rad Instruments. **(a)** This image represents the outcomes from a series of real-time multiplex RT-PCR experiments conducted on a Bio-Rad tabletop PCR analyzer. These tests used RNA standards with a serial dilution ranging from 10^5 to 0 copies per reaction, each conducted in six replicates. Detection of HIV-1, HCV, and RNase P via three different optical channels is presented in three distinct columns. **(b)** This chart illustrates the cycle threshold (Ct) values corresponding to various RNA concentrations for each analyzed target. The "Cq values" are determined by the time it takes for the relative fluorescence units (RFU) to surpass a set threshold of 100, as depicted by a dashed line on the graph.

5.3.4. Analyzer analytical evaluation

Further validation of our portable analyzer's quantitative accuracy involved rigorous systematic testing of a panel displaying real-time RT-PCR data for various serially diluted RNA samples. These tests, represented in **Figure 5-6a**, were conducted in triplicate for each RNA concentration level, from 10^5 to 0 copies/rnx, to confirm the assay's reproducibility and reliability under different testing scenarios. Comparative analysis between our portable device and the conventional Bio-Rad

analyzer revealed that both systems produced identical amplification curves for each RNA type tested. These comparative results, illustrated in **Figure 5-6b**, reveal correlation coefficients ranging from 0.96 to 0.99, underscoring the precise and consistent performance of our portable system relative to the established benchtop equipment.

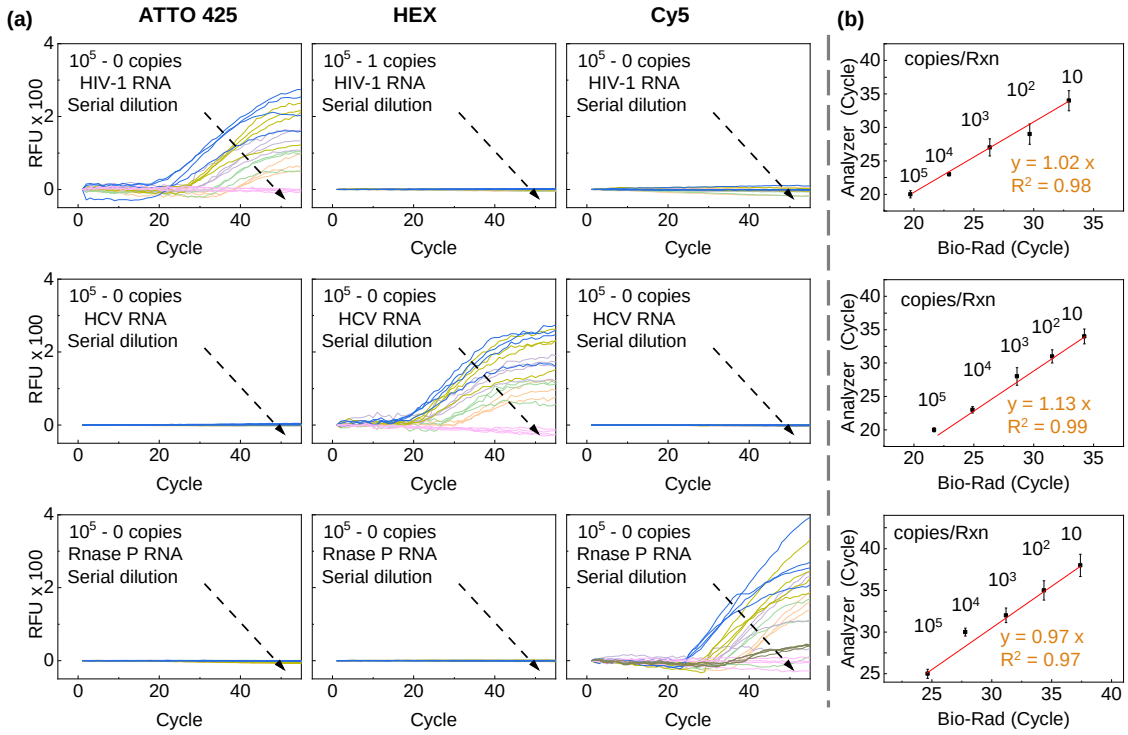

Figure 5-6. (a) A panel presenting real-time RT-PCR results from tests conducted on serially diluted RNA, ranging from 10^5 to 0 copies per reaction, with each concentration tested in triplicate. The optical signals for the three targets are displayed in three separate columns. **(b)** A comparative graph illustrating the Cq values for all three targets, obtained from both the Bio-Rad benchtop PCR analyzer and our portable analyzer.

In combination with the multiplex RT-PCR assay, our portable PCR analyzer achieved a detection limit of 10 copies per reaction. This confirms not only the reliability but also the equivalency of our portable device to traditional laboratory apparatus, emphasizing its utility in a wide array of environments, including those with restricted resources. The robust performance of our multiplex assay when implemented on our portable analyzer validates its suitability for diverse operational

contexts. This adaptability is critical, particularly in resource-limited settings where traditional lab facilities are scarce or non-existent.

Overall, the assay's ability to deliver sensitive, specific, and reliable results in a compact, portable format presents significant advantages for on-site diagnostics and real-time monitoring of viral loads. This makes our portable analyzer an essential tool in the global effort to control and manage HIV, particularly in regions where rapid, accurate testing is crucial but access to standard lab facilities is limited.

5.4. Summary

In this study, we have successfully developed a portable, battery-operated multiplex PCR system for the simultaneous detection of HIV and HCV viral loads. Our device is optimized for home self-testing, addressing the critical need for accessible and rapid diagnostics in resource-limited settings. The system integrates a portable sample preparation module with a three-channel detection mechanism, ensuring accurate and reliable measurements of viral loads. The developed device demonstrates strong correlation with traditional benchtop PCR systems, with correlation coefficients ranging from 0.96 to 0.99. The reduction in processing time from 70 minutes to 45 minutes further enhances its practicality for point-of-care applications. Our multiplex PCR assay is highly specific and sensitive, capable of detecting low viral loads with high accuracy, making it an excellent tool for managing HIV and HCV infections. This advancement represents a significant leap forward in the field of point-of-care diagnostics, providing a robust solution for timely and precise viral load testing. The device's portability, ease of use, and reliability make it particularly valuable for use in settings where conventional laboratory infrastructure is lacking. By facilitating early detection and continuous monitoring, our portable PCR system has the potential to greatly

improve health outcomes for individuals living with HIV and HCV, contributing to global efforts in controlling and managing these infections. Future work will focus on further miniaturizing the device, enhancing its user interface, and conducting extensive field evaluations to validate its performance in diverse real-world conditions. The ongoing development and refinement of this technology hold promise for expanding its applications to other infectious diseases, thereby broadening the impact of portable diagnostics on global health.

CHAPTER 6 Conclusions and Future Perspectives

6.1. Conclusions

This dissertation presents the development of a user-friendly portable device for quantitative HIV detection from finger-prick blood, addressing the need for accessible viral load testing in resource-limited settings. The work is divided into several key areas, each contributing to the overall aim of creating an efficient, accurate, and easy-to-use HIV testing device.

First, we developed an integrated nucleic acid testing (NAT) device for streamlined HIV self-testing using finger-prick whole blood. The device comprises a microfluidic reagent cartridge and an ultra-compact NAT-on-USB analyzer, which automatically handles sample preparation, purification, and real-time reverse-transcription loop-mediated isothermal amplification (RT-LAMP). The device demonstrated a limit of detection of 214 viral RNA copies/mL of whole blood within 60 minutes, making it suitable for high-risk populations seeking private self-testing.

Second, we enhanced the device to incorporate quantitative detection capabilities. This included designing a disposable plasma separation card and developing a syringe-based RNA extraction module for on-site plasma processing. These innovations achieved 80% efficiency in plasma separation and 86% viral recovery efficiency. A smartphone interface was integrated for real-time semi-quantitative RT-LAMP testing, ensuring stable performance over 16 weeks with lyophilized reagents. The device accurately categorized viral load into low, medium, and high levels with 95% accuracy, providing a convenient solution for home-based antiretroviral therapy (ART) monitoring.

Third, we advanced the device to perform multiplex PCR for HIV-1 and HIV-2 viral load determination from finger-prick whole blood. The portable PCR analyzer, designed for resource-

limited settings, incorporates multiplex RT-PCR technology with high specificity and sensitivity. The diagnostic performance showed 100% sensitivity for both HIV-1 and HIV-2 and high specificity, confirming its reliability in various testing environments.

Fourth, we refined the device to enable simultaneous self-testing detection of HIV and HCV viral loads. This battery-operated system significantly reduces the time required for point-of-care testing, completing PCR amplification in just 45 minutes. The system provides concurrent measurements of viral loads for HIV and HCV, with high accuracy and reliability, making it a critical tool for home-based self-testing.

In summary, the significant contributions of this thesis are as follows:

1. Development of an integrated NAT device for HIV self-testing using finger-prick whole blood, demonstrating high sensitivity and ease of use.
2. Enhancement of the device with quantitative detection capabilities and smartphone interface for real-time semi-quantitative testing.
3. Advancement of the device to perform multiplex PCR for HIV-1 and HIV-2 viral load determination, with high diagnostic performance.
4. Refinement of the device to enable simultaneous detection of HIV and HCV viral loads, providing a rapid, reliable, and user-friendly solution for home-based self-testing.

These contributions collectively advance the field of portable HIV diagnostics, addressing critical needs in resource-limited settings and improving accessibility to HIV viral load testing.

6.2. Future prospective

The research presented in this dissertation demonstrates significant advancements in portable and user-friendly devices for HIV detection. However, several aspects need further exploration to enhance the functionality and accessibility of these devices in resource-limited settings.

1. Integration of New Detection Methods: While the current device utilizes RT-LAMP and RT-PCR due to their simplicity and effectiveness, future research should explore integrating other amplification techniques such as recombinase polymerase amplification (RPA). Additionally, non-amplification detection methods, such as CRISPR-based diagnostics, could be considered. These methods might offer faster results, lower costs, and reduced complexity, improving the device's accessibility and efficiency.
2. Enhancement of RNA Extraction Efficiency: The syringe-based RNA extraction module has shown promising results, but further optimization is necessary. Future work should focus on enhancing the RNA recovery efficiency, possibly through advanced materials or novel extraction methods. Additionally, exploring automated or semi-automated extraction processes could reduce user intervention and improve consistency.
3. Miniaturization and Power Efficiency: While the current device is portable, there is room for further miniaturization. Reducing the size and weight of the analyzer and improving its power efficiency will make it more convenient for users in remote areas. Research into alternative power sources, such as solar or kinetic energy, could enhance the device's usability in areas with limited access to electricity.
4. Multiplexing Capabilities: The device currently supports multiplex PCR for HIV-1 and HIV-2. Future research should aim to expand these capabilities to include other sexually transmitted infections (STIs) like syphilis, gonorrhea, and chlamydia. Developing a comprehensive multiplex testing system will provide broader diagnostic capabilities and more holistic care for patients.

5. User Interface and Data Management: The integration with smartphones for real-time data display and management is a significant advancement. Future enhancements should focus on improving the graphical user interface (GUI) to make it more intuitive and user-friendly. Additionally, developing robust data management systems that ensure patient confidentiality and support remote healthcare provider consultations will be crucial for widespread adoption.
6. Field Testing and User Feedback: Extensive field testing in various resource-limited settings is essential to understand the practical challenges and gather user feedback. Future research should include large-scale clinical trials to validate the device's performance in real-world conditions and iteratively improve the design based on user experiences and needs.
7. Long-term Stability and Shelf-life: Ensuring the long-term stability and shelf-life of the reagents and components is crucial for the device's viability in resource-limited settings. Future research should focus on improving the stability of lyophilized reagents and ensuring that all components can withstand harsh environmental conditions without degradation.
8. Regulatory Approvals and Commercialization: Obtaining regulatory approvals from bodies such as the FDA and WHO is critical for the device's widespread adoption. Future efforts should focus on meeting the necessary regulatory requirements and developing a clear commercialization strategy. Collaborations with healthcare organizations and governments will be essential to facilitate the device's distribution and implementation.

By addressing these future research directions, the portable HIV detection device can be further refined and optimized, making it an invaluable tool for improving healthcare access and outcomes in resource-limited settings.

Bibliography

[1] "WHO. HIV Key facts," 2022. https://www.who.int/news-room/fact-sheets/detail/hiv-aids (accessed Jul. 05, 2023).

[2] WHO, "Summary of the Global HIV epidemic," 2023. https://www.who.int/data/gho/data/themes/hiv-aids

[3] S. G. Deeks *et al.*, "Research priorities for an HIV cure: International AIDS Society Global Scientific Strategy 2021," *Nat Med*, vol. 27, no. 12, pp. 2085–2098, Dec. 2021, doi: 10.1038/s41591-021-01590-5.

[4] P. Ehrenkranz *et al.*, "The revolving door of HIV care: Revising the service delivery cascade to achieve the UNAIDS 95-95-95 goals," *PLOS Medicine*, vol. 18, no. 5, p. e1003651, May 2021, doi: 10.1371/journal.pmed.1003651.

[5] A. Trickey *et al.*, "Survival of HIV-positive patients starting antiretroviral therapy between 1996 and 2013: a collaborative analysis of cohort studies," *The Lancet HIV*, vol. 4, no. 8, pp. e349–e356, Aug. 2017, doi: 10.1016/S2352-3018(17)30066-8.

[6] J. A. Sterne *et al.*, "Long-term effectiveness of potent antiretroviral therapy in preventing AIDS and death: a prospective cohort study," *The Lancet*, vol. 366, no. 9483. pp. 378–384, 2005.

[7] A. Phillips, A. Shroufi, L. Vojnov, J. Cohn, T. Roberts, and T. Ellman, "Working Group on Modelling of Antiretroviral Therapy Monitoring Strategies in Sub-Saharan Africa. Sustainable HIV treatment in Africa through viral-load-informed differentiated care," *Nature*, vol. 528, no. 7580. pp. S68-76, 2015.

[8] T. Roberts, J. Cohn, K. Bonner, and S. Hargreaves, "Scale-up of Routine Viral Load Testing in Resource-Poor Settings: Current and Future Implementation Challenges: Table 1.," *Clin Infect Dis.*, vol. 62, no. 8, pp. 1043–1048, Apr. 2016, doi: 10.1093/cid/ciw001.

[9] T. Notomi *et al.*, "Loop-mediated isothermal amplification of DNA," *Nucleic Acids Res*, vol. 28, no. 12, p. E63, Jun. 2000.

[10] I. V. Jani *et al.*, "Effect of point-of-care CD4 cell count tests on retention of patients and rates of antiretroviral therapy initiation in primary health clinics: an observational cohort study," *The Lancet*, vol. 378, no. 9802, pp. 1572–1579, Oct. 2011, doi: 10.1016/S0140-6736(11)61052-0.

[11] S. Palmer *et al.*, "New real-time reverse transcriptase-initiated PCR assay with single-copy sensitivity for human immunodeficiency virus type 1 RNA in plasma," *Journal of clinical microbiology*, vol. 41, no. 10. pp. 4531–4536, 2003.

[12] K. Nagamine, K. Watanabe, K. Ohtsuka, T. Hase, and T. Notomi, "Loop-mediated Isothermal Amplification Reaction Using a Nondenatured Template," *Clinical Chemistry*, vol. 47, no. 9, pp. 1742–1743, Sep. 2001, doi: 10.1093/clinchem/47.9.1742.

[13] M. Parida *et al.*, "Rapid Detection and Differentiation of Dengue Virus Serotypes by a Real-Time Reverse Transcription-Loop-Mediated Isothermal Amplification

Assay," *J Clin Microbiol*, vol. 43, no. 6, pp. 2895–2903, Jun. 2005, doi: 10.1128/JCM.43.6.2895-2903.2005.

[14] M. Parida, S. Sannarangaiah, P. K. Dash, P. V. L. Rao, and K. Morita, "Loop mediated isothermal amplification (LAMP): a new generation of innovative gene amplification technique; perspectives in clinical diagnosis of infectious diseases," *Rev. Med. Virol.*, vol. 18, no. 6, pp. 407–421, Nov. 2008, doi: 10.1002/rmv.593.

[15] C. N. Mnyani, J. A. McIntyre, and L. Myer, "The Reliability of Point-of-Care CD4 Testing in Identifying HIV-Infected Pregnant Women Eligible for Antiretroviral Therapy," *JAIDS Journal of Acquired Immune Deficiency Syndromes*, vol. 60, no. 3, pp. 260–264, Jul. 2012, doi: 10.1097/QAI.0b013e318256b651.

[16] G. H. Xun, S. T. Lane, V. A. Petrov, B. E. Pepa, and H. M. Zhao, "A rapid, accurate, scalable, and portable testing system for COVID-19 diagnosis," *Nature communications*, vol. 12, no. 1, May 2021.

[17] T. Liu, G. Choi, Z. Tang, A. Kshirsagar, A. J. Politza, and W. Guan, "Fingerpick Blood-Based Nucleic Acid Testing on A USB Interfaced Device towards HIV self-testing," *Biosensors and Bioelectronics*, vol. 209. p. 114255, 2022.

[18] Z. F. Tang *et al.*, "SLIDE: saliva-based SARS-CoV-2 self-testing with RT-LAMP in a mobile device," *ACS sensors*, Aug. 2022, doi: 10.1021/acssensors.2c01023.

[19] G. Choi and W. Guan, "Sample-to-Answer Microfluidic Nucleic Acid Testing (NAT) on Lab-on-a-Disc for Malaria Detection at Point of Need," in *Biomedical Engineering Technologies*, vol. 2393, M. R. Ossandon, H. Baker, and A. Rasooly, Eds. New York, NY: Springer US, 2022, pp. 297–313. doi: 10.1007/978-1-0716-1803-5_16.

[20] G. Choi and W. Guan, "An Ultracompact Real-Time Fluorescence Loop-Mediated Isothermal Amplification (LAMP) Analyzer," in *Biomedical Engineering Technologies*, vol. 2393, M. R. Ossandon, H. Baker, and A. Rasooly, Eds. New York, NY: Springer US, 2022, pp. 257–278. doi: 10.1007/978-1-0716-1803-5_14.

[21] E. A. Phillips *et al.*, "Microfluidic rapid and autonomous analytical device (microRAAD) to detect HIV from whole blood samples," *Lab Chip*, vol. 19, no. 20, pp. 3375–3386, Oct. 2019, doi: 10.1039/c9lc00506d.

[22] S. C. Liao *et al.*, "Smart Cup: A Minimally-Instrumented, Smartphone-Based Point-of-Care Molecular Diagnostic Device," *Sens Actuators B Chem*, vol. 229, pp. 232–238, Jun. 2016, doi: 10.1016/j.snb.2016.01.073.

[23] "ITAP for HCV POC Diagnostics - POCTRN - GAITS." https://www.poctrn.org/itap-for-hcv-poc-diagnostics (accessed Jun. 13, 2024).

[24] A. R. Bardon, J. M. Simoni, L. M. Layman, J. D. Stekler, and P. K. Drain, "Perspectives on the utility and interest in a point-of-care urine tenofovir test for adherence to HIV pre-exposure prophylaxis and antiretroviral therapy: an exploratory qualitative assessment among U.S. clients and providers," *AIDS Res Ther*, vol. 17, no. 1, p. 50, Dec. 2020, doi: 10.1186/s12981-020-00308-w.

[25] W. Tang *et al.*, "Diagnostic Accuracy of Point-of-Care HCV Viral Load Assays for HCV Diagnosis: A Systematic Review and Meta-Analysis," *Diagnostics*, vol. 12, no. 5, p. 1255, May 2022, doi: 10.3390/diagnostics12051255.

[26] H. Xu *et al.*, “An ultraportable and versatile point-of-care DNA testing platform,” *Sci. Adv.*, vol. 6, no. 17, p. eaaz7445, Apr. 2020, doi: 10.1126/sciadv.aaz7445.
[27] S.-M. Yang, S. Lv, W. Zhang, and Y. Cui, “Microfluidic Point-of-Care (POC) Devices in Early Diagnosis: A Review of Opportunities and Challenges,” *Sensors*, vol. 22, no. 4, p. 1620, Feb. 2022, doi: 10.3390/s22041620.
[28] WHO, “HIV/AIDS,” 2021.
[29] A. R. Zolopa, “The evolution of HIV treatment guidelines: current state-of-the-art of ART,” *Antiviral research*, vol. 85, no. 1. pp. 241–244, 2010.
[30] C. Iwuji and M. L. Newell, “HIV testing: the ‘front door’ to the UNAIDS 90-90-90 target,” *Public health action*, vol. 7, no. 2, p. 79, Jun. 2017, doi: 10.5588/ijtld.17.0046.
[31] F. Spielberg, R. O. Levine, and M. Weaver, “Self-testing for HIV: a new option for HIV prevention?,” *Lancet Infect Dis*, vol. 4, no. 10, pp. 640–6, Oct. 2004, doi: 10.1016/S1473-3099(04)01150-8.
[32] B. S. Parekh *et al.*, “Diagnosis of human immunodeficiency virus infection,” *Clinical microbiology reviews*, vol. 32, no. 1. pp. e00064-18, 2018.
[33] V. Frye and B. A. Koblin, “HIV self-testing in high-risk populations,” *The lancet. HIV*, vol. 4, no. 6, pp. e232–e233, Jun. 2017, doi: 10.1016/S2352-3018(17)30024-3.
[34] O. T. Ng and M. T. Tan, “HIV self-testing: money matters,” *Clin Infect Dis*, vol. 57, no. 5, pp. 771–2, Sep. 2013, doi: 10.1093/cid/cit361.
[35] L. Frith, “HIV self-testing: a time to revise current policy,” *Lancet*, vol. 369, no. 9557, pp. 243–5, Jan. 2007, doi: 10.1016/S0140-6736(07)60113-5.
[36] C. C. Johnson and E. L. Corbett, “HIV self-testing to scale up couples and partner testing,” *The lancet. HIV*, vol. 3, no. 6, pp. e243-4, Jun. 2016, doi: 10.1016/S2352-3018(16)00044-8.
[37] T. G. Fund, “List of HIV Diagnostic test kits and equipments classified according to the Global Fund Quality Assurance Policy,” *https://www.theglobalfund.org/media/5878/psm_productshiv-who_list_en.pdf*. 2022. [Online]. Available: https://www.theglobalfund.org/media/5878/psm_productshiv-who_list_en.pdf
[38] P. M. Mugo *et al.*, “Uptake and Acceptability of Oral HIV Self-Testing among Community Pharmacy Clients in Kenya: A Feasibility Study,” *PloS one*, vol. 12, no. 1, p. e0170868, 2017, doi: 10.1371/journal.pone.0170868.
[39] A. Sarkar *et al.*, “Feasibility of supervised self-testing using an oral fluid-based HIV rapid testing method: a cross-sectional, mixed method study among pregnant women in rural India,” *Journal of the International AIDS Society*, vol. 19, no. 1, p. 20993, 2016, doi: 10.7448/IAS.19.1.20993.
[40] L. de la Fuente *et al.*, “Are participants in a street-based HIV testing program able to perform their own rapid test and interpret the results?,” *PloS one*, vol. 7, no. 10, p. e46555, 2012, doi: 10.1371/journal.pone.0046555.
[41] O. T. Ng *et al.*, “Accuracy and user-acceptability of HIV self-testing using an oral fluid-based HIV rapid test,” *PloS one*, vol. 7, no. 9, p. e45168, 2012, doi: 10.1371/journal.pone.0045168.

[42] M. Stone *et al.*, “Comparison of detection limits of fourth-and fifth-generation combination HIV antigen-antibody, p24 antigen, and viral load assays on diverse HIV isolates,” *Journal of clinical microbiology*, vol. 56, no. 8, pp. e02045-17, 2018.

[43] L. Mazzola and C. Pérez-Casas, “HIV/AIDS diagnostics technology landscape 5th edition,” *UNITAID*. pp. 66–68, 2015.

[44] M. Mauk *et al.*, “Miniaturized devices for point of care molecular detection of HIV,” *Lab Chip*, vol. 17, no. 3, pp. 382–394, 2017.

[45] S. Fidler *et al.*, “A pilot evaluation of whole blood finger-prick sampling for point-of-care HIV viral load measurement: the UNICORN study,” *Sci Rep-Uk*, vol. 7, no. 1, p. 13658, Oct. 2017, doi: 10.1038/s41598-017-13287-2.

[46] S. Bertagnolio, N. T. Parkin, M. Jordan, J. Brooke, and J. G. Garcia-Lerma, “Dried blood spots for HIV-1 Drug Resistance and Viral Load Testing: A Review of Current Knowledge and WHO Efforts for Global HIV Drug Resistance Surveillance,” *Aids Reviews*, vol. 12, no. 4. pp. 195–208, 2010.

[47] E. Guichet *et al.*, “Comparison of different nucleic acid preparation methods to improve specific HIV-1 RNA isolation for viral load testing on dried blood spots,” *J Virol Methods*, vol. 251. pp. 75–79, 2018. doi: 10.1016/j.jviromet.2017.10.014.

[48] K. A. Curtis *et al.*, “Single-use, electricity-free amplification device for detection of HIV-1,” *J Virol Methods*, vol. 237. pp. 132–137, 2016. doi: 10.1016/j.jviromet.2016.09.007.

[49] J. Singleton *et al.*, “Electricity-free amplification and detection for molecular point-of-care diagnosis of HIV-1,” *PLoS One*, vol. 9, no. 11. p. e113693, 2014. doi: 10.1371/journal.pone.0113693.

[50] K. A. Curtis *et al.*, “Isothermal amplification using a chemical heating device for point-of-care detection of HIV-1,” *PLoS One*, vol. 7, no. 2. p. e31432, 2012. doi: 10.1371/journal.pone.0031432.

[51] F. B. Myers, R. H. Henrikson, J. M. Bone, and L. P. Lee, “A handheld point-of-care genomic diagnostic system,” *PLoS One*, vol. 8, no. 8. p. e70266, 2013. doi: 10.1371/journal.pone.0070266.

[52] M. Safavieh *et al.*, “Emerging Loop-Mediated Isothermal Amplification-Based Microchip and Microdevice Technologies for Nucleic Acid Detection,” *Acs Biomaterials-Science & Engineering*, vol. 2, no. 3. pp. 278–294, 2016. doi: 10.1021/acsbiomaterials.5b00449.

[53] E. A. Phillips, T. J. Moehling, S. Bhadra, A. D. Ellington, and J. C. Linnes, “Strand Displacement Probes Combined with Isothermal Nucleic Acid Amplification for Instrument-Free Detection from Complex Samples,” *Anal Chem*, vol. 90, no. 11. pp. 6580–6586, 2018. doi: 10.1021/acs.analchem.8b00269.

[54] G. Choi, T. Prince, J. Miao, L. W. Cui, and W. H. Guan, “Sample-to-answer palm-sized nucleic acid testing device towards low-cost malaria mass screening,” *Biosensors & Bioelectronics*, vol. 115. pp. 83–90, 2018. doi: 10.1016/j.bios.2018.05.019.

[55] G. Choi, D. Song, S. Shrestha, J. Miao, L. W. Cui, and W. H. Guan, “A field-deployable mobile molecular diagnostic system for malaria at the point of need,” *Lab on a Chip*, vol. 16, no. 22. pp. 4341–4349, 2016. doi: 10.1039/c6lc01078d.

[56] C. Liu *et al.*, “An isothermal amplification reactor with an integrated isolation membrane for point-of-care detection of infectious diseases,” *Analyst*, vol. 136, no. 10. pp. 2069–2076, 2011.

[57] G. L. Damhorst, C. Duarte-Guevara, W. Chen, T. Ghonge, B. T. Cunningham, and R. Bashir, “Smartphone-Imaged HIV-1 Reverse-Transcription Loop-Mediated Isothermal Amplification (RT-LAMP) on a Chip from Whole Blood,” *Engineering (Beijing)*, vol. 1, no. 3. pp. 324–335, 2015. doi: 10.15302/J-ENG-2015072.

[58] X. Wang, D. J. Seo, M. H. Lee, and C. Choi, “Comparison of conventional PCR, multiplex PCR, and loop-mediated isothermal amplification assays for rapid detection of Arcobacter species,” *J Clin Microbiol*, vol. 52, no. 2. pp. 557–63, 2014. doi: 10.1128/JCM.02883-13.

[59] D. L. Rudolph, V. Sullivan, S. M. Owen, and K. A. Curtis, “Detection of Acute HIV-1 Infection by RT-LAMP,” *PLoS One*, vol. 10, no. 5. p. e0126609, 2015. doi: 10.1371/journal.pone.0126609.

[60] K. E. Ocwieja, S. Sherrill-Mix, C. Liu, J. Song, H. Bau, and F. D. Bushman, “A reverse transcription loop-mediated isothermal amplification assay optimized to detect multiple HIV subtypes,” *PLoS One*, vol. 10, no. 2. p. e0117852, 2015. doi: 10.1371/journal.pone.0117852.

[61] E. O. Odari, A. Maiyo, R. Lwembe, L. Gurtler, J. Eberle, and H. Nitschko, “Establishment and evaluation of a loop-mediated isothermal amplification (LAMP) assay for the semi-quantitative detection of HIV-1 group M virus,” *J Virol Methods*, vol. 212. pp. 30–8, 2015. doi: 10.1016/j.jviromet.2014.10.012.

[62] K. A. Curtis, P. L. Niedzwiedz, A. S. Youngpairoj, D. L. Rudolph, and S. M. Owen, “Real-Time Detection of HIV-2 by Reverse Transcription-Loop-Mediated Isothermal Amplification,” *J Clin Microbiol*, vol. 52, no. 7. pp. 2674–6, 2014. doi: 10.1128/JCM.00935-14.

[63] K. A. Curtis, D. L. Rudolph, and S. M. Owen, “Rapid detection of HIV-1 by reverse-transcription, loop-mediated isothermal amplification (RT-LAMP),” *J Virol Methods*, vol. 151, no. 2. pp. 264–70, 2008. doi: 10.1016/j.jviromet.2008.04.011.

[64] K. A. Curtis, D. L. Rudolph, and S. M. Owen, “Sequence-specific detection method for reverse transcription, loop-mediated isothermal amplification of HIV-1,” *J Med Virol*, vol. 81, no. 6. pp. 966–72, 2009. doi: 10.1002/jmv.21490.

[65] S.-C. Liao *et al.*, “Smart cup: a minimally-instrumented, smartphone-based point-of-care molecular diagnostic device,” *Sensors and Actuators B: Chemical*, vol. 229. pp. 232–238, 2016.

[66] E. A. Phillips *et al.*, “Microfluidic rapid and autonomous analytical device (microRAAD) to detect HIV from whole blood samples,” *Lab Chip*, vol. 19, no. 20. pp. 3375–3386, 2019. doi: 10.1039/c9lc00506d.

[67] M. A. Dineva, L. Mahilum-Tapay, and H. Lee, “Sample preparation: a challenge in the development of point-of-care nucleic acid-based assays for resource-limited

settings," *The Analyst*, vol. 132, no. 12, pp. 1193–1199, 2007, doi: 10.1039/B705672A.

[68] LabCorp, "HIV Specimen Collection Guide," *https://monogrambio.labcorp.com/sites/default/files/2019-11/L12159-0516-5.pdf*.

[69] A. Beyzavi and N. T. Nguyen, "One-dimensional actuation of a ferrofluid droplet by planar microcoils," *J Phys D Appl Phys*, vol. 42, no. 1, Jan. 2009.

[70] A. Rida, V. Fernandez, and M. A. M. Gijs, "Long-range transport of magnetic microbeads using simple planar coils placed in a uniform magnetostatic field," *Appl Phys Lett*, vol. 83, no. 12, pp. 2396–2398, Sep. 2003.

[71] C.-H. Chiou, D. J. Shin, Y. Zhang, and T.-H. Wang, "Topography-assisted electromagnetic platform for blood-to-PCR in a droplet," *Biosensors and Bioelectronics*, vol. 50, pp. 91–99, 2013.

[72] N. Tomita, Y. Mori, H. Kanda, and T. Notomi, "Loop-mediated isothermal amplification (LAMP) of gene sequences and simple visual detection of products," *Nat Protoc*, vol. 3, no. 5, pp. 877–882, May 2008, doi: 10.1038/nprot.2008.57.

[73] C. A. Holstein, M. Griffin, J. Hong, and P. D. Sampson, "Statistical method for determining and comparing limits of detection of bioassays," *Analytical chemistry*, vol. 87, no. 19, pp. 9795–9801, 2015.

[74] T. M. Ellman, B. Alemayehu, E. J. Abrams, S. Arpadi, A. A. Howard, and W. M. El-Sadr, "Selecting a viral load threshold for routine monitoring in resource-limited settings: optimizing individual health and population impact," *Journal of the International AIDS Society*, vol. 20, no. Suppl 7. 2017.

[75] S. L. Manoto, M. Lugongolo, U. Govender, and P. Mthunzi-Kufa, "Point of care diagnostics for HIV in resource limited settings: an overview," *medicina*, vol. 54, no. 1. p. 3, 2018.

[76] V. Bewick, L. Cheek, and J. Ball, "Statistics review 13: receiver operating characteristic curves," *Critical care*, vol. 8, no. 6, pp. 1–5, 2004.

[77] M. H. Zweig and G. Campbell, "Receiver-operating characteristic (ROC) plots: a fundamental evaluation tool in clinical medicine," *Clin Chem*, vol. 39, no. 4, pp. 561–577, 1993.

[78] P. K. Drain *et al.*, "Point-of-Care HIV Viral Load Testing: an Essential Tool for a Sustainable Global HIV/AIDS Response," *Clin Microbiol Rev*, vol. 32, no. 3, pp. e00097-18, Jun. 2019, doi: 10.1128/CMR.00097-18.

[79] M. M. Hossain, A. Sultana, and H. Mazumder, "Munzur-E-Murshid," *Sexually transmitted infections among Rohingya refugees in Bangladesh. lancet HIV*, vol. 5. p. e342, 2018.

[80] M. Schank, J. Zhao, J. P. Moorman, and Z. Q. Yao, "The impact of HIV-and ART-induced mitochondrial dysfunction in cellular senescence and aging," *Cells*, vol. 10, no. 1. p. 174, 2021.

[81] P. K. Drain *et al.*, "Diagnostic point-of-care tests in resource-limited settings," *The Lancet Infectious Diseases*, vol. 14, no. 3, pp. 239–249, Mar. 2014, doi: 10.1016/S1473-3099(13)70250-0.

[82] A. N. Phillips *et al.*, “Point-of-Care Viral Load Testing for Sub-Saharan Africa: Informing a Target Product Profile,” *Open Forum Infectious Diseases*, vol. 3, no. 3, p. ofw161, May 2016, doi: 10.1093/ofid/ofw161.

[83] S. Bertagnolio, N. T. Parkin, M. Jordan, J. Brooke, and J. G. Garcia-Lerma, “Dried blood spots for HIV-1 Drug Resistance and Viral Load Testing,” *Aids Reviews*, vol. 12, no. 4, pp. 195–208, Dec. 2010.

[84] E. Guichet *et al.*, “Comparison of different nucleic acid preparation methods to improve specific HIV-1 RNA isolation for viral load testing on dried blood spots,” *J Virol Methods*, vol. 251, pp. 75–79, Jan. 2018, doi: 10.1016/j.jviromet.2017.10.014.

[85] H. T. Ngo *et al.*, “Sensitive and Quantitative Point-of-Care HIV Viral Load Quantification from Blood Using a Power-Free Plasma Separation and Portable Magnetofluidic Polymerase Chain Reaction Instrument,” *Anal. Chem.*, p. acs.analchem.2c03897, Dec. 2022, doi: 10.1021/acs.analchem.2c03897.

[86] Y. Mori, K. Nagamine, N. Tomita, and T. Notomi, “Detection of Loop-Mediated Isothermal Amplification Reaction by Turbidity Derived from Magnesium Pyrophosphate Formation,” *Biochemical and Biophysical Research Communications*, vol. 289, no. 1, pp. 150–154, Nov. 2001, doi: 10.1006/bbrc.2001.5921.

[87] N. Tomita, Y. Mori, H. Kanda, and T. Notomi, “Loop-mediated isothermal amplification (LAMP) of gene sequences and simple visual detection of products,” *Nature protocols*, vol. 3, no. 5, p. 877, 2008.

[88] K. A. Curtis *et al.*, “Single-use, electricity-free amplification device for detection of HIV-1,” *J Virol Methods*, vol. 237, pp. 132–137, Nov. 2016, doi: 10.1016/j.jviromet.2016.09.007.

[89] M. Safavieh *et al.*, “Emerging Loop-Mediated Isothermal Amplification-Based Microchip and Microdevice Technologies for Nucleic Acid Detection,” *Acs Biomater-Sci Eng*, vol. 2, no. 3, pp. 278–294, Mar. 2016, doi: 10.1021/acsbiomaterials.5b00449.

[90] E. A. Phillips, T. J. Moehling, S. Bhadra, A. D. Ellington, and J. C. Linnes, “Strand Displacement Probes Combined with Isothermal Nucleic Acid Amplification for Instrument-Free Detection from Complex Samples,” *Anal Chem*, vol. 90, no. 11, pp. 6580–6586, Jun. 2018, doi: 10.1021/acs.analchem.8b00269.

[91] G. Choi, T. Prince, J. Miao, L. Cui, and W. Guan, “Sample-to-answer palm-sized nucleic acid testing device towards low-cost malaria mass screening,” *Biosensors and Bioelectronics*, vol. 115, pp. 83–90, Sep. 2018, doi: 10.1016/j.bios.2018.05.019.

[92] G. Choi, D. Song, S. Shrestha, J. Miao, L. Cui, and W. Guan, “A field-deployable mobile molecular diagnostic system for malaria at the point of need,” *Lab Chip*, vol. 16, no. 22, pp. 4341–4349, Nov. 2016, doi: 10.1039/c6lc01078d.

[93] C. Liu *et al.*, “An isothermal amplification reactor with an integrated isolation membrane for point-of-care detection of infectious diseases,” *The Analyst*, vol. 136, no. 10, pp. 2069–2076, 2011, doi: 10.1039/C1AN00007A.

[94] G. L. Damhorst, C. Duarte-Guevara, W. Chen, T. Ghonge, B. T. Cunningham, and R. Bashir, “Smartphone-Imaged HIV-1 Reverse-Transcription Loop-Mediated Isothermal Amplification (RT-LAMP) on a Chip from Whole Blood,” *Engineering*, vol. 1, no. 3, pp. 324–335, Sep. 2015, doi: 10.15302/J-ENG-2015072.

[95] S. Palmer *et al.*, “New real-time reverse transcriptase-initiated PCR assay with single-copy sensitivity for human immunodeficiency virus type 1 RNA in plasma,” *Journal of clinical microbiology*, vol. 41, no. 10, pp. 4531–4536, 2003, doi: 10.1128/jcm.41.10.4531-4536.2003.

[96] K. A. Curtis *et al.*, “Isothermal amplification using a chemical heating device for point-of-care detection of HIV-1,” *PloS one*, vol. 7, no. 2, p. e31432, 2012, doi: 10.1371/journal.pone.0031432.

[97] H.-W. Chen and W.-M. Ching, “Evaluation of the stability of lyophilized loop-mediated isothermal amplification reagents for the detection of Coxiella burnetii,” *Heliyon*, vol. 3, no. 10, p. e00415, Oct. 2017, doi: 10.1016/j.heliyon.2017.e00415.

[98] S. Vemulapati and D. Erickson, “Portable Resource-Independent Blood–Plasma Separator,” *Anal. Chem.*, vol. 91, no. 23, pp. 14824–14828, Dec. 2019, doi: 10.1021/acs.analchem.9b04180.

[99] H. Zhang *et al.*, “A circular gradient-width crossflow microfluidic platform for high-efficiency blood plasma separation,” *Sensors and Actuators B: Chemical*, vol. 354, p. 131180, Mar. 2022, doi: 10.1016/j.snb.2021.131180.

[100] C. Liu *et al.*, “A high-efficiency superhydrophobic plasma separator,” *Lab Chip*, vol. 16, no. 3, pp. 553–560, 2016, doi: 10.1039/C5LC01235J.

[101] A. Nabatiyan, Z. A. Parpia, R. Elghanian, and D. M. Kelso, “Membrane-based plasma collection device for point-of-care diagnosis of HIV,” *Journal of Virological Methods*, vol. 173, no. 1, pp. 37–42, Apr. 2011, doi: 10.1016/j.jviromet.2011.01.003.

[102] K. R. Baillargeon, L. P. Murray, R. N. Deraney, and C. R. Mace, “High-Yielding Separation and Collection of Plasma from Whole Blood Using Passive Filtration,” *Anal. Chem.*, vol. 92, no. 24, pp. 16245–16252, Dec. 2020, doi: 10.1021/acs.analchem.0c04127.

[103] K. Kadimisetty *et al.*, “An integrated self-powered 3D printed sample concentrator for highly sensitive molecular detection of HIV in whole blood at the point of care,” *Analyst*, vol. 146, no. 10, pp. 3234–3241, 2021, doi: 10.1039/D0AN02482A.

[104] M. Robinson, H. Marks, T. Hinsdale, K. Maitland, and G. Coté, “Rapid isolation of blood plasma using a cascaded inertial microfluidic device,” *Biomicrofluidics*, vol. 11, no. 2, p. 024109, Mar. 2017, doi: 10.1063/1.4979198.

[105] W. Guo, J. Hansson, and W. Van Der Wijngaart, “Synthetic Paper Separates Plasma from Whole Blood with Low Protein Loss,” *Anal. Chem.*, vol. 92, no. 9, pp. 6194–6199, May 2020, doi: 10.1021/acs.analchem.0c01474.

[106] C.-H. Liu *et al.*, “Blood Plasma Separation Using a Fidget-Spinner,” *Anal. Chem.*, vol. 91, no. 2, pp. 1247–1253, Jan. 2019, doi: 10.1021/acs.analchem.8b04860.

[107] J. Hauser, G. Lenk, J. Hansson, O. Beck, G. Stemme, and N. Roxhed, "High-Yield Passive Plasma Filtration from Human Finger Prick Blood," *Anal. Chem.*, vol. 90, no. 22, pp. 13393–13399, Nov. 2018, doi: 10.1021/acs.analchem.8b03175.
[108] W. Tan, L. Zhang, J. C. G. Doery, and W. Shen, "Three-dimensional microfluidic tape-paper-based sensing device for blood total bilirubin measurement in jaundiced neonates," *Lab Chip*, vol. 20, no. 2, pp. 394–404, 2020, doi: 10.1039/C9LC00939F.
[109] R. Boom, C. J. Sol, M. M. Salimans, C. L. Jansen, P. M. Wertheim-van Dillen, and J. Van Der Noordaa, "Rapid and simple method for purification of nucleic acids," *J Clin Microbiol*, vol. 28, no. 3, pp. 495–503, Mar. 1990, doi: 10.1128/jcm.28.3.495-503.1990.
[110] K. L. Hill-Ambroz, G. L. Brown-Guedira, and J. P. Fellers, "Modified Rapid DNA Extraction Protocol for High Throughput Microsatellite Analysis in Wheat," *Crop Sci.*, vol. 42, no. 6, pp. 2088–2091, Nov. 2002, doi: 10.2135/cropsci2002.2088.
[111] S. Aljanabi, "Universal and rapid salt-extraction of high quality genomic DNA for PCR- based techniques," *Nucleic Acids Research*, vol. 25, no. 22, pp. 4692–4693, Nov. 1997, doi: 10.1093/nar/25.22.4692.
[112] R. J. Mogg and J. M. Bond, "A cheap, reliable and rapid method of extracting high-quality DNA from plants," *Mol Ecol Notes*, vol. 3, no. 4, pp. 666–668, Oct. 2003, doi: 10.1046/j.1471-8286.2003.00548.x.
[113] M. S. Saag *et al.*, "HIV viral load markers in clinical practice," *Nat Med*, vol. 2, no. 6, pp. 625–629, Jun. 1996, doi: 10.1038/nm0696-625.
[114] A. V. Ritchie *et al.*, "SAMBA HIV Semiquantitative Test, a New Point-of-Care Viral-Load-Monitoring Assay for Resource-Limited Settings," *J Clin Microbiol*, vol. 52, no. 9, pp. 3377–3383, Sep. 2014, doi: 10.1128/JCM.00593-14.
[115] T. Liu, A. J. Politza, A. Kshirsagar, Y. Zhu, and W. Guan, "Compact Point-of-Care Device for Self-Administered HIV Viral Load Tests from Whole Blood," *ACS Sens.*, vol. 8, no. 12, pp. 4716–4727, Dec. 2023, doi: 10.1021/acssensors.3c01819.
[116] A. J. Politza, T. Liu, A. Kshirsagar, M. Dong, M. A. Ahamed, and W. Guan, "A Portable Centrifuge for Universal Nucleic Acid Extraction at the Point-of-Care." Rochester, NY, Apr. 03, 2024. doi: 10.2139/ssrn.4781228.
[117] T. Liu, G. Choi, Z. Tang, A. Kshirsagar, A. J. Politza, and W. Guan, "Fingerpick Blood-Based Nucleic Acid Testing on A USB Interfaced Device towards HIV self-testing," *Biosensors & bioelectronics*, vol. 209, p. 114255, Aug. 2022, doi: 10.1016/j.bios.2022.114255.
[118] G. Choi, T. Prince, J. Miao, L. Cui, and W. Guan, "Sample-to-answer palm-sized nucleic acid testing device towards low-cost malaria mass screening," *Biosensors and Bioelectronics*, vol. 115, pp. 83–90, Sep. 2018, doi: 10.1016/j.bios.2018.05.019.
[119] G. Choi, D. Song, S. Shrestha, J. Miao, L. Cui, and W. Guan, "A field-deployable mobile molecular diagnostic system for malaria at the point of need," *Lab on a Chip*, vol. 16, no. 22, pp. 4341–4349, 2016, doi: 10.1039/C6LC01078D.
[120] A. Kshirsagar, G. Choi, V. Santosh, T. Harvey, R. C. Bernhards, and W. Guan, "Handheld Purification-Free Nucleic Acid Testing Device for Point-of-Need

Detection of Malaria from Whole Blood," *ACS Sens.*, vol. 8, no. 2, pp. 673–683, Feb. 2023, doi: 10.1021/acssensors.2c02169.
[121] Z. Tang *et al.*, "SLIDE: Saliva-Based SARS-CoV-2 Self-Testing with RT-LAMP in a Mobile Device," *ACS Sens.*, vol. 7, no. 8, pp. 2370–2378, Aug. 2022, doi: 10.1021/acssensors.2c01023.
[122] R. W. Eisinger, C. W. Dieffenbach, and A. S. Fauci, "HIV Viral Load and Transmissibility of HIV Infection: Undetectable Equals Untransmittable," *JAMA*, vol. 321, no. 5, pp. 451–452, Feb. 2019, doi: 10.1001/jama.2018.21167.
[123] M. S. Saag *et al.*, "HIV viral load markers in clinical practice," *Nat Med*, vol. 2, no. 6, pp. 625–629, Jun. 1996, doi: 10.1038/nm0696-625.
[124] H. Farzadegan *et al.*, "Sex differences in HIV-1 viral load and progression to AIDS," *The Lancet*, vol. 352, no. 9139, pp. 1510–1514, Nov. 1998, doi: 10.1016/S0140-6736(98)02372-1.
[125] D. P. Wilson, M. G. Law, A. E. Grulich, D. A. Cooper, and J. M. Kaldor, "Relation between HIV viral load and infectiousness: a model-based analysis," *The Lancet*, vol. 372, no. 9635, pp. 314–320, Jul. 2008, doi: 10.1016/S0140-6736(08)61115-0.
[126] A. N. Phillips *et al.*, "HIV Viral Load Response to Antiretroviral Therapy According to the Baseline CD4 Cell Count and Viral Load," *JAMA*, vol. 286, no. 20, pp. 2560–2567, Nov. 2001, doi: 10.1001/jama.286.20.2560.
[127] A. Calmy *et al.*, "HIV Viral Load Monitoring in Resource-Limited Regions: Optional or Necessary?," *Clinical Infectious Diseases*, vol. 44, no. 1, pp. 128–134, Jan. 2007, doi: 10.1086/510073.
[128] WHO, "HIV Key facts." 2022. [Online]. Available: https://www.who.int/news-room/fact-sheets/detail/hiv-aids
[129] D. B. Reeves *et al.*, "Impact of misclassified defective proviruses on HIV reservoir measurements," *Nat Commun*, vol. 14, no. 1, p. 4186, Jul. 2023, doi: 10.1038/s41467-023-39837-z.
[130] A. B. D. Djiyou *et al.*, "Viral load suppression in HIV-infected adolescents in cameroon: towards achieving the UNAIDS 95% viral suppression target," *BMC Pediatr*, vol. 23, no. 1, p. 119, Mar. 2023, doi: 10.1186/s12887-023-03943-0.
[131] P. Mancuso *et al.*, "CRISPR based editing of SIV proviral DNA in ART treated non-human primates," *Nat Commun*, vol. 11, no. 1, p. 6065, Nov. 2020, doi: 10.1038/s41467-020-19821-7.
[132] S. Prakash, R. Aasarey, Priyatma, M. Sharma, S. Khan, and Medha, "The development, evaluation, performance, and validation of micro-PCR and extractor for the quantification of HIV-1 &-2 RNA," *Sci Rep*, vol. 14, no. 1, p. 8700, Apr. 2024, doi: 10.1038/s41598-024-56164-5.
[133] P. K. Akakpo *et al.*, "High-risk human papillomavirus genotype distribution among women living with HIV; implication for cervical cancer prevention in a resource limited setting," *Infect Agents Cancer*, vol. 18, no. 1, p. 33, May 2023, doi: 10.1186/s13027-023-00513-y.
[134] M. D. Pham, L. Romero, B. Parnell, D. A. Anderson, S. M. Crowe, and S. Luchters, "Feasibility of antiretroviral treatment monitoring in the era of

decentralized HIV care: a systematic review," *AIDS Res Ther*, vol. 14, no. 1, p. 3, Dec. 2017, doi: 10.1186/s12981-017-0131-5.

[135] The Strategies for Management of Antiretroviral Therapy (SMART) Study Group, "Major Clinical Outcomes in Antiretroviral Therapy (ART)–Naive Participants and in Those Not Receiving ART at Baseline in the SMART Study," *J INFECT DIS*, vol. 197, no. 8, pp. 1133–1144, Apr. 2008, doi: 10.1086/586713.

[136] C. Charpentier *et al.*, "HIV-2EU: Supporting Standardized HIV-2 Drug Resistance Interpretation in Europe," *Clinical Infectious Diseases*, vol. 56, no. 11, pp. 1654–1658, Jun. 2013, doi: 10.1093/cid/cit104.

[137] I. Moranguinho, N. Taveira, and I. Bártolo, "Antiretroviral Treatment of HIV-2 Infection: Available Drugs, Resistance Pathways, and Promising New Compounds," *IJMS*, vol. 24, no. 6, p. 5905, Mar. 2023, doi: 10.3390/ijms24065905.

[138] B. K. Tchounga *et al.*, "Molecular confirmation of HIV-1 and HIV-2 coinfections among initially serologically dually-reactive samples from patients living in West Africa," *PLoS ONE*, vol. 18, no. 3, p. e0283602, Mar. 2023, doi: 10.1371/journal.pone.0283602.

[139] H. Diop-Ndiaye *et al.*, "m-PIMA™ HIV1/2 VL: A suitable tool for HIV-1 and HIV-2 viral load quantification in West Africa," *Journal of Virological Methods*, vol. 324, p. 114872, Feb. 2024, doi: 10.1016/j.jviromet.2023.114872.

[140] D. Mariani *et al.*, "The performance of a new point-of-care HIV virus load technology to identify patients failing antiretroviral treatment," *Journal of Clinical Virology*, vol. 122, p. 104212, Jan. 2020, doi: 10.1016/j.jcv.2019.104212.

[141] M. D. Pham, H. V. Nguyen, D. Anderson, S. Crowe, and S. Luchters, "Viral load monitoring for people living with HIV in the era of test and treat: progress made and challenges ahead – a systematic review," *BMC Public Health*, vol. 22, no. 1, p. 1203, Dec. 2022, doi: 10.1186/s12889-022-13504-2.

[142] J. Dorward *et al.*, "Diagnostic Accuracy of the Rapid Xpert HIV-1 Viral Load XC, Xpert HIV-1 Viral Load, & m-PIMA HIV-1/2 Viral Load in South African Clinics," *JAIDS Journal of Acquired Immune Deficiency Syndromes*, vol. 91, no. 2, pp. 189–196, Oct. 2022, doi: 10.1097/QAI.0000000000003037.

[143] L. L. Jagodzinski *et al.*, "Impact of Early Antiretroviral Therapy on Detection of Cell-Associated HIV-1 Nucleic Acid in Blood by the Roche Cobas TaqMan Test," *J Clin Microbiol*, vol. 57, no. 5, pp. e01922-18, May 2019, doi: 10.1128/JCM.01922-18.

[144] P. Bwana, J. Ageng'o, and M. Mwau, "Performance and usability of Cepheid GeneXpert HIV-1 qualitative and quantitative assay in Kenya," *PLoS ONE*, vol. 14, no. 3, p. e0213865, Mar. 2019, doi: 10.1371/journal.pone.0213865.

[145] T. Liu, G. Choi, Z. Tang, A. Kshirsagar, A. J. Politza, and W. Guan, "Fingerpick Blood-Based Nucleic Acid Testing on A USB Interfaced Device towards HIV self-testing," *Biosensors and Bioelectronics*, vol. 209, p. 114255, Aug. 2022, doi: 10.1016/j.bios.2022.114255.

[146] T. Liu, A. J. Politza, A. Kshirsagar, Y. Zhu, and W. Guan, “Compact point-of-care device for self-administered HIV viral load tests from whole blood,” *ACS Sens.*, p. acssensors.3c01819, Nov. 2023, doi: 10.1021/acssensors.3c01819.
[147] Z. Tang *et al.*, “SLIDE: saliva-based SARS-CoV-2 self-testing with RT-LAMP in a mobile device,” *ACS Sens.*, vol. 7, no. 8, pp. 2370–2378, Aug. 2022, doi: 10.1021/acssensors.2c01023.
[148] R. Nouri *et al.*, “STAMP-Based Digital CRISPR-Cas13a for Amplification-Free Quantification of HIV-1 Plasma Viral Loads,” *ACS Nano*, vol. 17, no. 11, pp. 10701–10712, Jun. 2023, doi: 10.1021/acsnano.3c01917.
[149] A. J. Politza, T. Liu, and W. Guan, “Programmable magnetic robot (ProMagBot) for automated nucleic acid extraction at the point of need,” *Lab on a Chip*, vol. 23, no. 17, pp. 3882–3892, 2023.
[150] A. J. Politza, T. Liu, A. Kshirsagar, M. Dong, Md. A. Ahamed, and W. Guan, “A Portable Centrifuge for Universal Nucleic Acid Extraction at the Point-of-Care.” 2024. doi: 10.2139/ssrn.4781228.
[151] Md. A. Ahamed *et al.*, “Sensitive and specific CRISPR-Cas12a assisted nanopore with RPA for Monkeypox detection,” *Biosensors and Bioelectronics*, vol. 246, p. 115866, Feb. 2024, doi: 10.1016/j.bios.2023.115866.
[152] M. A. Ahamed and W. Guan, “CRISPR-assisted solid-state nanopore sensor for rapid and sensitive point-of-care amendable of monkeypox virus detection via RPA amplification,” *Biophysical Journal*, vol. 123, no. 3, p. 145a, 2024.
[153] R. Nouri, Z. Tang, M. Dong, T. Liu, A. Kshirsagar, and W. Guan, “CRISPR-based detection of SARS-CoV-2: A review from sample to result,” *Biosensors and Bioelectronics*, vol. 178, p. 113012, Apr. 2021, doi: 10.1016/j.bios.2021.113012.
[154] S. Lecher *et al.*, “Progress with Scale-Up of HIV Viral Load Monitoring — Seven Sub-Saharan African Countries, January 2015–June 2016,” *MMWR Morb. Mortal. Wkly. Rep.*, vol. 65, no. 47, pp. 1332–1335, Dec. 2016, doi: 10.15585/mmwr.mm6547a2.
[155] H. Newman and D. Hardie, “HIV-1 viral load testing in resource-limited settings: Challenges and solutions for specimen integrity,” *Reviews in Medical Virology*, vol. 31, no. 2, p. e2165, Mar. 2021, doi: 10.1002/rmv.2165.
[156] R. Thomas *et al.*, “Cost and cost-effectiveness of a universal HIV testing and treatment intervention in Zambia and South Africa: evidence and projections from the HPTN 071 (PopART) trial,” *The Lancet Global Health*, vol. 9, no. 5, pp. e668–e680, May 2021, doi: 10.1016/S2214-109X(21)00034-6.
[157] P. H. Kilmarx and R. Simbi, “Progress and Challenges in Scaling Up Laboratory Monitoring of HIV Treatment,” *PLoS Med*, vol. 13, no. 8, p. e1002089, Aug. 2016, doi: 10.1371/journal.pmed.1002089.
[158] Z. Zhang, T. Liu, M. Dong, Md. A. Ahamed, and W. Guan, “Sample-to-answer salivary miRNA testing: New frontiers in point-of-care diagnostic technologies,” *WIREs Nanomed Nanobiotechnol*, vol. 16, no. 3, p. e1969, May 2024, doi: 10.1002/wnan.1969.
[159] L. Kreitmann *et al.*, “Next-generation molecular diagnostics: Leveraging digital technologies to enhance multiplexing in real-time PCR,” *TrAC Trends in*

Analytical Chemistry, vol. 160, p. 116963, Mar. 2023, doi: 10.1016/j.trac.2023.116963.
[160] V. Guiraud *et al.*, "Are Confirmatory Assays Reliable for HIV-1/HIV-2 Infection Differentiation? A Multicenter Study," *J Clin Microbiol*, pp. e00619-23, Jul. 2023, doi: 10.1128/jcm.00619-23.
[161] C. Gaebler *et al.*, "Sequence Evaluation and Comparative Analysis of Novel Assays for Intact Proviral HIV-1 DNA," *J Virol*, vol. 95, no. 6, pp. e01986-20, Feb. 2021, doi: 10.1128/JVI.01986-20.
[162] J. P. Broughton *et al.*, "CRISPR–Cas12-based detection of SARS-CoV-2," *Nature Biotechnology*, vol. 38, no. 7, pp. 870–874, Jul. 2020.
[163] P. Q. M. Nguyen *et al.*, "Modular micro-PCR system for the onsite rapid diagnosis of COVID-19," *Microsyst Nanoeng*, vol. 8, no. 1, p. 82, Jul. 2022, doi: 10.1038/s41378-022-00400-3.
[164] "People Coinfected with HIV and Viral Hepatitis | CDC," 2021. Accessed: Jun. 13, 2024. [Online]. Available: https://www.cdc.gov/hepatitis/populations/hiv.htm
[165] CDC, "Fast Facts: HIV in the United States," *HIV*, May 14, 2024. https://www.cdc.gov/hiv/data-research/facts-stats/index.html (accessed Jun. 13, 2024).
[166] CDC, "Hepatitis C Prevention and Control," *Hepatitis C*, May 29, 2024. https://www.cdc.gov/hepatitis-c/prevention/index.html (accessed Jun. 13, 2024).
[167] H. Zhang, A. A. Quadeer, and M. R. McKay, "Direct-acting antiviral resistance of Hepatitis C virus is promoted by epistasis," *Nat Commun*, vol. 14, no. 1, p. 7457, Nov. 2023, doi: 10.1038/s41467-023-42550-6.
[168] C. Dietz and B. Maasoumy, "Direct-Acting Antiviral Agents for Hepatitis C Virus Infection—From Drug Discovery to Successful Implementation in Clinical Practice," *Viruses*, vol. 14, no. 6, p. 1325, Jun. 2022, doi: 10.3390/v14061325.
[169] A. L. Cox *et al.*, "Progress towards elimination goals for viral hepatitis," *Nat Rev Gastroenterol Hepatol*, vol. 17, no. 9, pp. 533–542, Sep. 2020, doi: 10.1038/s41575-020-0332-6.
[170] C. Semá Baltazar *et al.*, "Prevalence and risk factors associated with HIV/hepatitis B and HIV/hepatitis C co-infections among people who inject drugs in Mozambique," *BMC Public Health*, vol. 20, no. 1, p. 851, Dec. 2020, doi: 10.1186/s12889-020-09012-w.
[171] J. Chapin-Bardales *et al.*, "Hepatitis C virus infection and co-infection with HIV among persons who inject drugs in 10 U.S. cities—National HIV Behavioral Surveillance, 2018," *International Journal of Drug Policy*, p. 104387, Mar. 2024, doi: 10.1016/j.drugpo.2024.104387.
[172] A. J. Kandathil *et al.*, "Plasma virome and the risk of blood-borne infection in persons with substance use disorder," *Nat Commun*, vol. 12, no. 1, p. 6909, Nov. 2021, doi: 10.1038/s41467-021-26980-8.
[173] A. Mukhatayeva *et al.*, "Hepatitis B, Hepatitis C, tuberculosis and sexually-transmitted infections among HIV positive patients in Kazakhstan," *Sci Rep*, vol. 11, no. 1, p. 13542, Jun. 2021, doi: 10.1038/s41598-021-92688-w.

[174] Y. Tassachew *et al.*, “Prevalence of HIV and Its Co-Infection with Hepatitis B/C Virus Among Chronic Liver Disease Patients in Ethiopia,” *HMER*, vol. Volume 14, pp. 67–77, May 2022, doi: 10.2147/HMER.S365443.
[175] S. Yousefpouran *et al.*, “The assessment of selected MiRNAs profile in HIV, HBV, HCV, HIV/HCV, HIV/HBV Co-infection and elite controllers for determination of biomarker,” *Microbial Pathogenesis*, vol. 147, p. 104355, Oct. 2020, doi: 10.1016/j.micpath.2020.104355.
[176] A. J. Jeyarajan and R. T. Chung, “Insights Into the Pathophysiology of Liver Disease in HCV/HIV: Does it End With HCV Cure?,” *The Journal of Infectious Diseases*, vol. 222, no. Supplement_9, pp. S802–S813, Nov. 2020, doi: 10.1093/infdis/jiaa279.
[177] A. Abutaleb and K. E. Sherman, “A changing paradigm: management and treatment of the HCV/HIV-co-infected patient,” *Hepatol Int*, vol. 12, no. 6, pp. 500–509, Nov. 2018, doi: 10.1007/s12072-018-9896-4.
[178] R. Mukherjee *et al.*, “Diagnosis and Management of Hepatitis C Virus Infection,” *SLAS Technology*, vol. 20, no. 5, pp. 519–538, Oct. 2015, doi: 10.1177/2211068214563794.
[179] G. C. M. Kalla, E. V. Voundi, F. Angwafo, L. Bélec, and F.-X. Mbopi-Keou, “Mass screening for hepatitis B and C and HIV in sub-Saharan Africa,” *The Lancet Infectious Diseases*, vol. 18, no. 7, p. 716, Jul. 2018, doi: 10.1016/S1473-3099(18)30343-8.

VITA
Tianyi Liu

Education

- Ph.D. in Electrical Engineering
  The Pennsylvania State University, University Park, Pennsylvania, USA
- M.S. in Electrical Engineering
  The Pennsylvania State University, University Park, Pennsylvania, USA
- B.S. in Electrical Engineering
  The Pennsylvania State University, University Park, Pennsylvania, USA

Journal Publication (5/13)

1. **Liu, T.**, Choi, G., Tang, Z., Kshirsagar, A., Politza, A. J., & Guan, W. (2022). Fingerpick Blood-Based Nucleic Acid Testing on A USB Interfaced Device towards HIV self-testing. *Biosensors and Bioelectronics*, *209*, 114255.
2. Politza, A. J., **Liu, T.**, & Guan, W. (2023). Programmable magnetic robot (ProMagBot) for automated nucleic acid extraction at the point of need. Lab on a Chip, 23(17), 3882–3892.
3. **Liu, T.**, Politza, A. J., Aneesh Kshirsagar, Zhu, Y., & Guan, W. (2023). Compact Point-of-Care Device for Self-Administered HIV Viral Load Tests from Whole Blood. ACS Sensors.
4. **Liu, T.**, Politza, A. J., Aneesh Kshirsagar, Zhu, Y., & Guan, W. (2024). Compact Multiplex PCR Device for HIV-1 and HIV-2 Viral Load Determination from Finger-Prick Whole Blood in Resource-Limited Settings. Under Review.
5. **Liu, T.**, Politza, A. J., Aneesh Kshirsagar, Zhu, Y., & Guan, W. (2024). Portable Multiplex Rapid PCR Device for Simultaneous Self-Testing Detection of HIV and HCV Viral Loads. Under Review.

Conference Presentation (3 of 7)

- **Tianyi Liu**, Anthony J. Politza and Weihua Guan, HIV Quantitative Viral Load Self-Testing From Fingerpick Blood For ART Treatment Rebound Monitoring. BMES 2023, Seattle, WA, 2023
- **Tianyi Liu**, Aneesh Kshirsagar, Anthony J. Politza and Weihua Guan, Fingerpick Blood-Based HIV Self-Nucleic Acid Testing on USB At The Point of Need. Chemical and Biological Defense Science & Technology (CBD S&T) Conference, San Francisco, CA, 2022

Award

- Melvin P. Bloom Memorial Graduate Fellowship in Electrical Engineering
- Excellent Undergraduate Research Exhibition Award
- 2018 Penn State REU Scholarship